LUCAS MONOGIOS KOLEFF

Analysis of the impact of stray coupling effects on power grid filters

Trabalho apresentado à Escola Politécnica da Universidade de São Paulo para obtenção do título de Bacharel em Engenharia

Darmstadt

São Paulo

2015

LUCAS MONOGIOS KOLEFF

Analysis of the impact of stray coupling effects on power grid filters

Darmstadt

São Paulo

2015

LUCAS MONOGIOS KOLEFF

Analysis of the impact of stray coupling effects on power grid filters

Área de Concentração: Engenharia Elétrica com Ênfase em Energia e Automacao

Orientador: M.Sc. Illia Manushyn
Supervisor: Prof. Dr. Gerd Griepentrog
Coordenador: Prof. Dr. Lourenço Matakas Jr.

Darmstadt
São Paulo
2015

Catalogação-na-publicação M2015D

[2751098]

Koleff, Lucas
Analysis of the Impact of Stray Coupling Effects on Power Grid Filters / L. Koleff -- São Paulo, 2015.
131 p.

Trabalho de Formatura - Escola Politécnica da Universidade de São Paulo. Departamento de Engenharia de Energia e Automação Elétricas.

1.COMPATIBILIDADE ELETROMAGNÉTICA 2.ELETRÔNICA DE POTÊNCIA 3.FILTROS ELÉTRICOS 4.ENGENHARIA ELÉTRICA 5.CONVERSORES ELÉTRICOS I.Universidade de São Paulo. Escola Politécnica. Departamento de Engenharia de Energia e Automação Elétricas II.t.

RESUMO

O objetivo deste trabalho é desenvolver um método geral como analisar efeitos de acoplamento parasitas em filtros de EMI passivos. Os componentes de um filtro de EMI comercial são modelados em uma ferramenta de análise por método dos elementos finitos. Simulações magnetostáticas e eletrostáticas são feitas para obter as matrizes de capacitância e indutância. Esses parâmetros sao inseridos em um modelo de circuito equivalente, que é validado através de comparação com medições das perdas de inserção do filtro. Os componentes parasitas são classificados de acordo com a relevância de seu impacto nas perdas de inserção do filtro. Medidas para mitigar os componentes parasitas mais relevantes são avaliadas. Conclue-se que através da compensação dos componentes parasitas e otimização do posicionamento dos componentes a performance do filtro pode ser melhorada.

Palavras-Chave: Filtros de EMI. Método dos Elementos Finitos. Componentes Parasitas. Compatibilidade Eletromagnética.

Kurzfassung

Ziel dieser Masterarbeit ist es eine Methode zu entwickeln, um Streueffekte in einen passiven Netzfilter zu analysieren. Die Auslegung der Komponenten eines kommerziellen Netzfilters ist durch Nachmodellierung mit einem Finite-Elemente-Analyse Programm untersucht worden. Magnetostatische und elektrostatische Simulationen werden durchgeführt, um die Induktivitäts- und Kapazitäts-Matrizen für die Anordnung zu berechnen. Die Parameter sind in ein Ersatzschaltbild eingefügt, das mittels Vergleich mit Messungen der Filtereinfügungsdämpfung validiert ist. Die Streukomponenten und Streukopplungen sind nach ihrer Relevanz entsprechend ihres Einflusses auf die Filtereinfügungsdämpfung klassifiziert. Maßnahmen zur Verringerung der relevanten Streukomponenten werden untersucht. Zur Validierung der Maßnahmen ist ein modularer Prototyp aufgebaut worden. Es folgt, dass durch die Kompensation der Streugrößen und die Optimierung der Anordnung der passiven Komponenten die Filterfunktionalität verbessert wird.

Schlüsselwörter: Netzfilter, FEM, Streukomponenten, EMV

Abstract

The goal of this master's thesis is to develop a general method, how to analyze stray coupling effects on a passive EMI filter. The component arrangement of a retail EMI filter is modelled in a finite element analysis tool. Magnetostatic and electrostatic simulations are done to obtain the capacitance and inductance matrices for the configuration. These parameters are implemented on an equivalent circuit model, which is validated through comparison with measurements of the insertion losses of the filter. The stray components and couplings are classified in their relevance according to their degradation impact on the insertion losses of the filter. Measures to mitigate the most relevant stray components are investigated. A filter prototype with a modular approach is built and the proposed measures are evaluated. It is concluded that through parasitics compensation of the filter components and optimization of the component arrangement the performance of the filter can be improved.

Keywords: EMI filter, FEM, stray components, EMC

To my family, I owe you everything.

Contents

List of Figures

List of Tables

Abbreviations and Symbols

Abbreviations

Abbreviation	Description
EMI	Electromagnetic Interference
FEM	Finite Element Method
PEEC	Partial Element Equivalent Circuit Method
IEC	International Electrotechnical Comission
EN	European Norm
FCC	Federal Communications Commission (USA)
ABNT	Associacao Brasileira de Normas Tecnicas
NB	Norma Brasileira
EMC	Electromagnetic Compatibility
PCB	Printed Circuit Board
3D	Three Dimensional
AC	Alternated Current
BNC	Bayonet Connector
RMS	Root Mean Square
DM	Diffential Mode
CM	Common Mode
EN	European Norm
CM	Common Mode
ISM	Industrial, Scientific and Medical
CNS	Chinese National Standard
ICES	Industry Canada Interference-Causing Equipment Standard
GOST	Gosudarstvenii(Russian Standard)
VCCI	Voluntary Control Council for Interference
DSTU	State Committee of Ukraine for Standardization, Metrology and Certification
MIL-STD	Military Standard

Symbols

Symbol	Description	Unit
U	Voltage	V
R	Resistance	Ω

Continues on next page ...

Symbol	Description	Unit
I	Current	A
B	Flux Density	T
H	Magnetic Field Intensity	A/m
J	Current Density	A/m^2
B	Flux Density	T
μ	Permeability	H/m
E	Electric Field	V/m
ϕ	Electric Potential	V
ρ	Charge Density	C/m^2
ϵ	Permittivity	F/m
Q	Electric Charge	C
C	Capacitance	F
L	Inductance	H
K	Coupling Factor	
f	Frequency	Hz
N	Number of Turns	
A	Area	m^2
l	Length	m
X	Reactance	Ω
S	Scattering Parameter	
IL	Insertion Loss	
λ	Wave Length	m
m	Transformer Winding Ratio	
Z	Impedance	Ω
R_m	Reluctance	A/(Vs)
ρ	Resisitivity	Ω / m
δ	Sheet Thickness	m
ω	Angular Frequency	1/s
l	Length	m
D	Electric Displacement Field	C/m^2

1 Introduction

Part 1.1: Vocabulary and Terms

The vocabulary and terms used in this work are listed below. They are further explained and analyzed in the next chapters.

- Filter Element: one of the passive components found in EMI filters, such as the common mode choke or the film capacitors.
- Stray Component: unintended and undesired component of a filter element that degrades its characteristics, like the stray inductance of the capacitors.
- Stray Coupling: inductive and capacitive coupling between filter elements, unintended or not. The stray inductive coupling between two capacitors is an example.
- Filter Parasitics: any element or effect that causes degradation of the filter performance. Stray components and stray couplings are filter parasitics.
- Ideal Filter: EMI filter, without consideration of filter parasitics.
- Real Filter: ideal filter, with consideration of the stray components and stray couplings.
- Filter Arrangement: combination of filter elements with defined electrical and physical properties, positioned in a certain layout.
- Filter Attenuation: is a measure of the ability to reduce conducted emissions, which can be evaluated through the insertion losses, for example.
- Compensation or Cancellation Technique: measures taken to compensate the effects of a filter parasitic, such as the cancellation of the stray inductance of the capacitors.

Part 1.2: Motivation of this Work

Power electronics have been evolving steadily in the last 20 years, with a very rapid increase in the power density and switching frequency in the recent years.

Unfortunately, fast switching of high currents and high voltages, the basic principle of modern power electronic systems, has got a high potential in emitting electromagnetic interference. [31] The radiated emissions consist in the high-frequency electromagnetic fields. The conducted emissions consist of the low-frequency harmonics, flicker and high-frequency conducted emissions, in which this work focuses.

The immunity is also an important aspect of the electromagnetic compatibility, so that the system is not influenced by the interferences emitted by other equipment. The radiated immunity is against high-

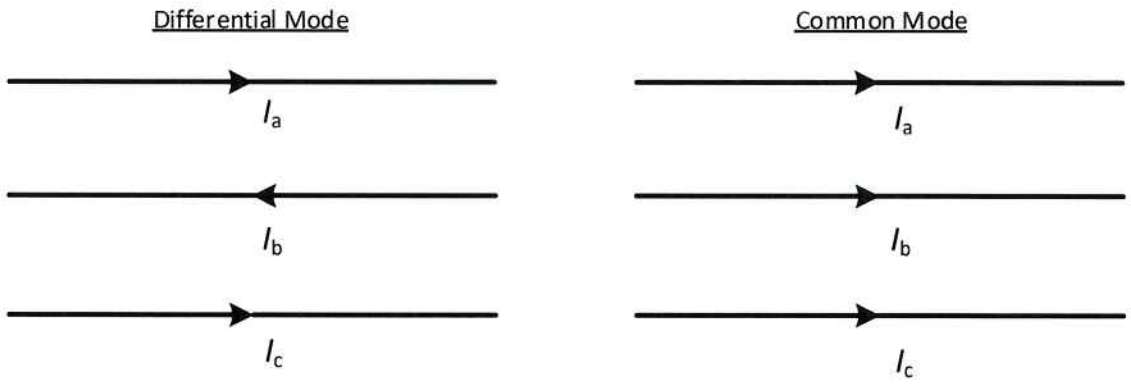

Figure 1.1.: Common and Differential Mode Signals

frequency electromagnetic fields. The conducted immunity is against electrostatic discharge, conducted signals, high energy surges, electric fast transients, voltage dips and interruptions. [24]

The high-frequency conducted emissions of a power electronics system can be reduced by means of passive EMI filters, which are the scope of the present work. Passive EMI filters are in general a combination of coils and capacitors with a characteristic impedance curve arranged in order to attenuate interferences generated by power electronics system or other sources.

The conducted emissions are classified in common mode and differential mode. Common mode signals happen simultaneously in the carrying conductors. That means, for example in a three-phase system, this signal does not have phase shift between phases. This leads to the fact that line frequent common mode signals are zero sequence symmetrical components. Differential mode signals happen independently in one carrying conductor or, in other words, between two phases in the three-phase system.

Usually, differential mode interference is caused by magnetic or galvanic coupling or either by common to differential mode conversion. Common mode interference on the other hand is mostly caused by capacitive coupling or ground potential and thus appears generally at higher frequencies than differential mode interference.

A comparison between both signal modes is depicted in Figure 1.1. The differential mode and common mode voltages can be calculated from the phase voltages according to Equations 1.1 and 1.2 [24]. This differentiation between the two signal modes is done in order to separate their effects and take effective mitigation procedures.

$$\begin{bmatrix} I_{\mathrm{DM,a}} \\ I_{\mathrm{DM,b}} \\ I_{\mathrm{DM,c}} \end{bmatrix} = \begin{bmatrix} 2/3 & -1/3 & -1/3 \\ -1/3 & 2/3 & -1/3 \\ -1/3 & -1/3 & 2/3 \end{bmatrix} \cdot \begin{bmatrix} I_{\mathrm{a}} \\ I_{\mathrm{b}} \\ I_{\mathrm{c}} \end{bmatrix} \tag{1.1}$$

$$I_{CM} = 1/3 \cdot (I_a + I_b + I_c) \tag{1.2}$$

In the Figures 1.2 and 1.5, the schematics and the plot of the filter attenuation for the Schaffner FN3100 series, which is an example of a conventional EMI filter developed for motor drives and other industrial applications, are presented.

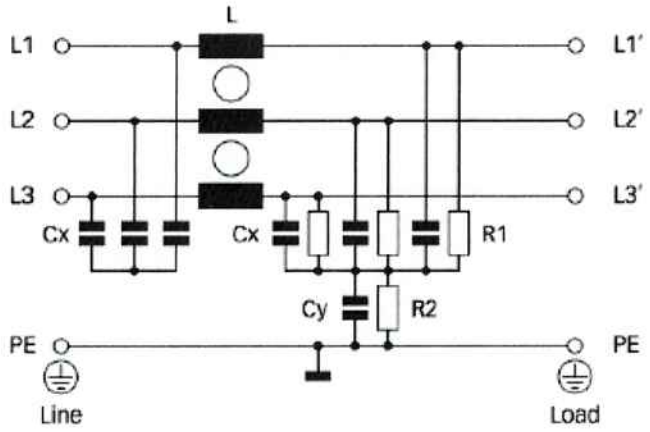

Figure 1.2.: FN3100 Schematics [33]

One of the main components of the filter is the common mode choke (Figure 1.3), which is represented as the inductances together with their respective couplings. The common mode choke, as its name suggests, is intended to attenuate common mode components. The sum of the flux in the three windings must be zero, and thus, the sum of the currents too. Since in common mode the current in all phases must be equal, the only solution is zero.

For differential mode signals, the common mode choke is behaving differently. The current in one of the coils creates flux and is exciting the other coils, therefore creating a flux which is counter-acting the first one. Only the stray flux, which closes outside of the core, remains.

X capacitors are used to attenuate differential mode signals and are connected between two phases. As the impedance of the capacitor decreases with an increase of the frequency, they are providing a path for differential mode currents to flow between phases at higher frequencies. The Y capacitors are used to attenuate common mode signals and are connected between one phase and the earth. They shunt the common mode currents to the earth at higher frequencies. Resistors are introduced in order to dampen resonance effects and/or to discharge the capacitors.

In the plot, curve A is the 50 Ω / 50 Ω symmetrical attenuation curve, curve B is the 50 Ω / 50 Ω asymmetrical attenuation curve, curve C is the 0.1 Ω / 100 Ω symmetrical attenuation curve and curve D is the 0.1 Ω / 100 Ω asymmetrical attenuation curve. It possible to see that the maximal attenuation of the filter is in the interval between 100kHz and 800kHz.

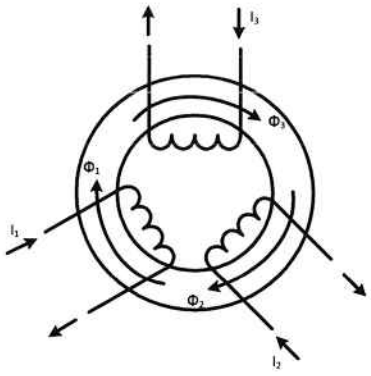

Figure 1.3.: Three-Phase Common Mode Choke

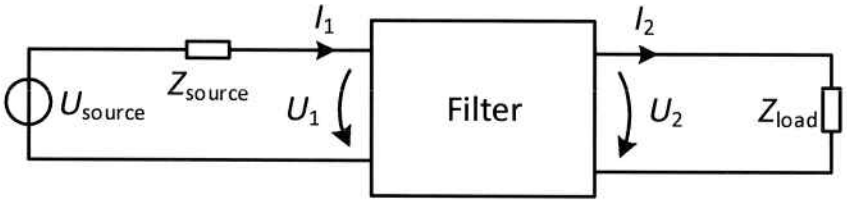

Figure 1.4.: Filter with Source and Load Impedances

Figure 1.4 depicts a filter connected to a voltage source, together with the source impedance and the load impedance. The filter insertion losses depend on the source impedance, on the load impedance and on the filter parameters, as described by Equations 1.3 and 1.4 [14].

$$IL = 20 \cdot log_{10} \frac{A \cdot Z_{\text{load}} + B + C \cdot Z_{\text{load}} \cdot Z_{\text{source}} + D \cdot Z_{\text{source}}}{Z_{\text{load}} + Z_{\text{source}}} \tag{1.3}$$

$$\begin{bmatrix} U_1 \\ I_1 \end{bmatrix} = \begin{bmatrix} A & B \\ C & D \end{bmatrix} \cdot \begin{bmatrix} U_2 \\ I_2 \end{bmatrix} \tag{1.4}$$

Part 1.3: Relevant EMC Emission Standards

Electromagnetic compatibility is concerned with the generation, transmission and reception of electromagnetic energy. A system is defined as electromagnetically compatible if it does not cause interference with other systems, it is not susceptible to emissions from other systems or it does not cause interference with itself. Devices must meet certain legal requirements in order to be operate and be sold in the market. [6] Power electronics system are potential sources of conducted emissions and therefore of special interest.

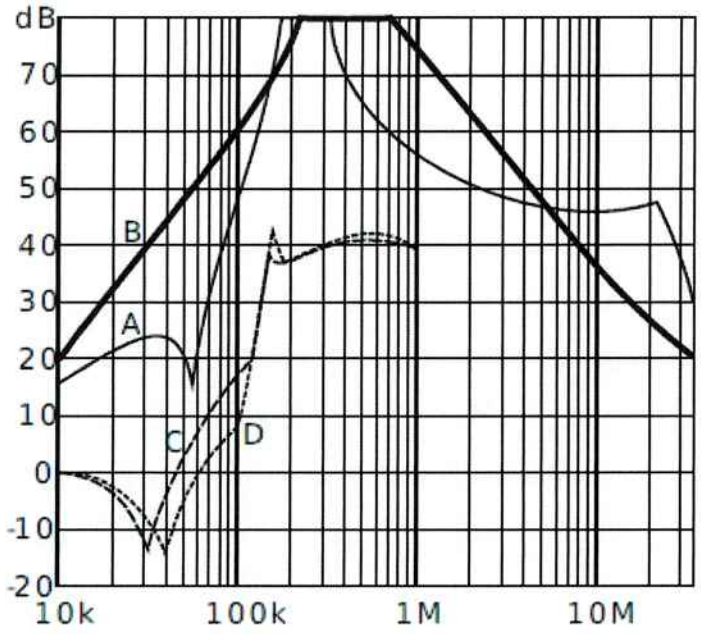

Figure 1.5.: FN3100 Attenuation Plot for 35A Version [33]

There are many standards associated with the CISPR 22 emissions limits for information technology equipment, where power electronics are used in the power supply unit. For example, the CISPR 22 emission limits are adopted in the ICES-003:2004 Issue 4 in Canada, ABNT NBR 12304 in Brazil, VCCI V-3/2014.04 in Japan and DIN EN 55022:2011-12 in Germany. The FCC Part 15 and the military standard MIL-STD 461F CE102 in the United States adopt different limits for the emissions of general electronic equipments. These standards are listed in Table 1.1. The values of the limits for this standards are summarized in Tables 1.2, 1.3 and 1.4.

The EN55022 norm defines class B as equipment, device and apparatus, that are intended to be used in the domestic environment and meets class B emission requirements. Class A is defined as equipment, device and apparatus, that do not meet the class B emission requirements, but complies with class A emission requirements.

Emission limits defined by the EN 55014-1 standard are valid for electrical equipments, whose main functions are performed by motors, switching and regulating devices, including separate parts of previously mentioned equipment. The limits are the same as EN55022 Class B. The EN 61000-6-3 standard applies to electrical equipment, that is intended to be used in residential, commercial and light industrial environments. If the equipment has no specific standard or family, this norm applies. The conducted emissions limits are the same as EN55022 Class B. For electrical equipment, that is used or intended to be used in industrial environment supplied by high or medium voltage transformer, or for equipment intended to operate near an industrial environment the EN 61000-6-4 standard is applicable. The conducted emission limits are the same as in EN55022 Class A.

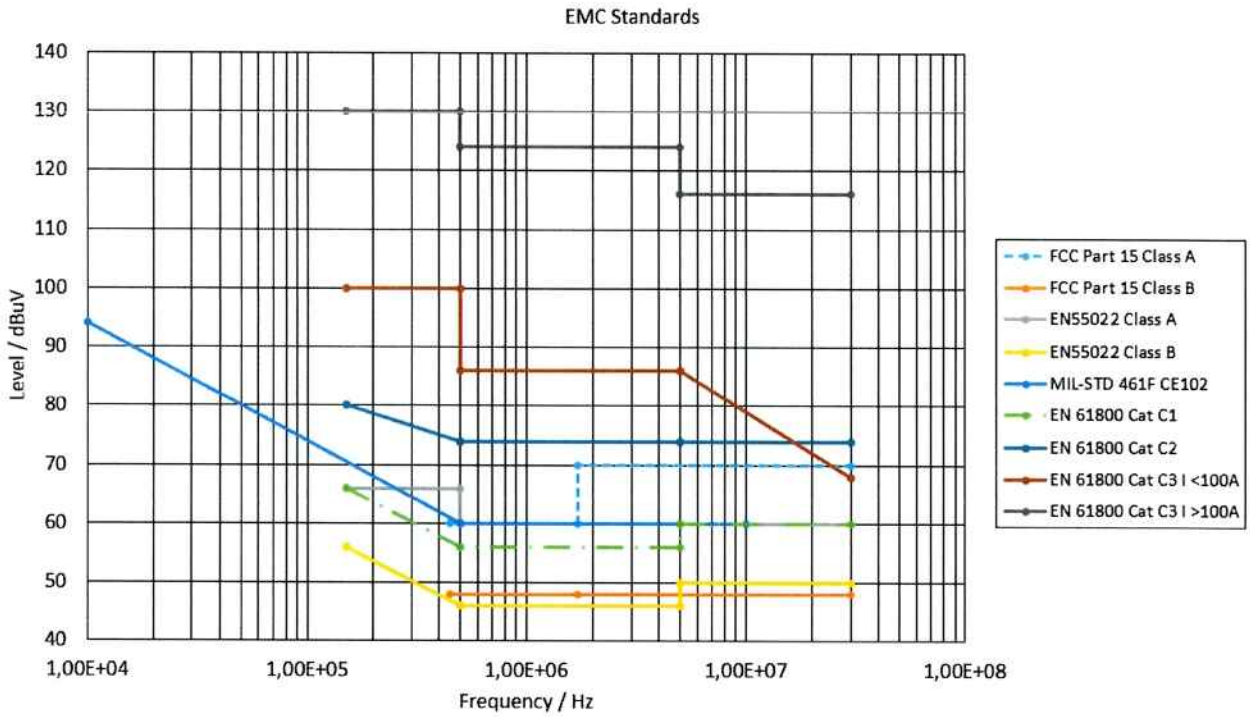

Figure 1.6.: EMC Standards Overview

For adjustable speed electrical power drive systems, the EN 61800 norm specifies different requirements for the following classes [42]. The emission limits are listed in Table 1.5.

Class 1: Low-level electromagnetic radiation environment. Typical level where radio/television stations are located at a distance of more than 1 km and typical level for low power transceivers.

Class 2: Moderate electromagnetic radiation environment. Low-power portable transceivers (typically less than 1 W rating) are in use, but with restrictions on use in proximity to the equipment. A typical commercial environment.

Class 3: Severe electromagnetic radiation environment. Portable transceivers (2 W and more) are in use relatively close to the equipment but at a distance not less than 1 m. High-powered broadcast transmitters are in proximity to the equipment and ISM equipment may be located close by. A typical industrial environment.

In Figure 1.6, the emission limits of the standards cited in this section are plotted.

Part 1.4: EMI Filters

Devices and installation must meet the legal requirements, creating the need to introduce mitigation measures to avoid electromagnetic compability problems. Power electronics devices, due to their non-linearities and switching processes are known for generating undesirable currents waveforms in the mains, with low frequency and high frequency harmonics. In Figure 1.7, the conducted emissions for

Table 1.1.: EMI Limiting Standards

Country	Standard
United States	FCC Part 15
Canada	ICES-003:2004 Issue 4
European Union	EN55022 (CISPR 22)
Japan	VCCI V-3/2014.04
Brazil	ABNT NBR 12304
Russia	GOST R51318.22
Ukraine	DSTU EN 55022:2004
China	CNS 134338

Table 1.2.: FCC Standard Overview

FCC Part 15 Class A		FCC Part 15 Class B	
Frequency	Voltage / dBuV	Frequency	Voltage / dBuV
450kHz - 1.705 MHz	60	450 kHz - 30 MHz	48
1.705 MHz - 30 MHz	70		

Table 1.3.: European Standard Overview

EN55022 AV Class A		EN55022 22 AV Class B	
Frequency	Voltage / dBuV	Frequency	Voltage / dBuV
150kHz - 500 kHz	66	150kHz - 500 kHz	56 - 46
500 kHz - 30 MHz	60	500 kHz - 5 MHz	46
		5 MHz - 30 MHz	50

Table 1.4.: Military Standard Overview

MIL-STD 461F CE102	
Frequency	Voltage / dBuV
10kHz - 500kHz	94 - 60
500 kHz - 10 MHz	60

Table 1.5.: EN 61800 Emission Limits

EN 61800 Cat C1		EN 61800 Cat C2	
Frequency	Voltage / dBuV	Frequency	Voltage / dBuV
150 kHz - 500 kHz	66 - 56	150 kHz - 500 kHz	80 - 74
500 kHz - 5 MHz	56	500 kHz - 5 MHz	74
5 MHz - 30 MHz	60	5 MHz - 30 MHz	74
EN 61800 Cat C3 I <100A		EN 61800 Cat C3 I >100A	
Frequency	Voltage / dBuV	Frequency	Voltage / dBuV
150 kHz - 500 kHz	100	150 kHz - 500 kHz	130
500 kHz - 5 MHz	86	500 kHz - 5 MHz	124
5 MHz - 30 MHz	90-68	5 MHz - 30 MHz	116

a passive diode front-end are represented together with the CISPR 22 AV Class B limit. The task of the electromagnetic interference filter is to attenuate the undesired high-frequency components.

There are many filter topologies with different characteristics available in the market. In order to select and purchase the appropriate one, the emissions of the equipment must be measured to determine the dampening requirements. A typical application is the connection of the filter between the power grid and a drive system to eliminate of the interference of the front-end of the motor drive.

In figure 1.8, the schematics for the Schurter FMBC-R91 filter are depicted and it is possible to see the two common-mode chokes and the X and Y capacitor stages. Here a double-stage approach is used. The employment of filters with multiple inductive stages, for a given attenuation, is advantageous from the volume perspective. [24]

The circuit of the Schaffner FN258 filter is more complex. Its schematics are represented in Figure 1.9. It has two common-mode chokes, two Y capacitor stages and one X capacitor. Another approach is used in the Schaffner FN351H filter. There is only one common-mode choke, but two Y capacitor stages and two X capacitor stages, as in Figure 1.10.

To successfully design an EMI filter, many aspects must be considered. First, the environment where the filter is going to be installed must defined and evaluated. For that, studying and measuring the noise sources and the EMC standards is needed. After this, a filter topology and the components are selected, with consideration of the required emission attenuation levels, efficiency, mechanical dimensions, nominal current, withstand voltage and others. [24]

In this work, the Siemens Micromaster 4 6SE6400-2FA00-6AD0 EMI filter is going to be studied. The topology is equivalent to the Schaffner FN3100, and its application area is electric motor drives. It is of relative simple construction, what facilitates the understanding of the components and their interactions. It has a nominal current of 6A, nominal voltage of 380/480 V and operates at network frequencies from 47 to 63 Hz.

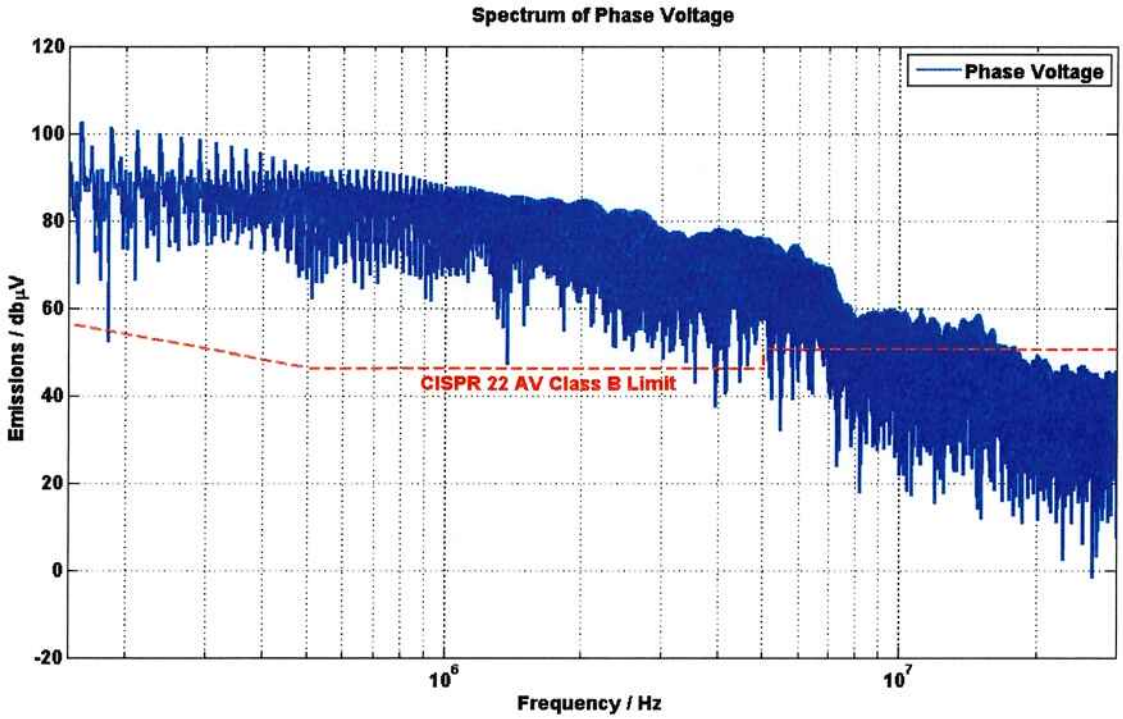

Figure 1.7.: Conducted Emissions Spectra for a Passive Rectifier

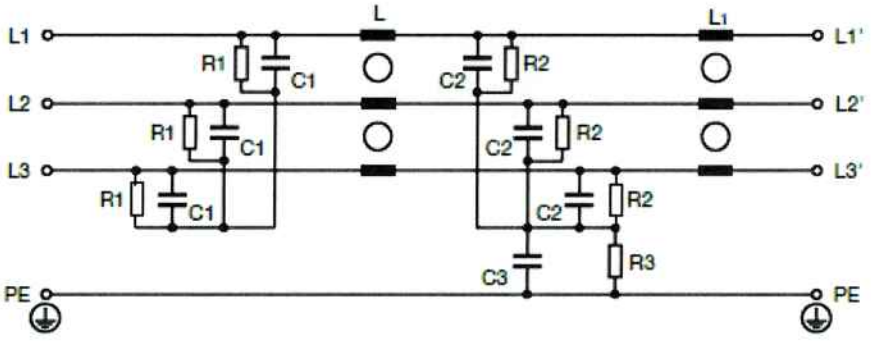

Figure 1.8.: Schurter FMBC-R91 Schematics [36]

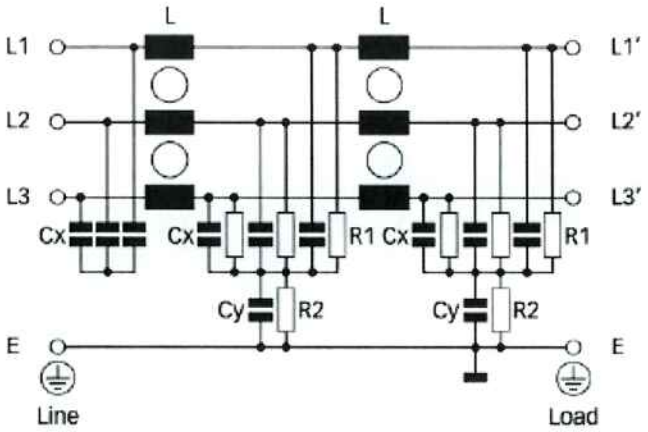

Figure 1.9.: Schaffner FN258 Schematics [34]

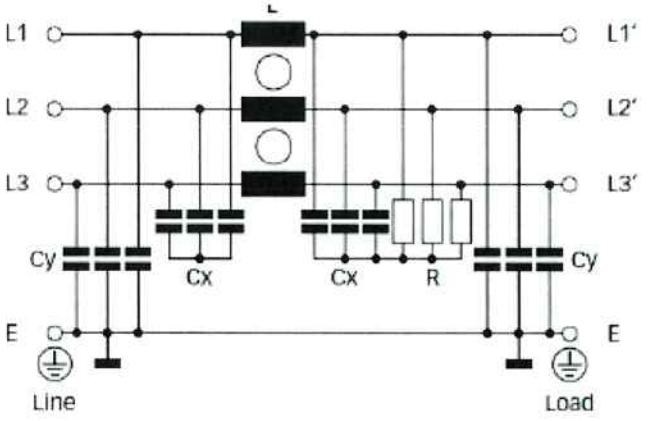

Figure 1.10.: Schaffner FN351H Schematics [35]

Apparently, the performance of EMI filters is directly dependent on the components inside it. The material of the common-mode choke core plays a crucial role, for example. Nanocrystalline materials have an improved frequency behaviour of the permeability when compared to ferrite. [11] Table 1.6 lists the materials commonly used to design common mode and differential mode inductors. A detailed comparison of core materials is presented in Chapter 6.

Table 1.6.: Core Materials

Material	Typical Application
Ferrite (NiZn and MnZn)	Common mode
Nanocrystalline (83-89 % or 74 % Fe)	Common mode
Amorphous alloys (Co, Fe and Ni Ribbon)	Both, depends on composition
Powder cores (AlSiFe, FeSiB, NiFe, FeSi, Fe, NiFeMo)	Differential mode

Part 1.5: Stray Components

Parasitic effects play a crucial role on performance of EMI filters. It has been found that these interactions can degrade the EMI-filter performance at high frequencies. [45] Therefore profound analysis of the degradation effects is needed in order to propose changes on the design of the EMI filters.

In [44] the impact of parasitic parameters on a single-phase EMI filter performance is analysed. Six different types of couplings are studied: the coupling between the inductor and capacitors, a filter inductor and trace loops, two filter inductors, two capacitor parasitic inductances, a filter inductor and ground plane and two trace loops. Measurements of the transfer gains and verificated simulations are done in order to evaluate the importance of each of the coupling effects. It is found that the inductive coupling between the capacitors and the coupling between the trace loops are the most relevant. Also the ground plane is found to be important in that analysis.

Another study, [23], proposed a new design for a single-phase filter. In this work, simulations using the finite element method were made in order to calculate an impedance matrix. With this calculation it is possible to create an equivalent circuit model in order to simplify the understanding of the coupling phenomena. Physical measurements are made in order to validate simulation results, and they have good correlation. It is concluded then that the finite element method is useful to determine parasitic effects.

A three-phase T-type EMI fiter has been analysed in [13]. Here stray couplings are determined with scattering parameter measurements. The analysis shows that the mutual coupling between the capacitors and the common-mode choke have an impact on filter performance, so as the couplings created by PCB traces and ground as well.

In [7], the genetic algorithm is used in order to optimize a component arrangement in a single-phase filter. In that case the objective function of the optimization process is the filter transfer function, and the variables are derived from the physical layout. A new filter design is proposed, with the drawback of

having more resonance peaks, which are due to way that the objective function is calculated. Validation of the results shows reasonable but not perfect correlation between experimental and calculated results, with deviations up to 27 %.

It has been shown in [1] that a basic rule should be followed when placing components in EMI filters. When placing components near each other, they have be orthogonal, otherwise they can be placed parallel to each other. A numerical analysis of the coupling factors in relation to distance and angle between the capacitors is still due.

Most of the cited works are focused in single-phase EMI filters. An in-depth analysis of three-phase filters, with simultaneous consideration of the stray components of the filter elements themselves and of the stray couplings between the filter elements, together with an analysis of the economic aspects, is still missing and the main goal of the present work.

Simulations enable a detailed analysis in order to understand how electromagnetic couplings work in an EMI filter. There are many numerical methods to simulate electromagnetic fields such as the Partial Element Equivalent Circuit Method, the Finite Element Method and the Finite Difference Method. The PEEC consists on the creation of a mesh on the surface of the model and direct derivation of an equivalent circuit model from the nodes of the mesh. It is more efficient in problems with a higher volume-surface ratio. The second one is the FEM, which is a well-established computational tool to simulate electromagnetic fields, which involves the creation of a mesh in the whole volume of the solution domain. With adaptive meshing, the FEM is more efficient in the simulation of irregular geometries. It can derive capacitance and inductance matrices in order to create an equivalent circuit model.

Both methods can calculate inductances and capacitances, either in form of an equivalent circuit diagram or as inductance and capacitance matrices. With determination of the inductance and capacitance values, it is possible to evaluate the relevance of the coupling effects. The simulations allow changes in the model to be made, for optimization purposes. Depending on the amount of variables to be optimized, one may use least-squares calculations, or the more complex genetic algorithms and neural networks.

Part 1.6: Goals and Objectives

The main goal of the present work is to develop a general method how to analyse stray coupling effects between components of a passive EMI filter. It should deliver results from the finite element modelling of a filter with optimization and validation, with both magnetostatic and electrostatic simulations.

The steps in this study comprise the analysis of the coupling between filter elements inside of an EMI filter, including analysis of the components themselves. A filter topology shall be chosen, and simulations should be done with the developed geometry using a FEM simulation tool. The stray components (stray couplings or parasitics) between capacitors and inductors (filter elements) and the stray components of the elements themselves (stray components) should then be calculated.

Furthermore, the calculated parameters should be implemented in an equivalent circuit model for validation, improvement and optimization purposes. With the results the component arrangement is to be

optimized, the stray components are to be mitigated and a new filter model is to be done in order to evaluate results of the changes.

Last but not at least, a list of measures, how to enhance the performance of an EMI filter should be presented.

2 Modelling of the Filter

Part 2.1: Introduction to the Modelling of the Filter

The capacitors, inductors, PCB and housing are called filter elements. The stray components of the filter elements themselves are called stray components. The parasitic electromagnetic couplings between the filter components are called stray couplings.

As already discussed in the previous chapter, finite element analysis is going to be applied to determine the stray components and couplings of an EMI filter. In order to do the simulations, a three dimensional model of the device must be available. The filter housing is opened and the internal construction is studied and the components are measured. In Figure 2.1 it is possible to see the structure of the filter. The X capacitors, the common mode choke and the Y capacitors (with resistors) are pointed.

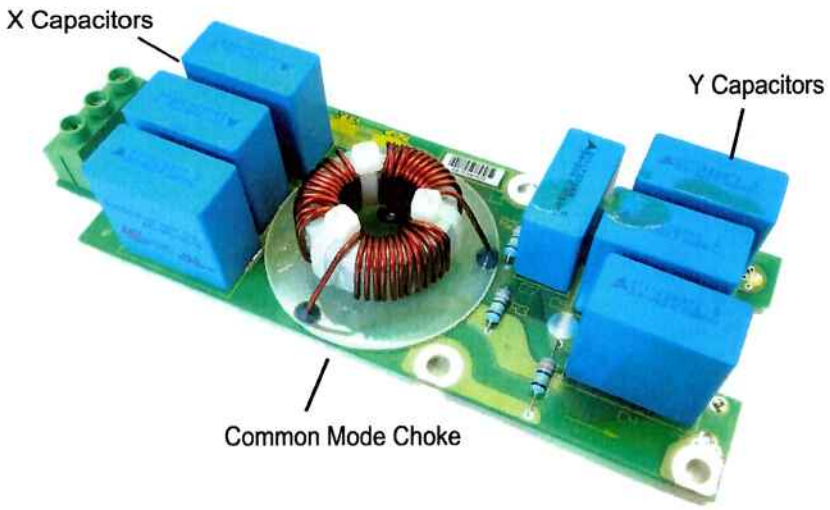

Figure 2.1.: Perspective View of the Filter

In order to create an appropriate model for the capacitors, one film capacitor of similar properties is transversally cut, as it can be seen in Figure 2.2.

The conducting part of the capacitor is smaller than the capacitor itself, and this must be taken in consideration in the 3D model. Also, the whole current inside of the capacitor is going to flow through the pins, which should be included in the model. A conductive material is assigned to the capacitor and the pins.

The common mode choke is modeled as a toroidal core with three windings. The magnetic core is assigned to be of ferrite material with an initial relative permeability of 10000. At this point the frequency

Figure 2.2.: Transversal Cut of Capacitor

behavior is still not taken into consideration. It is going to be considered in Chapter 3. The windings are modeled as concentrated windings, that means that all turns from one coil are assumed as being one group, allowing straightforward analysis of coupling effects. This is a common practice when using finite element analysis in electric machines [5]. The conductor paths and routes of the printed circuit board are also included in the model.

The 3D model of the Siemens Micromaster 4 6SE6400-2FA00-6AD0 EMI filter, depicted in Figure 2.3 is used to perform all proposed simulations, magnetostatic and electrostatic, in Ansys Maxwell. A detailed description of the simulations follows.

Part 2.2: Magnetostatics

A - Magnetostatic Simulations

The finite element methods divides the solution domain in small elements, in which the the magnetostatic solver from Ansys Maxwell solves the Gauss Law(Equation (2.1)) and the Ampere Circuital Law(Equation (2.2)).

$$\nabla \cdot \mathbf{B} = 0 \tag{2.1}$$

$$\nabla \times \mathbf{B} = \mu \cdot \mathbf{J} \tag{2.2}$$

As is it possible to see from (2.2), integrating the differential equation will result in the magnetic flux density. However, in order to do this calculation, the current densities in the model must be known. Consequently, the currents that flow in the filter are set in the capacitors and the windings of common mode choke. The inductances between the conduction paths from these currents can be derived in

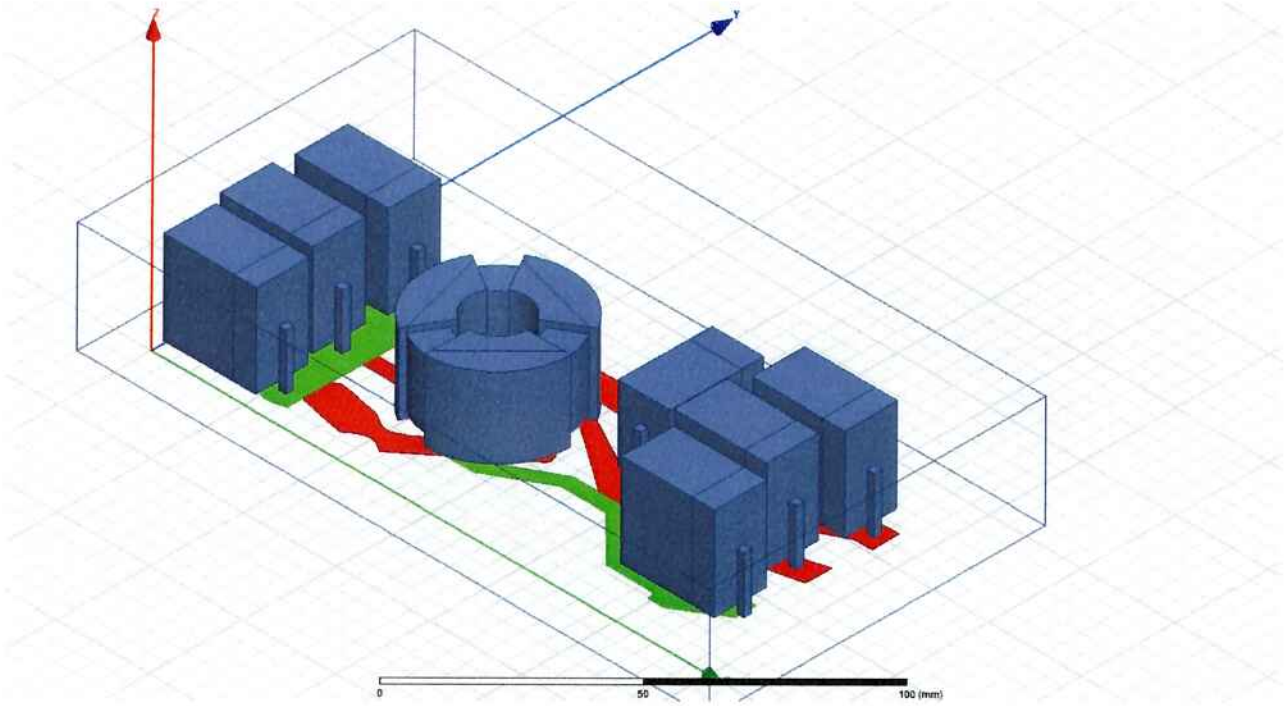

Figure 2.3.: 3D Model of Filter

matrix form. For volume meshing, a tetrahedral mesh generally provides a more automatic solution with the ability to add mesh controls to improve the accuracy in critical regions. Conversely, a hexahedral mesh generally provides a more accurate solution but is more difficult to generate [5]. Therefore, a tetrahedral mesh is created, and then the values of the magnetic field are derived. Adaptive meshing refines the mesh where the calculated field changes the most, in order to minimize computational errors.

In Figure 2.4 it is possible to see the excitations defined in the model, together with their names, which will define the inductance matrix. These current excitations are directed according with the power flow in the filter. The current enters the filter through the X capacitor bank, proceeds to the common mode choke and then exits the filter through the Y capacitor bank. At this stage, the frequency behavior of the core material of the common mode choke is not considered. That means, the stray inductance of the coil and not the real inductance of the coil can be calculated here. An appropriate model for the characteristics of ferrite is introduced in Chapter 3.

In Figure 2.5 it is possible to see the mesh used in the first calculations. The maximum length of one element in the mesh is set to 10 mm. The solutions from this mesh converged to a energy error of 0.01547 %, with in total 49737 tetrahedra, after 10 adaptive passes. This matches the expectations of the project. Another mesh with a maximum length of one element set to 2 mm is also generated, to be used if further reductions of the energy error are necessary. This second mesh can be seen in Figure 2.6.

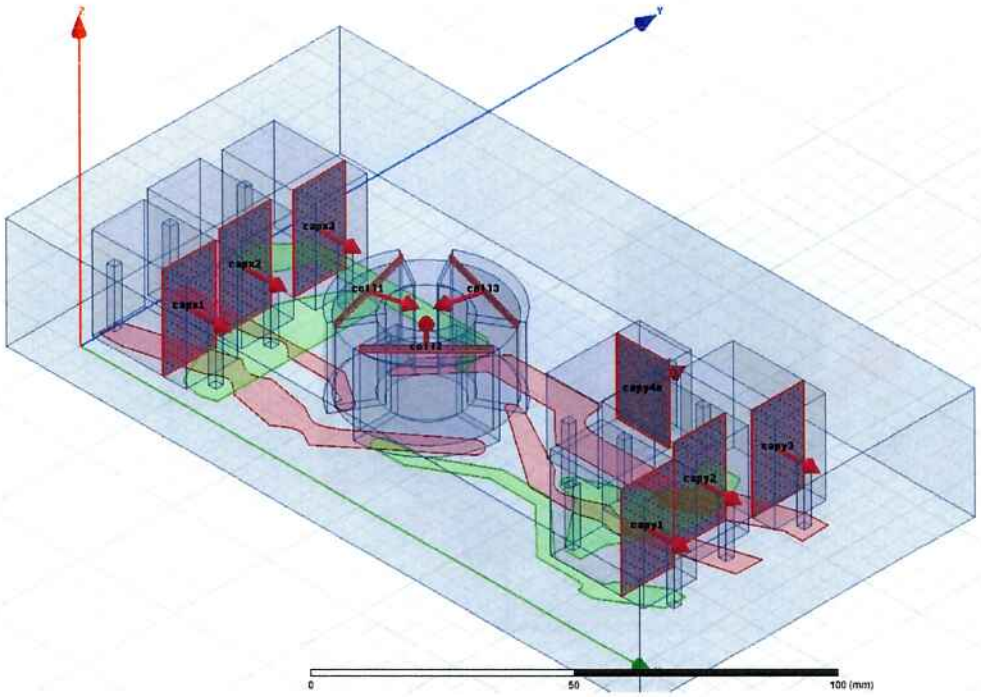

Figure 2.4.: Current Excitations

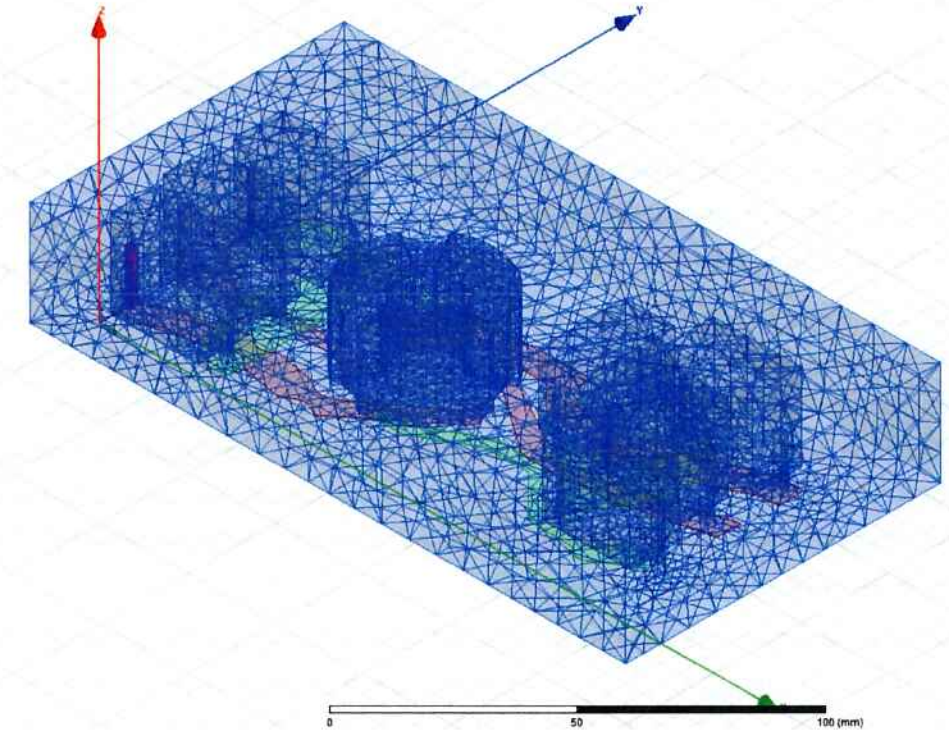

Figure 2.5.: 10 mm Mesh

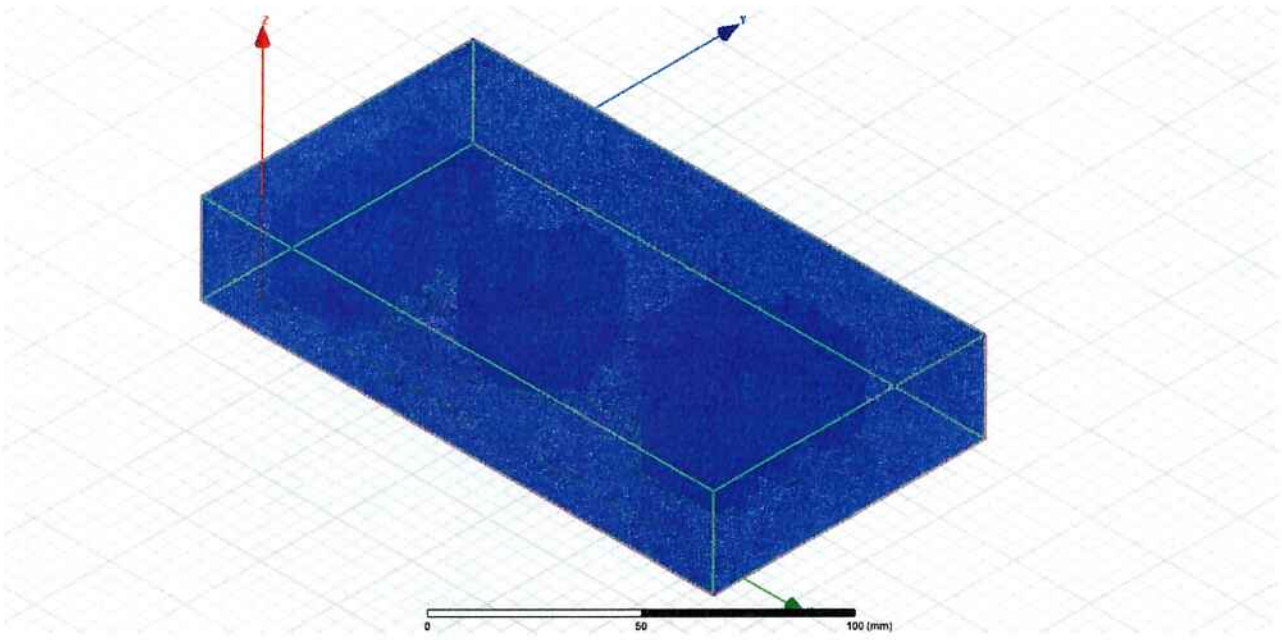

Figure 2.6.: 2 mm Mesh

B - Results of the Magnetostatic Simulations

In Figure 2.7, the magnetic field intensity vector field is plotted. It is possible to see how the flux lines close through observation of the rotation and the divergence of the field vectors. This plays a crucial role on the mutual coupling, because when a flux line crosses two windings, it will create a coupling between the currents of them. For example, when current flows in one of the capacitors and creates a flux line which crosses one of the coils of the common mode choke, a voltage is induced in the coil, and therefore a current is also induced. The higher the mutual inductance (and therefore the coupling coefficient), the higher the induced current, in relation to the original current, is.

Given two coils that are mutually coupled, if current flows in the first coil, a voltage is induced in the second coil. If current flows in the second coil, a voltage is induced in the first coil. That means that the mutual coupling is bidirectional. Thus, as in Equation 2.5, the matrix is diagonal for real systems, as M_{12} is equal to M_{21}.

It is also possible to identify which locations have the strongest magnetic field. In the region between each capacitor of the X or the Y capacitor bank and between each coil of the common mode choke, one finds the highest absolute values for the H-field vectors, in the range from 100 A/m to 200 A/m. In the arrangement the magnetic field ranges from 0.01 A/m to 200 A/m. Therefore, one predicts that the coupling inside the capacitor banks is going to be a relevant stray component.

In Annex A.1 a table with the inductance and coupling factor matrices is found. In the inductance matrix, the values in mH for self and mutual inductances for all components in the model are represented. In the coupling coefficient matrix, the values of the coupling factors, where a value of 1 means perfect coupling and a value of 0 means no coupling at all, are represented.

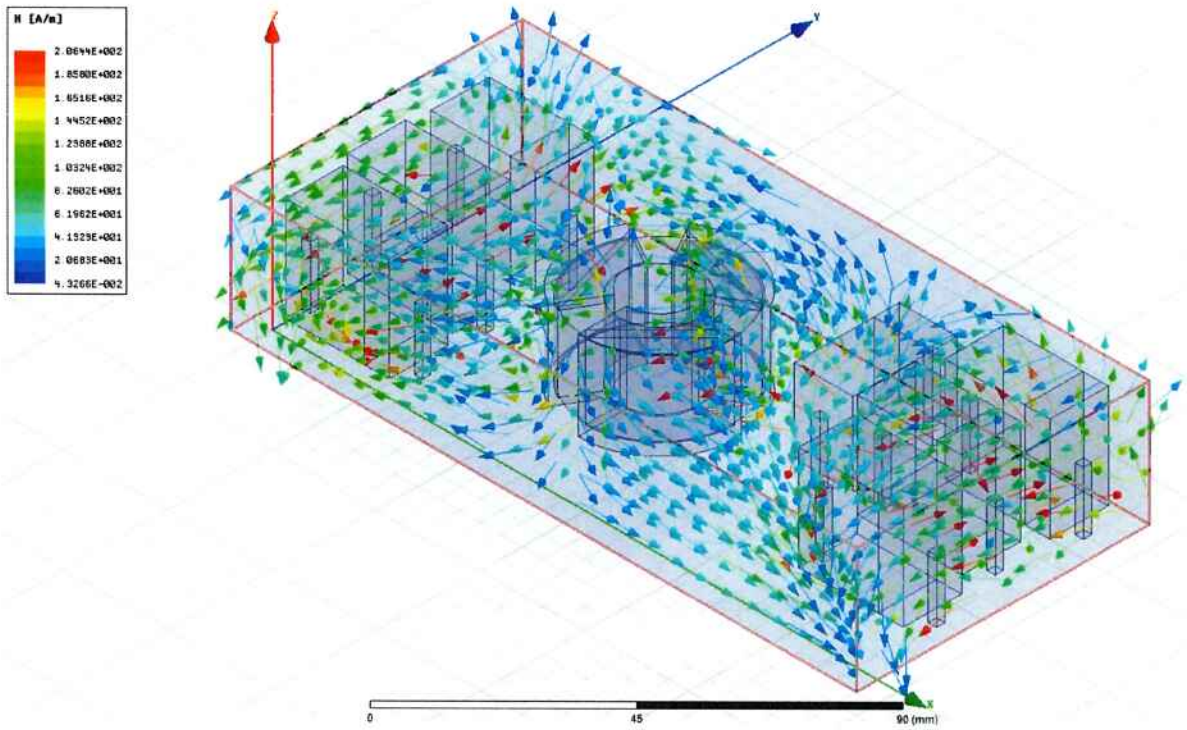

Figure 2.7.: H-Field Plot

As expected, the value of the coupling factor between the coils is very high, at least of 0.99. This is influenced by the high permeability of the ferrite material. Also, the values of the coupling between components of the capacitor groupings is higher than expected, reaching values up to 0.15. The analysis of the relevance of the stray couplings is done in Chapter 5.

The inductances can be calculated from the magnetic energy density as in Equation 2.3. With the inductances, the coupling factors are calculated as in Equation 2.4. The values of the inductances have a very wide range. Starting by values in the μH range, up to values in the nH range, which are expected to have influence on the filter attenuation in the MHz and GHz range.

$$E_{\text{mag}} = \frac{L \cdot I^2}{2} = \frac{1}{2} \cdot \int H \cdot B dV \tag{2.3}$$

$$k = \frac{\sqrt{L_{11} \cdot L_{22}}}{M} \tag{2.4}$$

$$\begin{bmatrix} \Psi_1 \\ \Psi_2 \\ \Psi_3 \end{bmatrix} = \begin{bmatrix} L_{11} & M_{12} & M_{13} \\ M_{12} & L_{22} & M_{23} \\ M_{13} & M_{23} & M_{33} \end{bmatrix} \cdot \begin{bmatrix} I_1 \\ I_2 \\ I_3 \end{bmatrix} \tag{2.5}$$

It is important to note that due to the asymmetries in the placement of the components of the filter, the couplings between the components of each phase are uneven. Differences between the transfer functions and other characteristic curves for each phase of the filter are expected.

Part 2.3: Electrostatics

A - Electrostatic Simulations

The electrostatic solver of Ansys Maxwell solves the Poisson equation (2.6) applied to the electric potential through integration. With knowledge of the free charge density ρ or of the electric potential φ it is possible to solve the partial differential equation for the electric field.

$$\nabla \cdot \mathbf{E} = \nabla \cdot (-\nabla \varphi) = -\nabla^2 \varphi = \frac{\rho}{\varepsilon} \tag{2.6}$$

Thus, in order to calculate the values of the electric field, setting the voltages in the components of the filter is necessary. This is done in the capacitors and the common mode choke and can be seen in Picture 2.8.

Capacitances are calculated between the parts of the model. Voltage excitations of 100V are assigned to all internal components. The type (AC or DC) and the value of the voltage is irrelevant for the calculation of the capacitances. Setting a ground surface is needed in order to determine the capacitances of the components to the ground, so a parallelepiped surrounding the filter with the dimensions of the housing is assigned to have zero voltage potential. The assumptions for the materials are the same as in the magnetostatic simulations.

B - Results of the Electrostatic Simulations

In Figure 2.9, the electric field vectors are plotted. The vectors are mostly aligned in the direction of the ground potential, parting from the components with voltage excitation. From the theory, the capacitances between the common mode choke and the capacitors to the ground are relevant in this case.

In Annex A.2, the values of the capacitances in pF and the coupling factors between the components of the filter are listed. Again, an absolute value for the coupling coefficient of 1 is associated with perfect coupling, and of 0 with no coupling at all.

The values of the capacitances are derived from the electric fields as in Equation 2.7.

$$C = \int E \cdot D dV \tag{2.7}$$

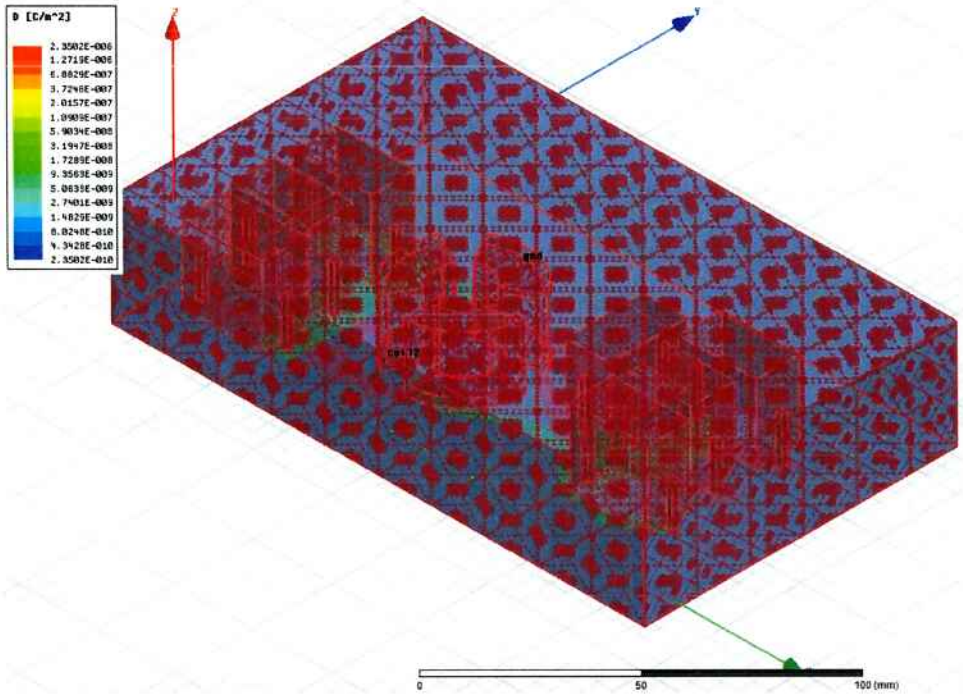

Figure 2.8.: Voltage Excitations

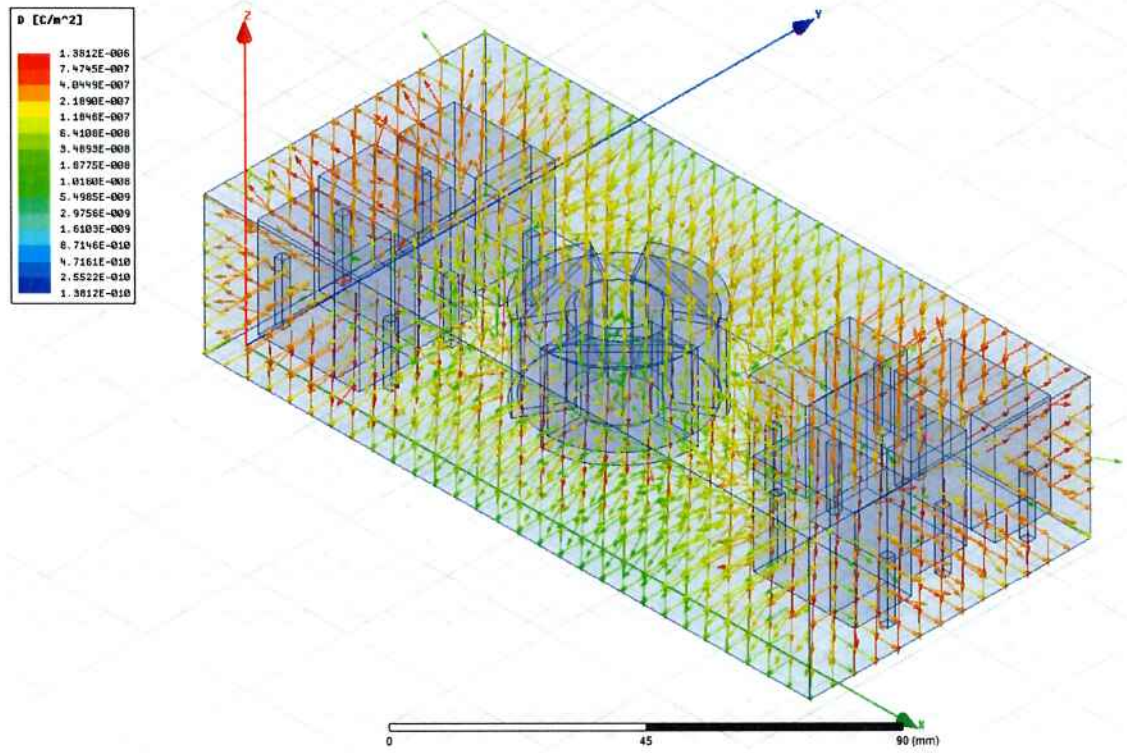

Figure 2.9.: E-Field Vector Plot

It is very important to understand the capacitance matrix, which represents the proportionality between the charge and the voltages. The values in the diagonal of the matrix are equal to the sum of the own capacitance of the object with the capacitances of this object to all other objects. The non-diagonal values of the matrix are equal to the value of the capacitance between the objects. An example for this relationship is found in Equation (2.8).

$$\begin{bmatrix} Q_1 \\ Q_2 \\ Q_3 \end{bmatrix} = \begin{bmatrix} C_{10}+C_{12}+C_{13} & -C_{12} & -C_{13} \\ -C_{12} & C_{20}+C_{12}+C_{23} & -C_{23} \\ -C_{13} & -C_{23} & C_{30}+C_{13}+C_{23} \end{bmatrix} \cdot \begin{bmatrix} V_1 \\ V_2 \\ V_3 \end{bmatrix} \tag{2.8}$$

As already stated, the model is surrounded by a parallelepiped with ground potential, which means that the ground is represented as an element in the matrix. It is possible to see that the most relevant capacitances are exactly the ones of the components to the ground, with values more than 10000 times bigger than the other stray capacitances. The relevance of the stray components is studied in Chapter 5.

C - Determination of the Coil Stray Capacitance

In order to calculate the parallel stray capacitance of the coils, additional simulations need to be performed. In this part, only one coil and the core of the common mode choke are simulated. In Figure 2.10, it is possible to see that the two lateral faces of the coil are excited, and the capacitance between them is calculated. The voltage drop in the coil is plotted in Figure 2.11. From this calculation, a capacitance of 1.151 pF results. This value is below the expectations and a different approach must be used to calculate the parallel stray capacitance of the coils.

Even though precise enough to analyse coupling effect with other components, the model of the coil as a concentrated winding is insufficient to calculate the parallel stray capacitance. This is due to the fact that this ignores the now relevant interactions inside of the winding. A preciser representation of the winding with individual coil turns needs to be done.

The winding is remodelled and the plot of the voltage drop is in Figure 2.12. The simulation leads to a turn-to-turn capacitance of 3.6 pF.

According to [25], the parallel stray capacitance of a single-layer winding is calculated from the turn-to-turn capacitance and the number of turns of the winding as in Equation 2.9, which is derived from the equivalent circuit of all turn-to-turn capacitances of the winding. The tolerance of this calculation is of 20 % for windings with 12 to 15 turns, and of 10 % for winding with higher number of turns.

$$C_s(n) = \frac{C_{tt}}{2 + \frac{C_{tt}}{C_s(n-2)}} + C_{tt} \tag{2.9}$$

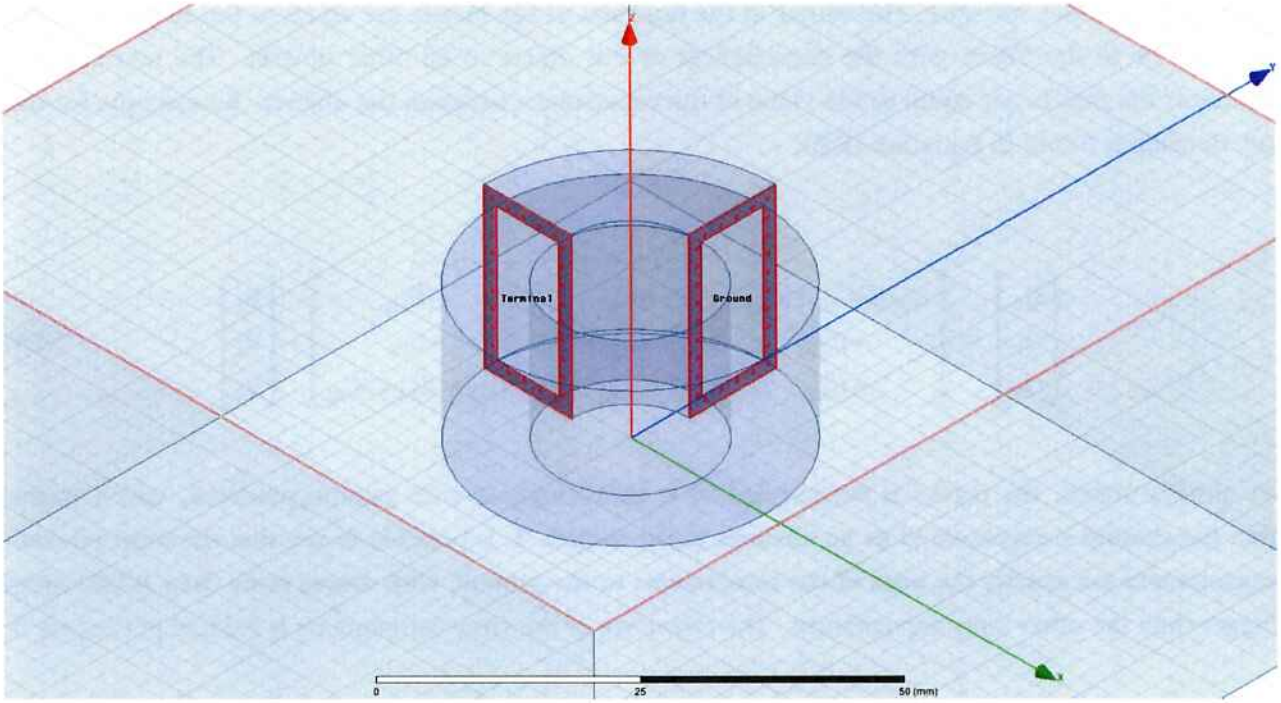

Figure 2.10.: Voltage Excitations for Determination of Coil Capacitance

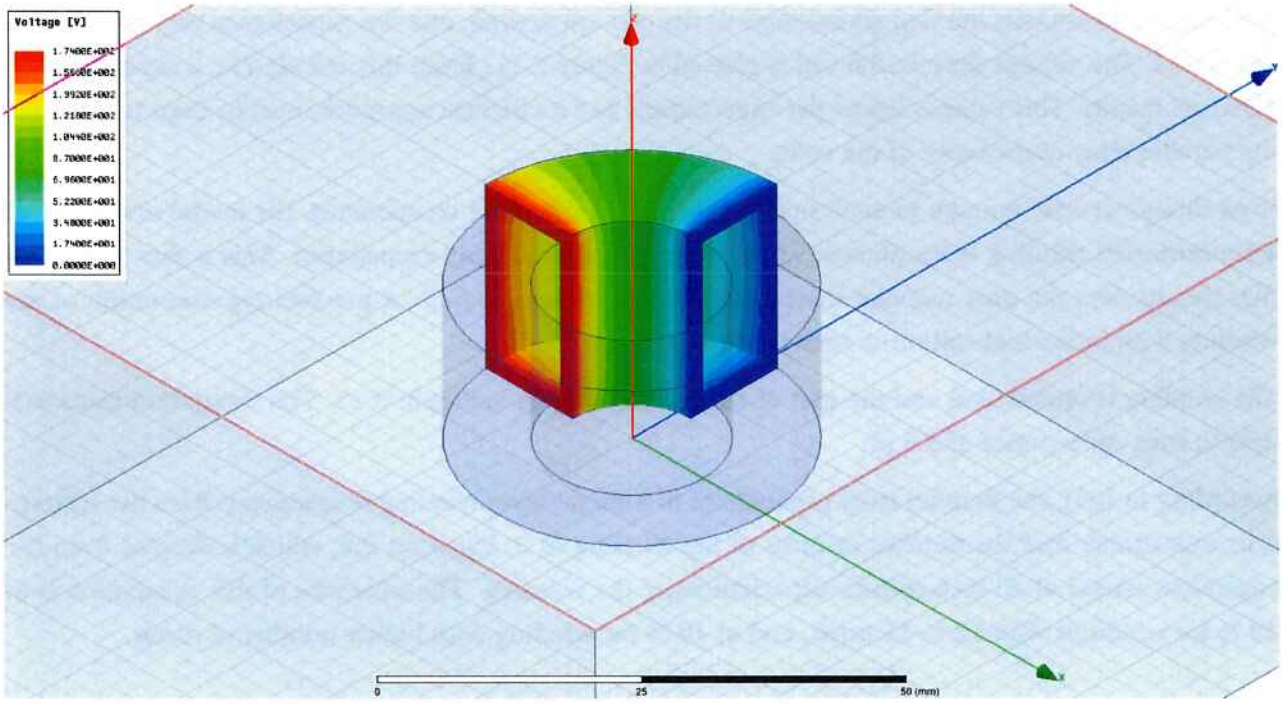

Figure 2.11.: Voltage Drop of the Concentrated Winding

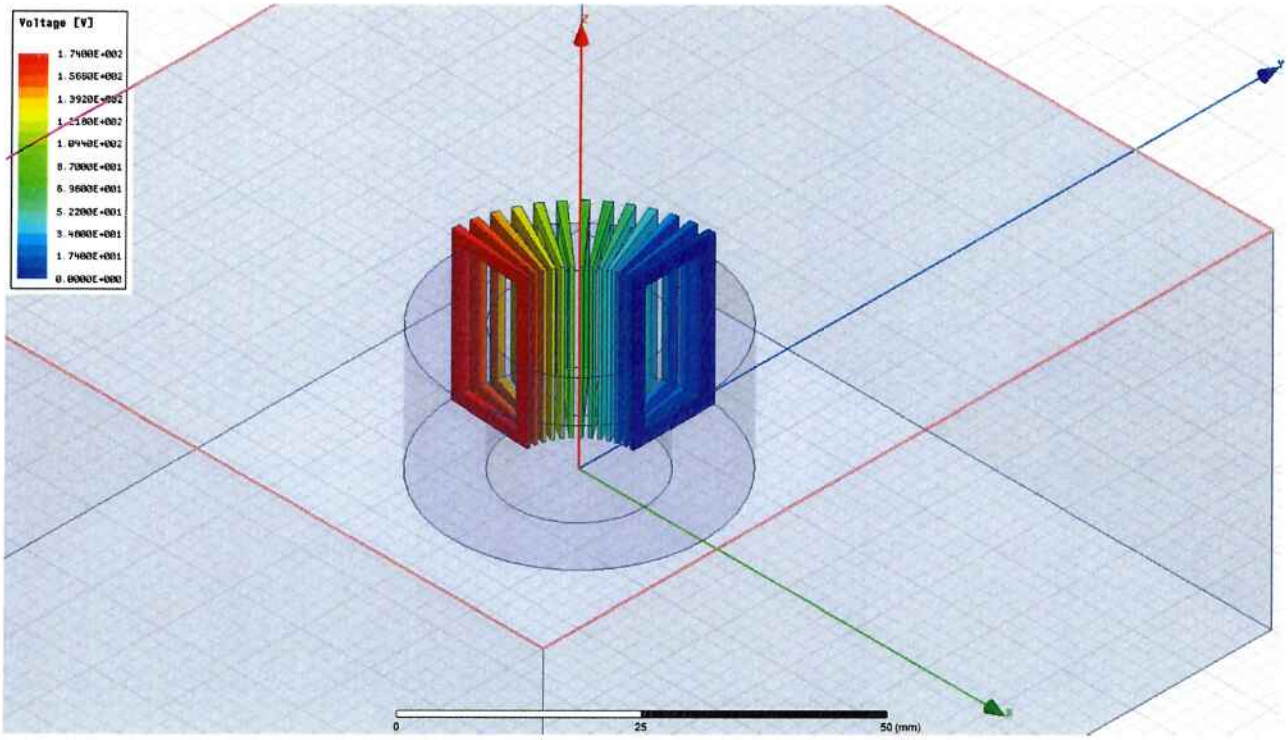

Figure 2.12.: Voltage Drop of the Distributed Winding

For a number of turns bigger than 10, this sequence converges and the coil parallel stray capacitance is then calculated in Equation 2.10 using the turn-to-turn capacitance obtained with the FEM simulations.

$$C_s \cong 1.366 \cdot C_{tt} \cong 5pF \tag{2.10}$$

The convergence of the coil parallel stray capacitance for a high number of turns is verified in Chapter 6.

Part 2.4: Summary of the Modelling

In this chapter, the physical and electrical characteristics of the filter are modelled in Ansys Maxwell, in order to obtain the values of the stray components and couplings of the EMI filter studied in this work, coupling between filter components, PCB and housing, as well as values of stray components of the filter elements themselves.

The results of the calculation of the inductances and capacitances using finite element analysis are presented. The obtained stray couplings, as well as the stray components of the filter elements are included in the equivalent circuit of the filter in Chapter 3. The validation of the developed model and the comparison with the measurement results is presented in Chapter 4. With the validated model, it is possible to propose changes and create new filter arrangements.

3 Development of an Equivalent Circuit

Part 3.1: Equivalent Circuit Model Introduction

In order to observe and assess the effects of the stray components in a different range of frequencies, an equivalent circuit model of the filter has to be developed. For this purpose the software LTSpice IV has been chosen. The values of the stray components of the filter elements as well as the values of the stray couplings between the filter elements have been obtained with the finite element method. At the equivalent circuit model all those values are represented by lumped capacitances and inductances, together with the ideal filter elements. Later on, AC sweeps are performed in the frequency range between 1 KHz and 100 MHz.

Moreover, the circuit model allows investigation of all currents and voltages (and their relations) in the circuit without using a physical model. The insertion losses characteristics obtained from the equivalent circuit model are validated by means of measurements with the network analyser in Chapter 4.

Part 3.2: Equivalent Circuit of the Ideal Filter

In order to determine the deterioration of the filter performance through the stray components and couplings, it is necessary to know the characteristics of the filter without any stray components. The ultimate goal is that the filter performance reaches the idealized curves. The equivalent circuit model in this case is called ideal filter.

With the nominal values of the capacitances and the resistances, together with the simulated values for the inductance, it is possible to obtain the insertion losses for two cases, namely common mode and differential mode. It is possible to find the values of the cited components in Table 3.1. The circuit used for the simulations can be found in Figure 3.3.

Table 3.1.: Values of Non-Stray Components

Parameter	Value
C_x	3.3 μF
C_y	3.3 μF
C_{ye}	2.2 μF
R_y	3.3 $M\Omega$
L	23.1 μH
K_m	0.98

The plots of the insertion losses over the frequency can be found in Figure 3.13.2 and respectively.

In the differential mode curve it is possible to see that the ideal filter has insertion losses in the range of 10 dB in low frequencies. It also shows a small resonance around 40 kHz. The switching frequency of the drive system for which this filter is designed must be 2 or 3 times lower than this resonant frequency. Then the curve falls continuously with a rate of 40 dB/decade. The common mode curve is also continuously falling with a rate of 40 dB/decade.

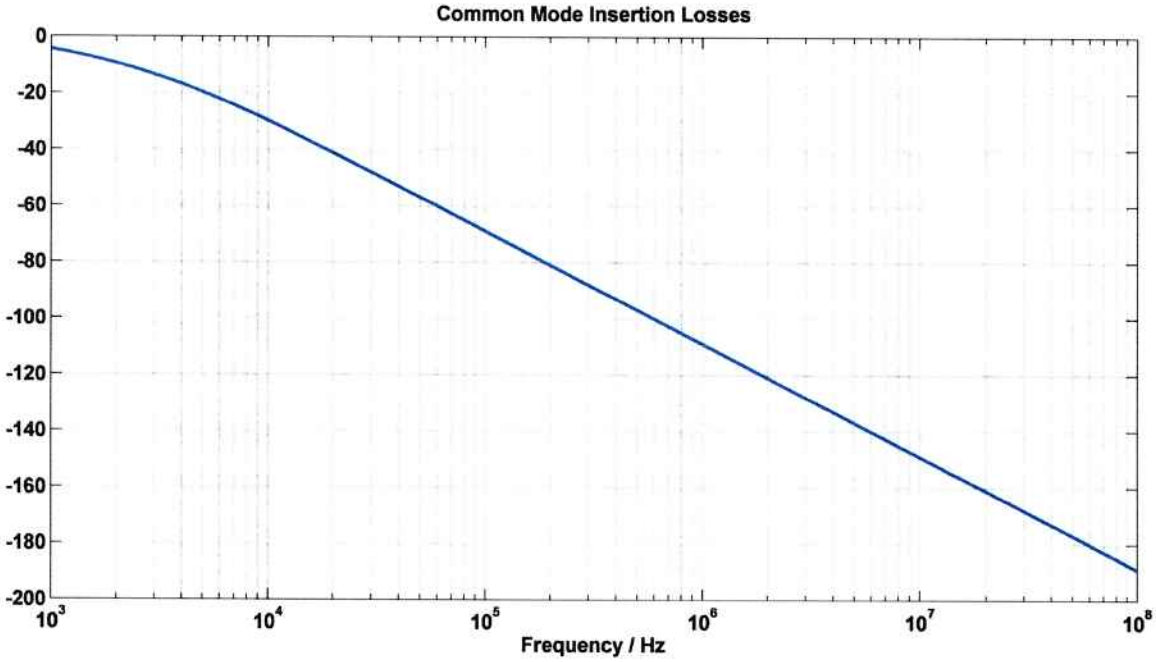

Figure 3.1.: Common Mode Insertion Loss for Ideal Filter

Part 3.3: Equivalent Circuit of the Real Filter

The stray components calculated in Chapter 2 are then inserted in the equivalent circuit model and the same AC sweeps are performed for the common mode and differential mode insertion losses of the filter. Furthermore, additional components due to the real properties of the core material, which cause a behavior change and degradation of the damping at higher frequencies, need to be taken into account. The magnetic material used in the core of the common mode choke is MnZn ferrite, which has a strong frequency dependent behavior and a ferrimagnetic resonance typically around 1 MHz. Those are main contributors to the difference between real and ideal filter behavior of the EMI filters.

As mentioned in Chapter 1, nanocrystalline materials are increasingly being used for this application, because they have a higher initial permeability and a better high-frequency behavior.

The characteristics of the complex permeability of the ferrite (Equation (3.1)) are obtained from [43] and approximated using exponential equations, with a tolerance of 10 %. The equivalent series resistance and reactance are calculated in Equations (3.2) and (3.3). The resulting equations can be found in Table 3.2. The iron length is of 86 mm and the cross section of 152 mm^2. For the same volume of material,

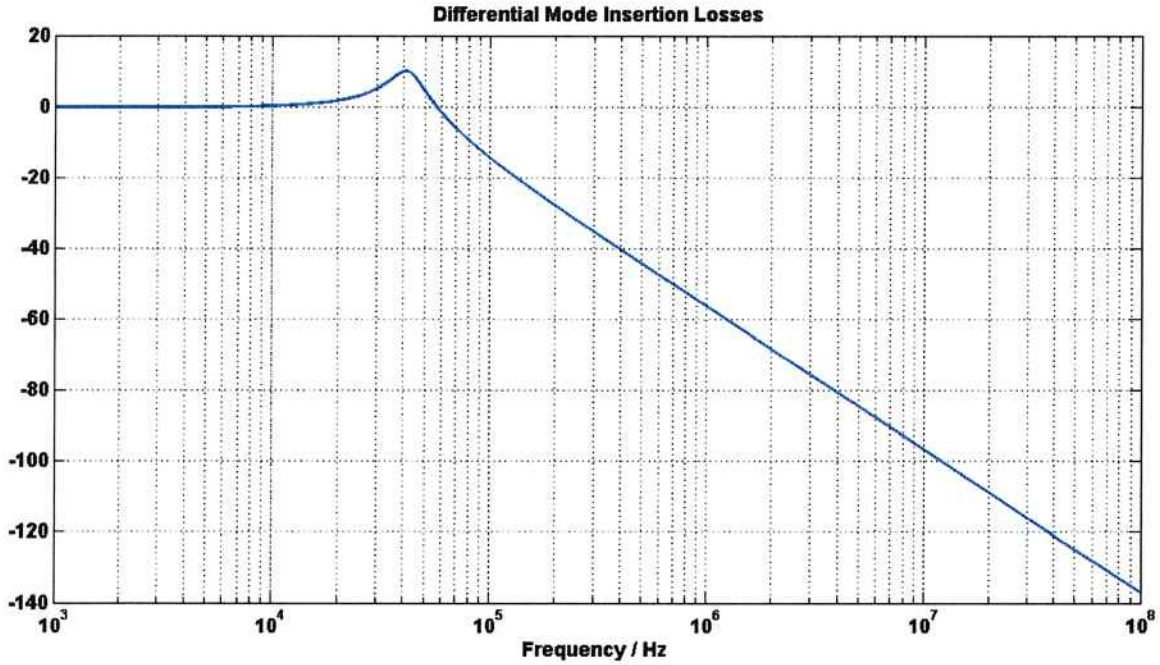

Figure 3.2.: Differential Mode Insertion Loss for Ideal Filter

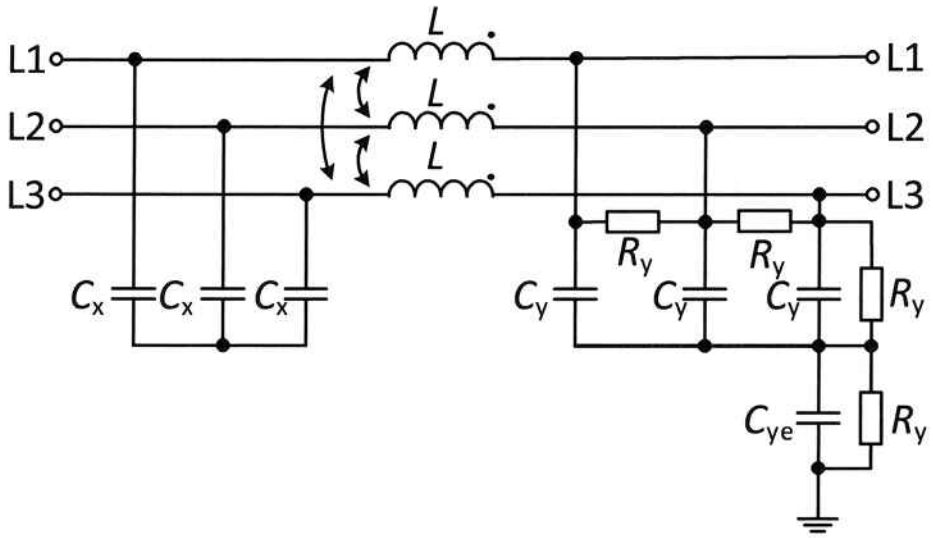

Figure 3.3.: Ideal Filter Circuit Model

if the iron length is smaller, the cross section increases. Consequently the equivalent series components increase strongly.

$$\mu_s = \mu_s^{'} + j \cdot \mu_s^{''} \tag{3.1}$$

$$R_s = 2 \cdot \pi \cdot f \cdot \mu_0 \cdot \mu_s^{''} \cdot N_1^2 \cdot \frac{A_{Fe}}{l_{Fe}} \tag{3.2}$$

$$X_s = 2 \cdot \pi \cdot f \cdot \mu_0 \cdot \mu_s^{'} \cdot N_1^2 \cdot \frac{A_{Fe}}{l_{Fe}} \tag{3.3}$$

A list of the additional components inserted in the circuit model of the ideal filter due to stray couplings between the filter elements follows next:

- Stray Capacitance between the Windings of the Common Mode Choke
- Stray Capacitance of the Components to Earth
- Stray Inductive Coupling Coefficients between the X Capacitors
- Stray Inductive Coupling Coefficients between the Y Capacitors
- Stray Inductive Coupling Coefficients between the X and Y Capacitors and the Common Mode Choke

The stray components of the filter elements themselves are listed below.

- Ohmic Resistance of PCB Traces, Wires and Connections
- Stray Inductance of the X and Y capacitors
- Stray Resistance of the X and Y capacitors
- Stray Parallel Capacitance of the Windings of the Common Mode Choke
- Stray Resistance of the Windings of the Common Mode Choke

The components added to represent the magnetic core of the common mode choke with the exponential approximation follow:

- Ferrite Equivalent Series Inductance of Magnetic Core
- Ferrite Equivalent Series Resistance of Magnetic Core

An overview of the circuit model with all components can be found in Figure 3.4. The mutual couplings are not represented in order to simplify the understanding.

In Figure 3.5, the equivalent circuit model of the capacitors with the stray components is shown. L_{Str} is the equivalent series stray inductance and R_{Str} is the equivalent series resistance.

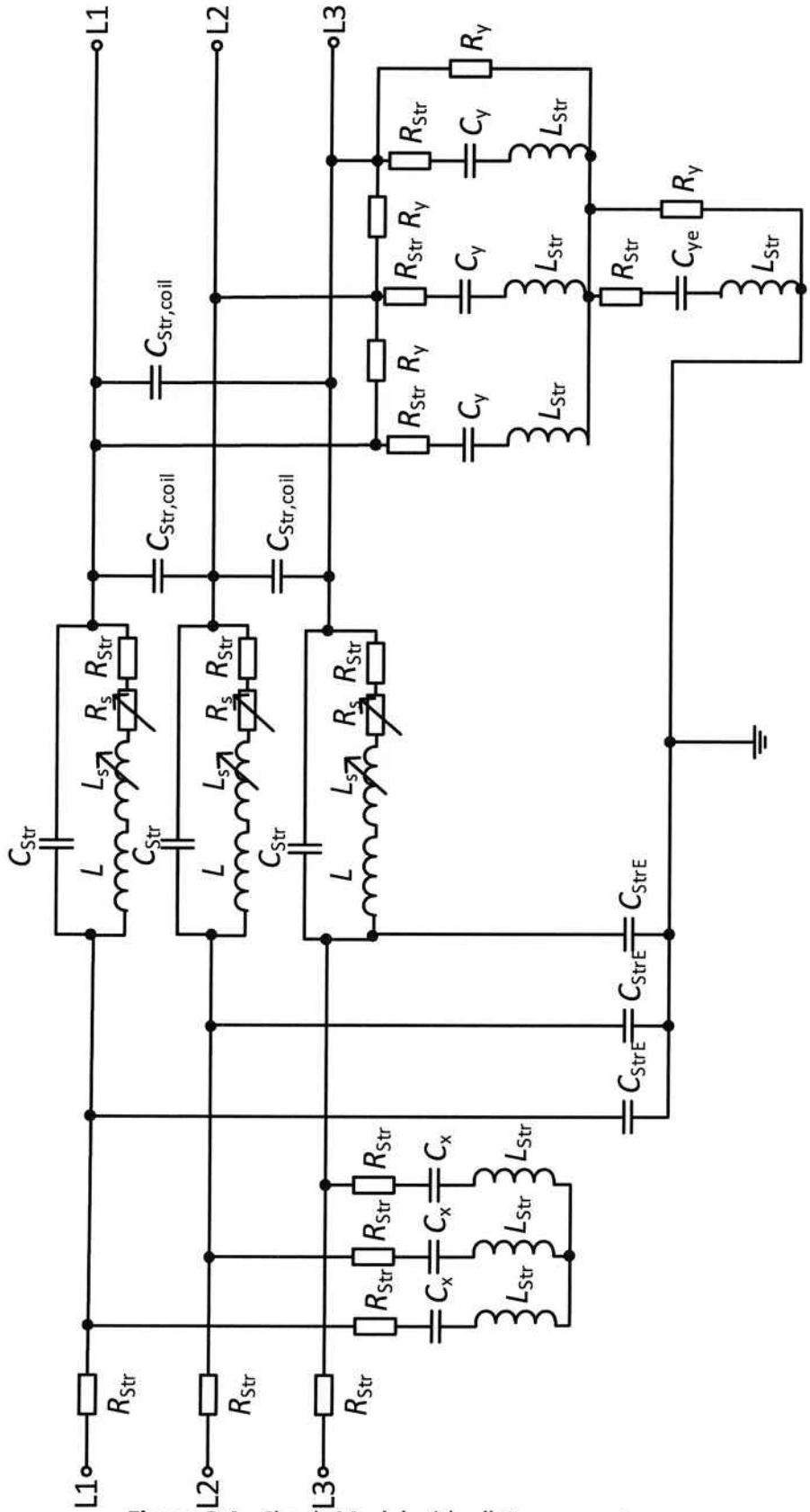

Figure 3.4.: Circuit Model with all Components

Table 3.2.: Values for Ferrite

Parameter	Equation
R_s	$0.0015 \cdot \omega \cdot (e^{-2 \cdot 10^{-6} \cdot f} - e^{-2 \cdot 10^{-7} \cdot f})$
X_s	$0.0021 \cdot \omega \cdot e^{-3 \cdot 10^{-7} \cdot f}$

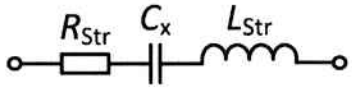

Figure 3.5.: Circuit Model of Capacitor with Stray Components

In Figure 3.6, the equivalent circuit model of the coil with the stray components is represented. L is the equivalent series stray inductance, L_s is the equivalent ferrite inductance, R_s is the equivalent ferrite resistance and R_{Str} is the equivalent series stray resistance.

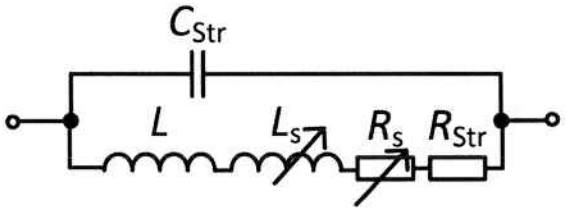

Figure 3.6.: Circuit Model of the Coil with Stray Components

Part 3.4: Summary of the Development of the Equivalent Circuit Model

Starting from the idealized equivalent circuit of the filter, the stray components and couplings are added and it is possible to see their deterioration effects. After this process, up to a hundred of lumped components are found in the circuit model, what makes understanding of the filter behavior difficult. Therefore, there is the need to classify the relative importance of the stray components. The skin effect and the proximity effect are not taken into account, due to their big complexity and small significance as second order effects in this application.

There is an exponential growth in the analysis effort between one-phase and three-phase filters, due to higher number of components of the later ones. However, the simulation of the couplings in the three-phase filters cannot be scaled down to one-phase filters, because they do not have the same structure (for example, there is no coupling between X capacitors in one-phase filters, because there is usually only one X capacitor). Nevertheless, it is still possible to simulate the common mode and differential mode insertion losses, and to see how changing the values of the components - stray or not - is influencing the filter performance. This creates the possibility for the development of a Matlab program that simulates the filter insertion losses.

The magnetic materials of the common mode choke need to be considered in the equivalent circuit model as a frequency-dependent reactance and resistance. Neglecting these parameters in the circuit is not possible, as they are of primary importance in the filter behaviour.

At this stage, almost the totality of the stray components and couplings are considered in the equivalent circuit model. In Chapter 5, the relevance of each of the components and couplings is analyzed, and then the least relevant are neglected.

4 Validation of the Simulations

Part 4.1: Introduction to the Validation Procedure

In order to validate the equivalent circuit model created in Chapter 3, the common mode and differential mode insertion losses are obtained using the Agilent E5061B network analyser (Figure 4.2). The instrument uses the following measurement principle: a test signal is sent from one port and the reflection and transmission of this signal are measured. The procedure is repeated from the second port. An overview of the measurement equipment is given in Annex E.

The S_{11}, S_{12}, S_{21}, S_{22} scattering parameters are obtained. The insertion loss, which is defined as the relation of the voltage of the system with and without the filter, as in Equation (4.1), is determinated from the S_{21} parameter. The sweep range of the measurements is from 1 KHz up to 100 MHz. The Device under Test (DUT) is connected to the Ports 1 and 2, which have a impedance of 50 Ω.

The equivalent circuit for the load and source impedances of Figure 1.4 applies to the measurements. The behavior of the filter in measured with the 50 Ω / 50 Ω arrangements and other impedance arrangements are simulated further.

$$IL_{\mathrm{dB}} = S_{21,\mathrm{dB}} = 20\log_{10}\left(\frac{V_{\mathrm{ins}}}{V_0}\right)\mathrm{dB} \tag{4.1}$$

The filter is installed inside of a metallic housing with one input and output for each of the three phases, totaling six N-type connectors, as in Figure 4.1. The shielding reduces external influences on the measurement setup. Additionally, the earthing impedance is low when the filter is connected to the grounded housing, because of the big conductive surface. A two-port calibration using open, short and load impedances is done before all measurements.

For the differential mode measurements, the network analyzer is connected to the input and to the output of one phase and the other ports are connected to the earth through 50 Ω impedances, as in Figure 4.3 (unsymmetrical). For the common mode measurements, the three inputs are connected together and the three outputs too, as in Figure 4.4 (asymmetrical). These measurement techniques are in accordance to the EN 55017 norm recommendations.

Part 4.2: Measurements and Comparison with Simulations

In Figure 4.6 the common mode insertion losses and in Figure 4.7 the differential mode insertion losses in the frequency range from 1 kHz to 100 MHz are plotted.

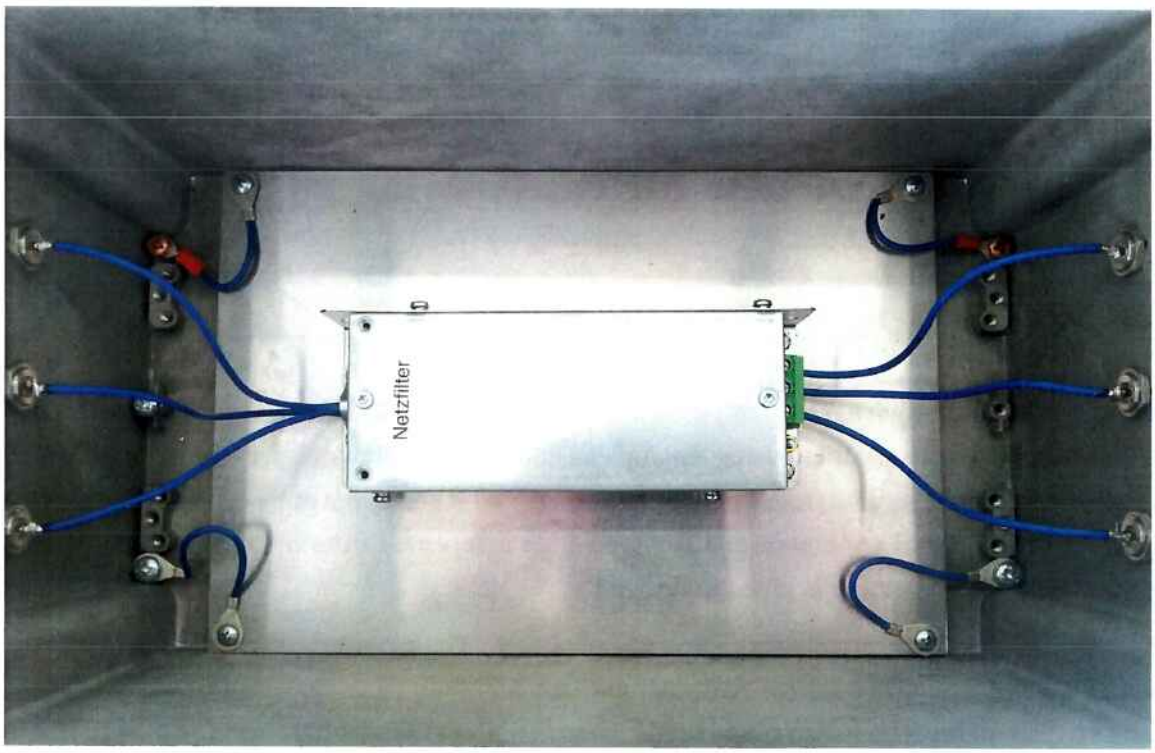

Figure 4.1.: Filter in Housing

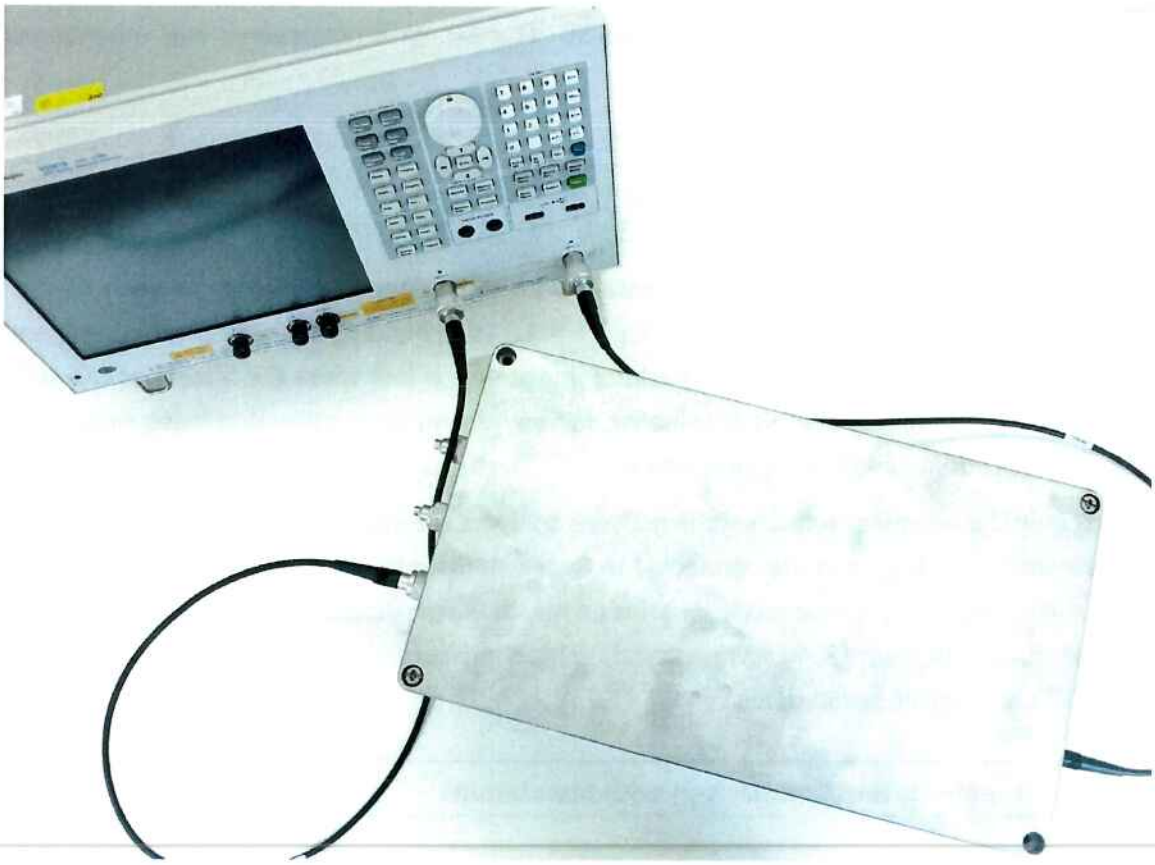

Figure 4.2.: Measurement Setup

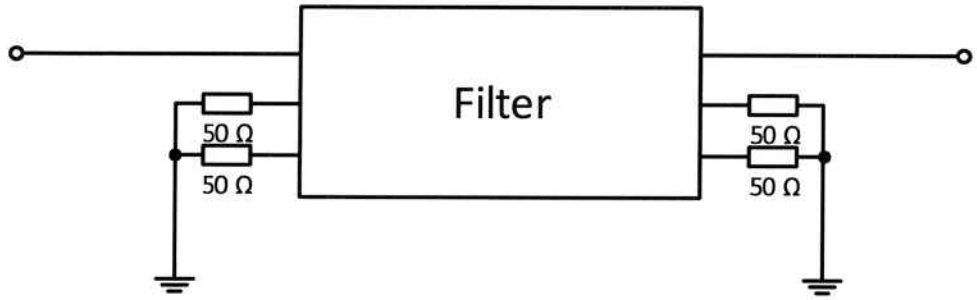

Figure 4.3.: Connection for Differential Mode Measurements

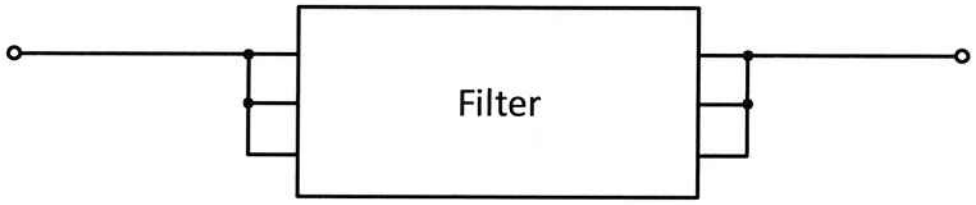

Figure 4.4.: Connection for Common Mode Measurements

It is possible to see that there is a resonant valley in the frequency of 800 KHz with insertion losses of 95 dB in the common mode and 700 KHz with insertion losses of 90 dB in the differential mode. In these frequencies, the filter attenuation reaches its maximum value. This valley is due to the stray inductance of the capacitor and the core material properties. After the resonance frequency, the filter attenuation is degraded and reaches around 20 dB at a frequency of 100 MHz.

As expected, the curves differ strongly from the ones from the ideal filter. Additionally, it is important to note that the measurements obtained from the network analyzer have an accuracy of 10 %, related to the dB values. The most common sources of errors in vector network analyzers are listed below. They are influenced by the quality of the instrument and of the accessories used. The differential mode insertion losses in different phases differ less than 5 % from each other so only one phase is plotted.

- Phase Noise
- Absolute Power Accuracy
- Displayed Average Noise Level
- Third Order Intercept
- Dynamic Range

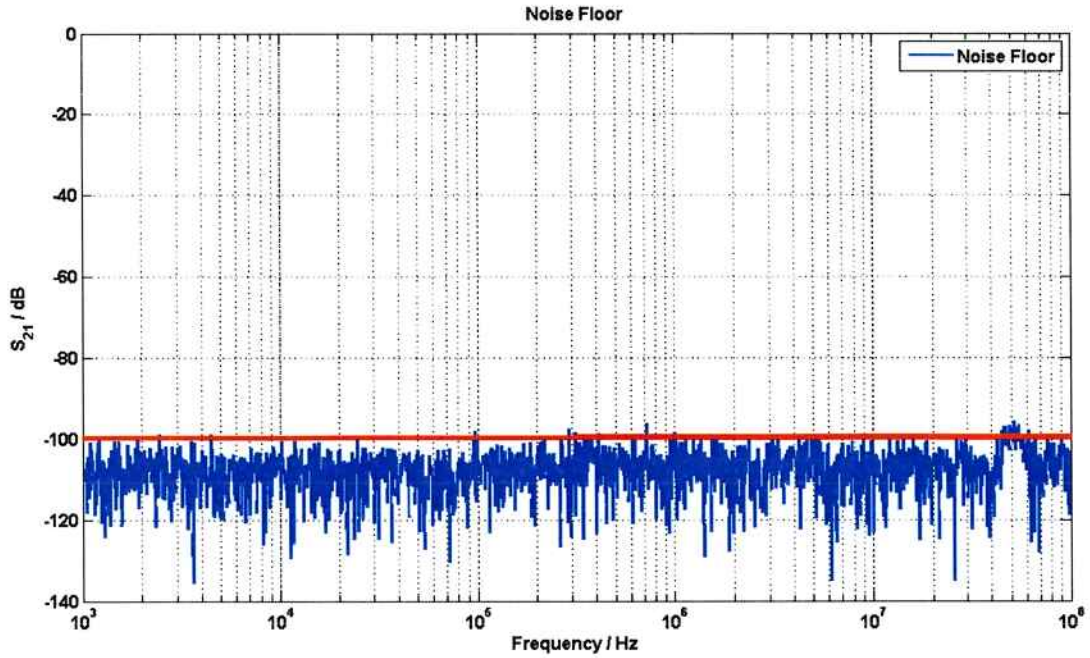

Figure 4.5.: Noise Floor

In Figure 4.5, the noise floor from the S_{21} measurements of the network analyzer is plotted. The lower limit for the measurements is -100 dB, and values below this threshold (which is unlikely) are not measurable with this equipment.

With consideration of the factors listed in Table 4.1 an accuracy of 10 % related to the dB values is assumed for the simulations.

Table 4.1.: Factors for Confidence Range

Factor	Range
Tolerance of Capacitors	20 %
Assumptions for Magnetic Material	10 %
Assumptions in the Model	5 %
Tolerance of Other Components	5 %
Simulation Errors and Other Factors	5 %

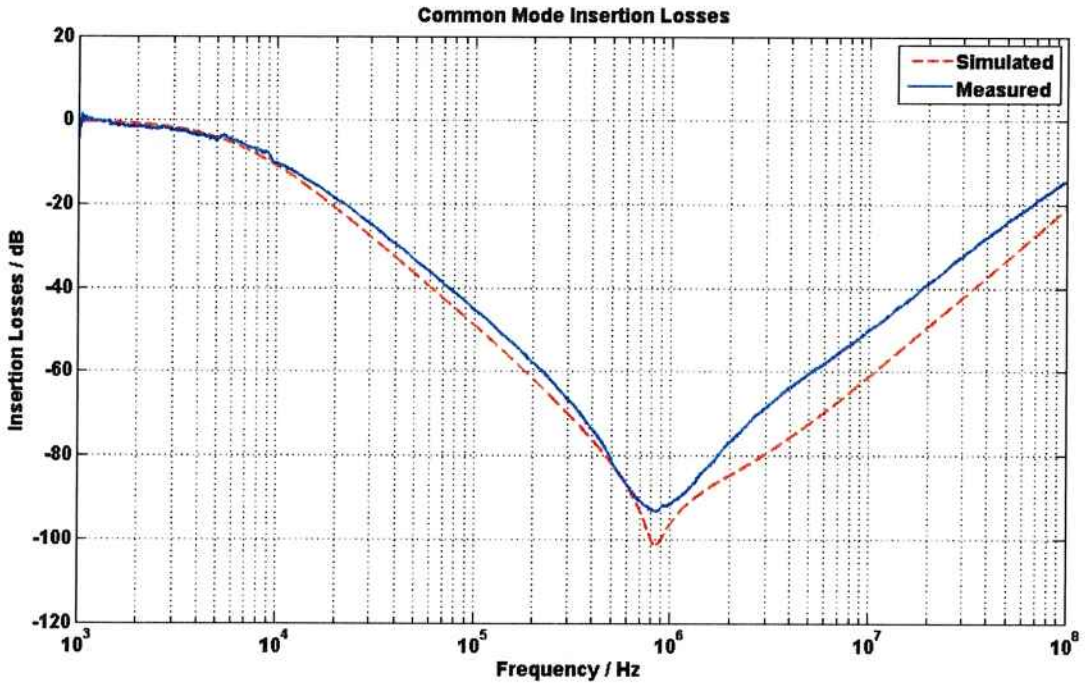

Figure 4.6.: Common Mode Insertion Losses

Part 4.3: Effect of Load and Source Impedances

In order to determine the effect of the load and source impedances in the filter attenuation, simulations with 50 Ω / 50 Ω, 100 Ω / 0.1 Ω and 0.1 Ω / 100 Ω impedances, as recommended in CISPR 17, are made and the results plotted in Figure 4.8. The measurements and/or simulations with 100 Ω / 0.1 Ω and 0.1 Ω / 100 Ω load and source impedances are defined in the CISPR 17 as "Approximate Worst Case Method".

It is possible to see that the insertion losses are increased in up to 40 dB, when the load impedance is decreased from 50 Ω to 0.1 Ω and the source impedance is increased from 50 Ω to 100 Ω.

Thereby the filter performance is better the lower the load impedance is and the higher the source impedance is. Unfortunately, in most applications, the inverse is true, as the network impedance is normally low and the load impedance generally high, and the performance of this filter is degraded. A careful analysis of the impedances of the system where the filter is going to be installed is therefore necessary.

Part 4.4: Summary of the Validation Process

In this chapter, the insertion losses of the filter are measured with a network analyzer and compared with the values obtained with the equivalent circuit model created in the previous chapter.

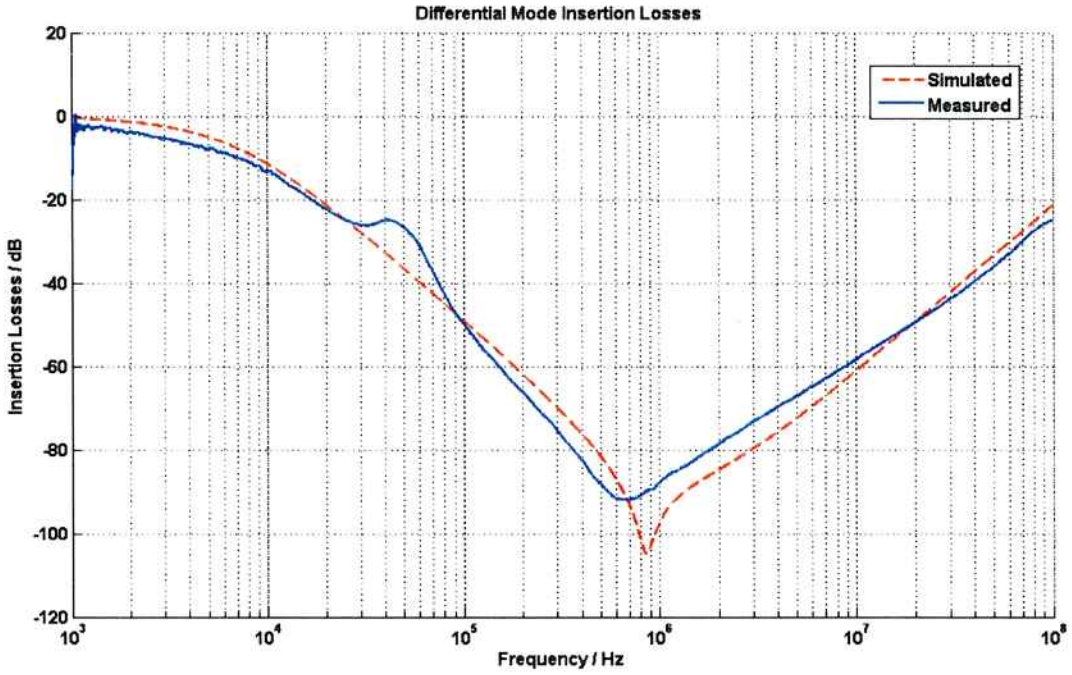

Figure 4.7.: Differential Mode Insertion Losses

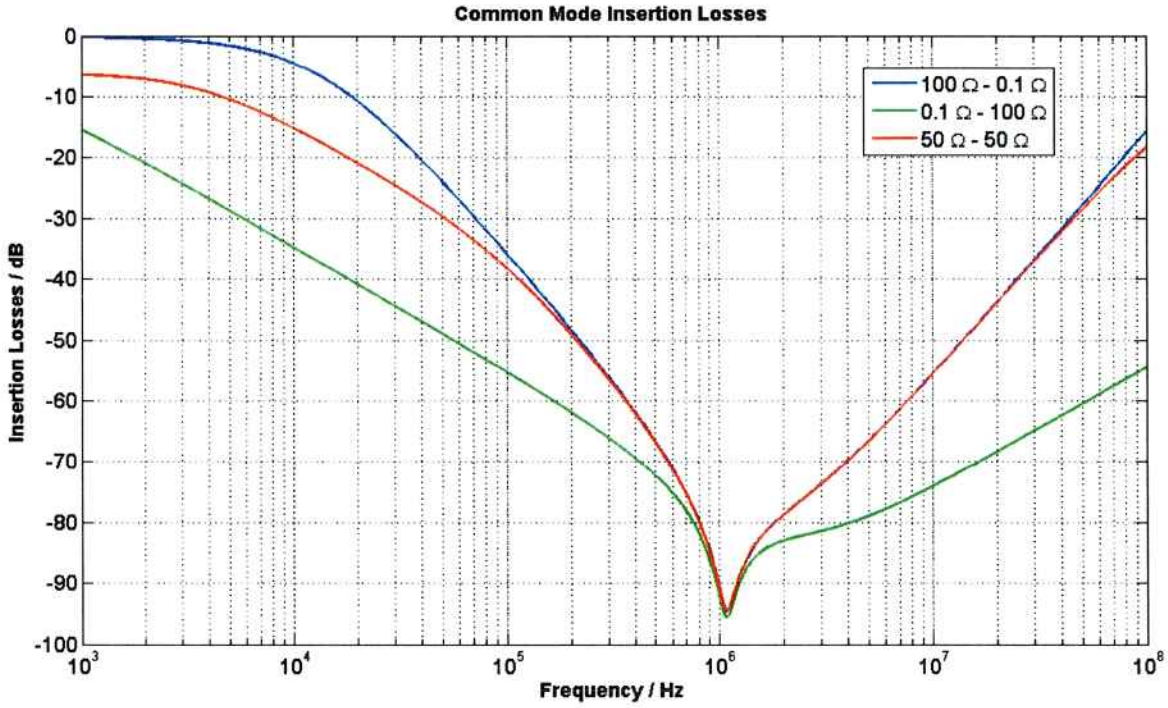

Figure 4.8.: Impact of Impedance (Load - Source)

Table 4.2.: Deviation

Frequency	Common Mode Deviation	Differential Mode Deviation
1 KHz	1 %	1 %
10 KHz	1 %	1 %
100 kHz	11%	1 %
1 MHz	5 %	11 %
10 MHz	20 %	5 %
100 MHz	25 %	15 %
Average	10 %	6 %

The sources of errors both in measurements and simulation are determined and the confidence ranges are evaluated. It is found that, within an adequate confidence range, the simulations correspond to the reality. In Table 4.2, the average deviation between simulations and measurements is of 10 % for the common mode and of 6 % for the differential mode.

Furthermore, the resonant frequencies, as seen in Pictures 4.6 and 4.7, are matching between the model and the simulations. These resonances are explained through the core material characteristics and the stray inductance of the capacitors. Considering that the tolerance is of 10 % , the model is then successfully validated.

Unfortunately the accuracy of the model is limited by the assumptions, mainly the material of the common mode choke core and the earth impedance which are not exactly known. One important factor which limits the accuracy of the model in relation to the measurements is the tolerance of the components (for example, the film capacitors have a tolerance of 20 %).

5 Effect of the Stray Components on the Filter Performance

Part 5.1: Evaluation of the Relevance

In Chapter 2, a total number of 221 inductances and capacitances are calculated using the finite element method. In order to have a better oversight of the filter parasitics and to keep track of their impact in the equivalent circuit of the filter, their relevance has to be determined.

In order to make a objective evaluation of the relevance, numerous simulations are made using the equivalent circuit model, removing, adding or changing the values of the parasitic components. The list of the criteria used to evaluate the relevance of the stray components follows. The coupling coefficients inside the filter stages are calculated in RMS mean of the individual coupling coefficients of the components.

1. Impact in the insertion losses (bigger than 5 dB)
2. Frequency range that is affected (between 10 KHz and 100 MHz)
3. Inductive coupling coefficient (bigger than 0.05)
4. Capacitive coupling coefficient (bigger than 0.15)

Part 5.2: Stray Components of Filter Elements

A - Most Relevant Components

I - Stray Inductances of Capacitors

The stray inductance is connected in series with the capacitor itself, as in Figure 3.5. The capacitance together with the inductance resonate at the frequency calculated in Equation (5.1). As higher the stray inductance of the capacitor, as lower the resonance frequency is.

$$f_o = \frac{1}{2 \cdot \pi \cdot \sqrt{L \cdot C}} \tag{5.1}$$

To see the impact of this stray component in the common mode insertion losses, its value in the equivalent circuit model is changed. In Figure 5.1 the common mode insertion losses are plotted for a stray

inductance of 1 nH, 10 nH and 100 nH. A three-dimensional plot of the insertion losses in relation to the frequency and the stray inductance is presented in Figure 5.2. The changes in the insertion losses are summarized in Table 5.1.

Table 5.1.: Effect of the Stray Inductance in the Insertion Losses

Stray Inductance	Resonant Frequency	Insertion Losses at Resonance	Insertion Losses at 10 MHz
1 nH	3 MHz	100 dB	81 dB
10 nH	853 KHz	92 dB	57 dB
100 nH	324 KHz	80 dB	40 dB

The stray inductance of the capacitor is one of the most important stray components and affects the filter performance significantly. At frequencies higher than their resonance frequency the apparent capacitance reduces, and the capacitor cannot shunt interferences anymore.

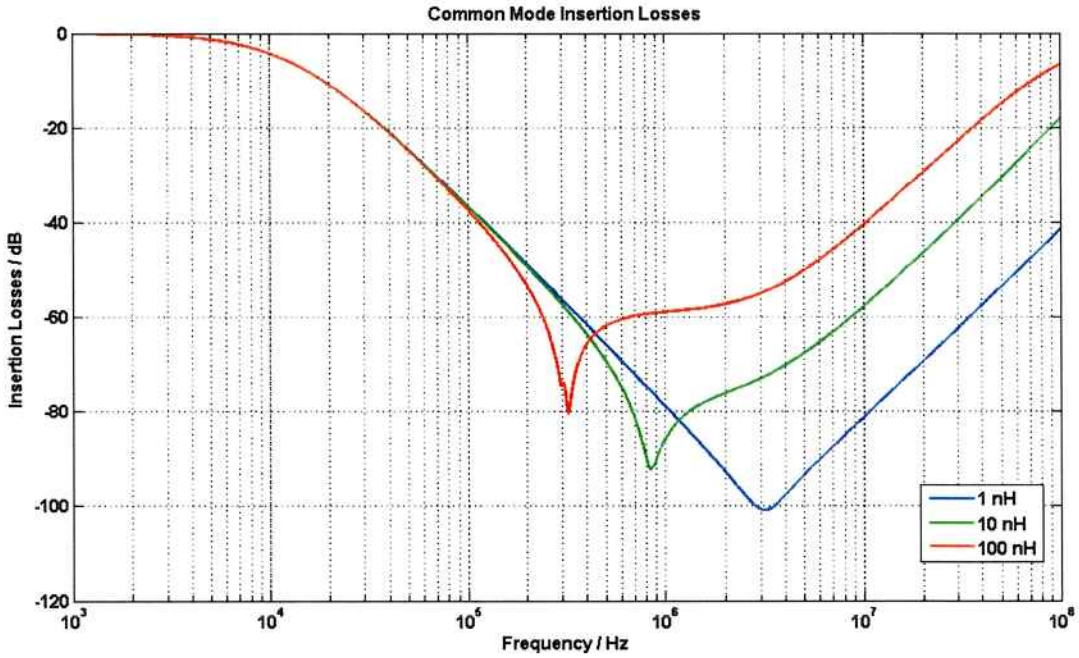

Figure 5.1.: Common Mode Insertion Losses for Stray Inductances of 1, 10 and 100 nH

According to Equation (2.3), the magnetic energy integral is proportional to the inductance of a given coil. The pins of the capacitor have a very high magnetic energy density, as is Picture 5.3, and thus a high contribution to the stray inductance of the capacitor. Therefore, the pins should be as short and thick as possible to avoid magnetic energy concentration.

II - Parallel Stray Capacitance of the Coil

The parallel stray capacitance (the whole capacitance, not the turn-to-turn capacitance) is set to 0.5 pF, 5 pF and 50 pF in the equivalent circuit model and the common mode insertion losses are plotted in

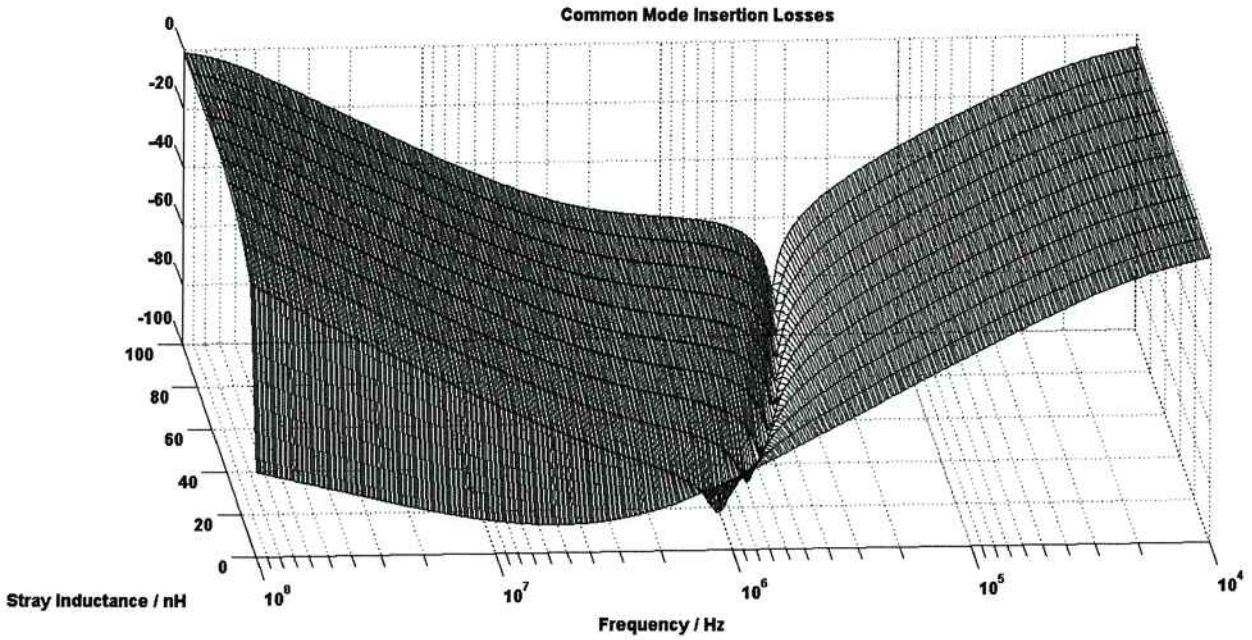

Figure 5.2.: Three Dimensional Plot of the Common Mode Insertion Losses for Stray Inductances

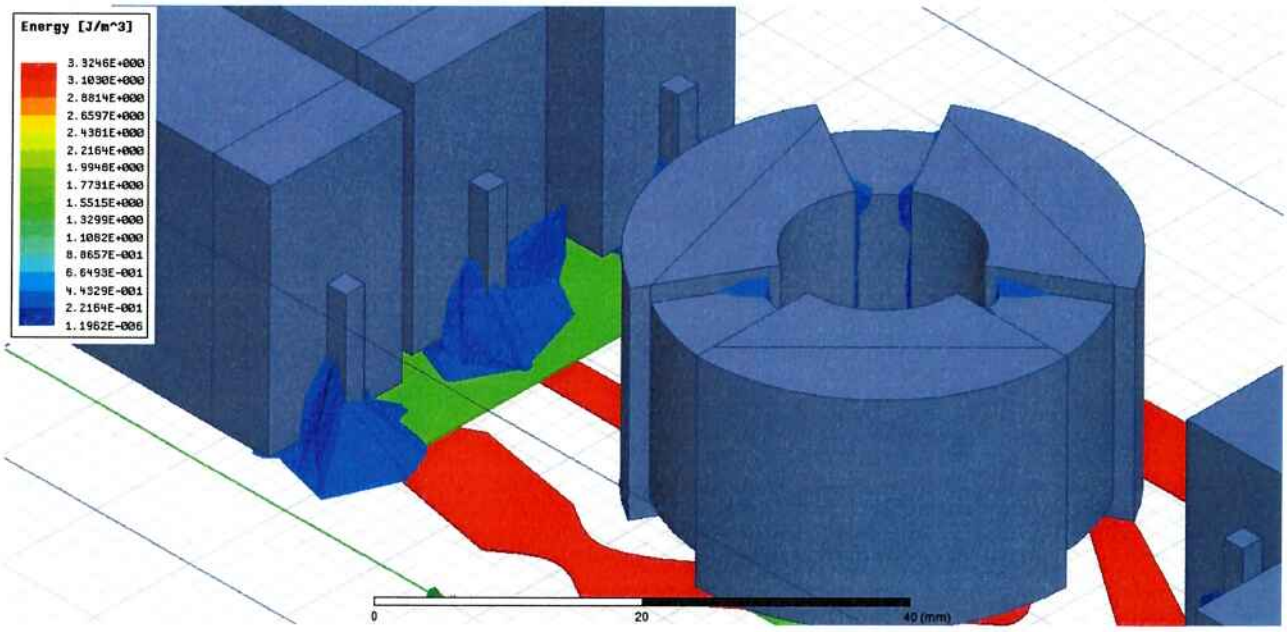

Figure 5.3.: Energy Density Plot

Figure 5.4. In Table 5.2, the results of the simulations are summarized. A three-dimensional plot of the insertion losses in relation to the frequency and the stray capacitance is presented in Figure 5.5.

Table 5.2.: Effect of the Stray Capacitance in the Insertion Losses

Stray Capacitance	Insertion Losses at 10 MHz	Insertion Losses at 100 MHz
0.5 pF	71 dB	38 dB
5 pF	56 dB	18 dB
50 pF	38 dB	12 dB

The parallel stray capacitance of the coil is also affecting the filter performance significantly, and thus is one of the most important stray components. Again, for frequencies higher that their resonant frequency, the coils will show a decreasing apparent inductance, affecting the filter performance.

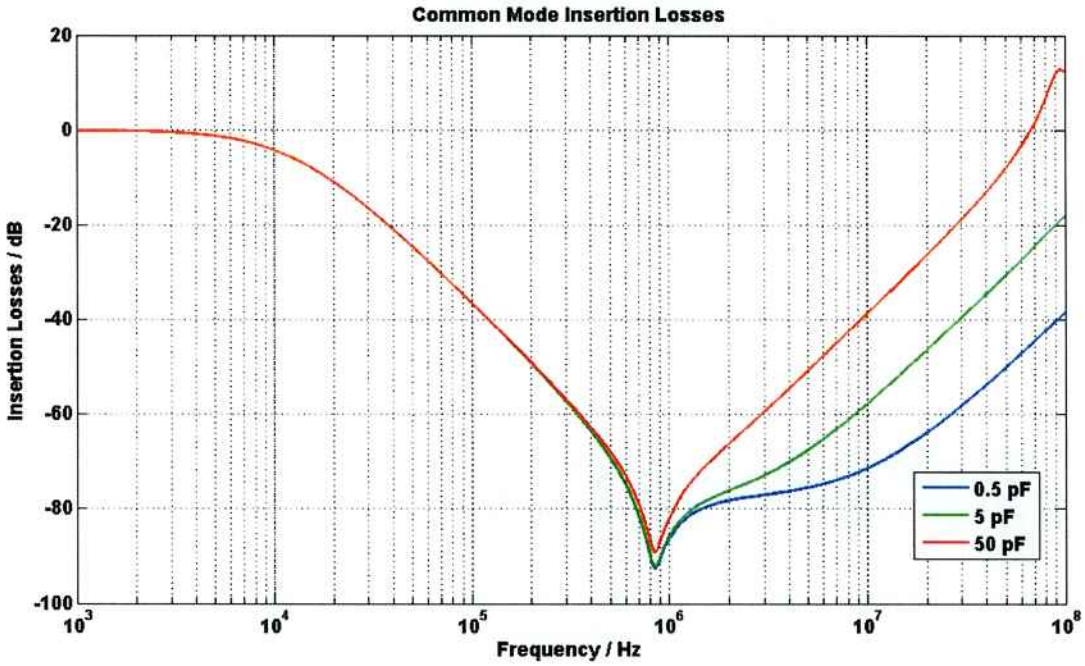

Figure 5.4.: Common Mode Insertion Losses of a Stray Capacitance of 0.5 pF, 5 pF and 50 pF

Part 5.3: Stray Couplings Between Filter Elements

A - Relevant Components

I - Coupling between X Capacitors

The coupling factors between the X capacitors are of 0.20 for capacitive coupling and of 0.09 for inductive coupling, in RMS mean. These stray capacitances fortunately improve the filter performance, since they

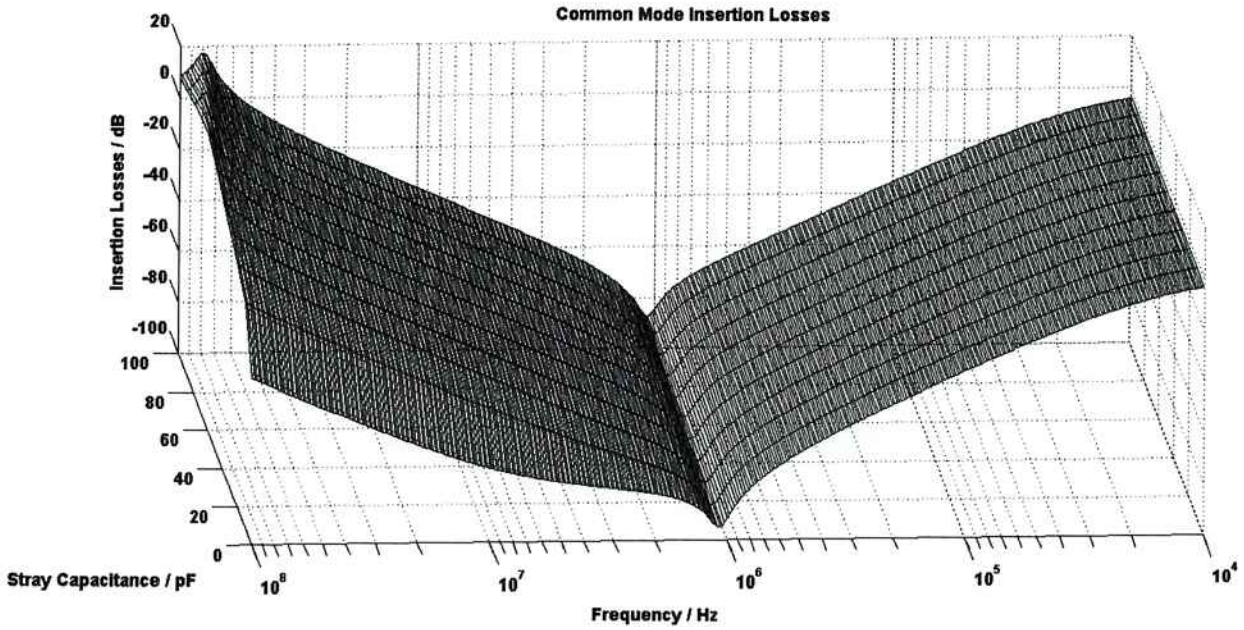

Figure 5.5.: Three Dimensional Plot of the Common Mode Insertion Losses for Stray Capacitance

act like an additional X capacitor bank. However, reducing the distance between the capacitors in order to increase the capacitive coupling has the drawback of potentially increasing the inductive coupling. Also, due to the values of the capacitances(in the pF range), their effect is small.

In Figure 5.6, the inductive coupling between the components of the X capacitor bank is represented. With transformation of the mutual couplings, as in Chapter 6, the equivalent circuit model of Figure 5.7 is obtained. The stray inductances and thus the resonance frequencies of the capacitors change due to this effect, which is summarized in Table 5.3.

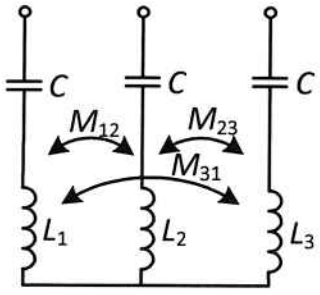

Figure 5.6.: Coupling between X Capacitors

The coupling between the X capacitors is asymmetrical. This reflects in the differences between the differential mode insertion loss characteristic between each of the phases of the filter. The simulated differential mode insertion losses in each of the phases are represented in Figure 5.8. This effect changes the behavior of the filter up to 5 dB. Therefore, the effect of this coupling is classified as relevant.

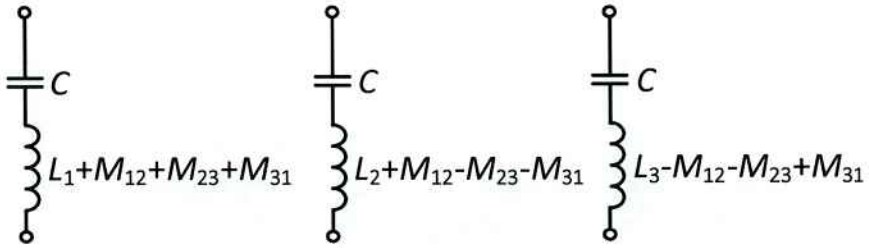

Figure 5.7.: X Capacitor Equivalent Circuit

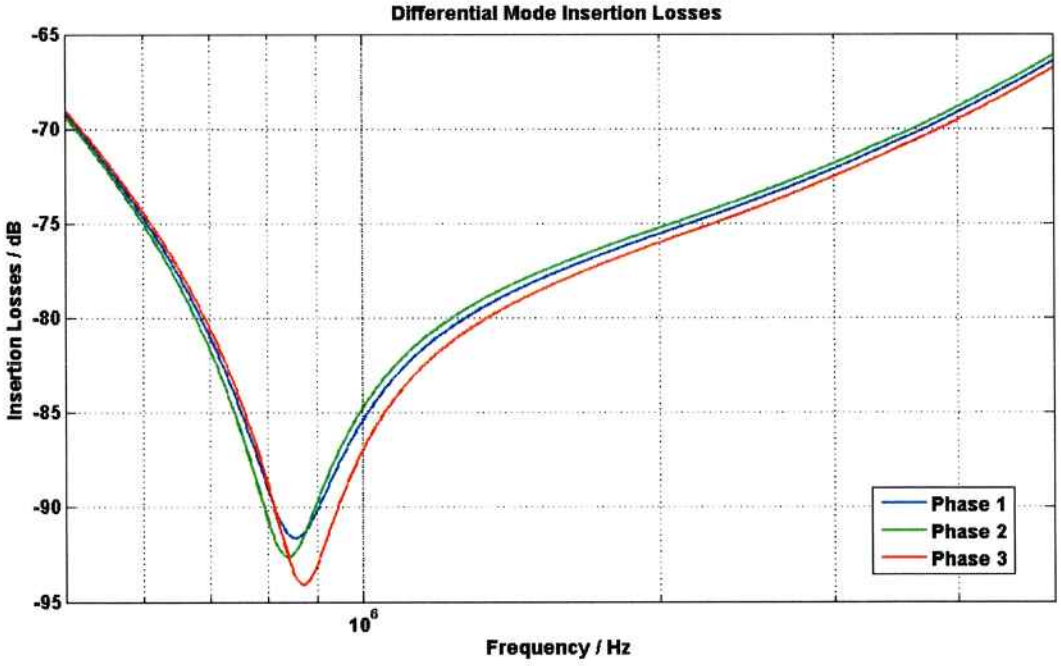

Figure 5.8.: Comparison of the Simulated Differential Mode Insertion Losses

Table 5.3.: Effect of the Mutual Coupling in the Resonance of the Capacitors

Stray Inductance	Resonant Frequency
$L_1 + M_{12} + M_{23} + M_{31} = 12.53$ nH	782 kHz
$L_2 + M_{12} - M_{23} - M_{31} = 10.03$ nH	875 kHz
$L_3 - M_{12} - M_{23} + M_{31} = 10.49$ nH	855 kHz

II - Coupling between Y Capacitors

The coupling factors between the Y capacitors are of 0.07 for inductive coupling and of 0.15 for capacitive coupling, in RMS mean. This coupling is classified as relevant, as in Annex C. The capacitive coupling acts as an additional X capacitor stage with very slight effect in the filter performance.

The stray mutual inductive coupling between the Y capacitors degrades the performance of the filter, because of conversion of differential mode signals in common mode signals. As one current flows in one of the stray inductances of the capacitors it also induces currents in the other capacitor because of the mutual coupling, creating a common mode disturbance. This phenomenon occurs with higher intensity at higher frequencies, as the mutual coupling impedance is the product of the angular frequency and the mutual inductance.

The common mode conversion factor is proportional to the coupling coefficient between the capacitors, which is of 0.07 RMS mean, resulting in a factor of -20 dB. This conversion has a negative effect because the additional common mode current contributes to the saturation of the common mode choke.

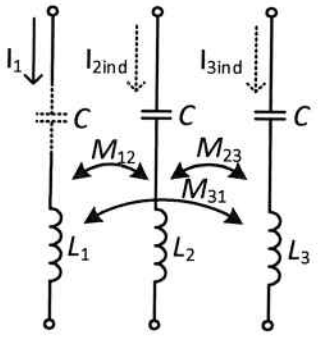

Figure 5.9.: Conversion of Differential Mode Signals in Common Mode Signals

In order to study the effects of the coupling in the Y capacitor bank, the insertion losses are simulated and plotted in Figure 5.11. The coupling factor between all capacitors is of 0, 0.1 and 0.2 in the simulations, and the impact of this stray coupling in the insertion losses is up to 10 dB.

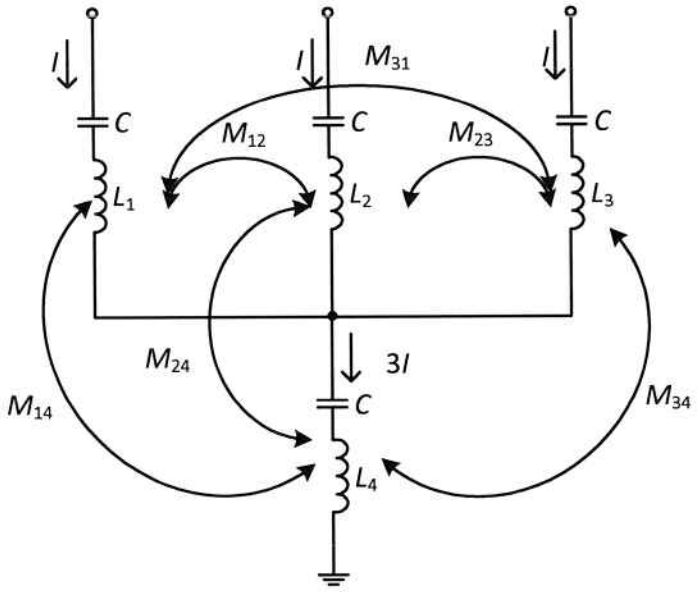

Figure 5.10.: Y Capacitor Coupling

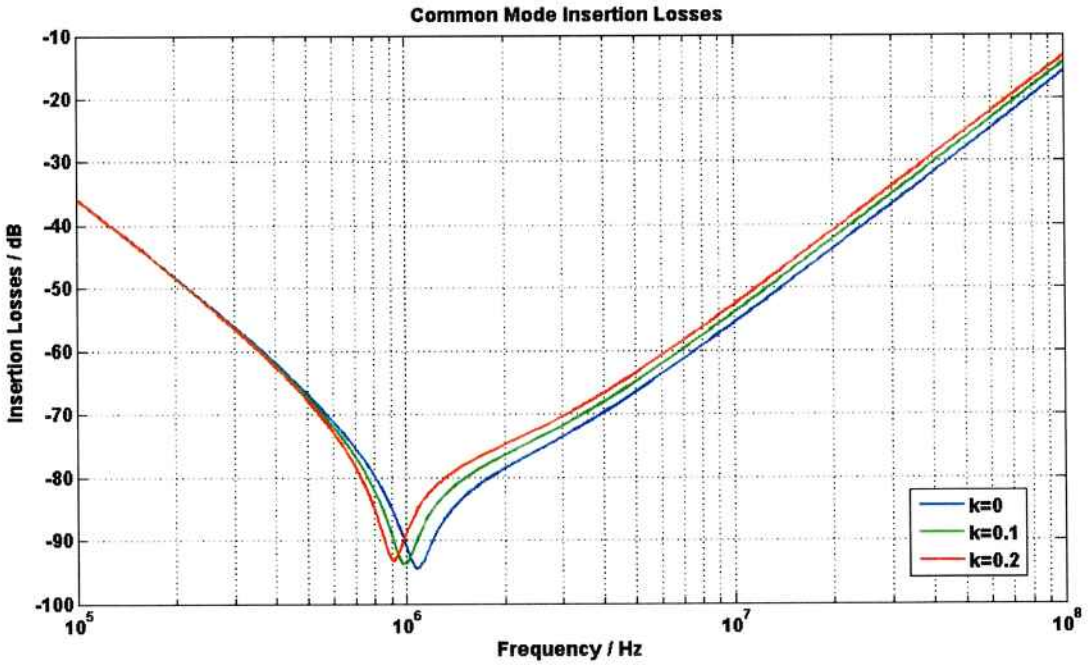

Figure 5.11.: Effect of the Stray Coupling between the Y Capacitors

All filter components have a stray capacitive coupling to the housing, with coupling coefficient that range from 0.16 to 0.26 RMS mean. This coupling acts like an additional Y capacitor stage, and is influencing the higher-frequency resonance peak. In Figure 5.12, the common mode insertion losses in the higher frequency range are represented for equivalent component-housing capacitances of 10 pF and of 100 pF.

It is possible to see that the resonant frequency changed from 70 MHz to 200 MHz. The magnitude of the peak changed in 10 dB. That means, the component-housing stray capacitance influences the filter behavior in higher frequencies.

The coupling between the filter components and the housing is then classified as relevant, especially on higher frequencies. If the whole frequency range up to 100 MHz is considered, this coupling is useful to increase the insertion losses at very high frequencies. However, as most applications of filters consider frequencies only up to 30 MHz, the usefulness of this effect is limited.

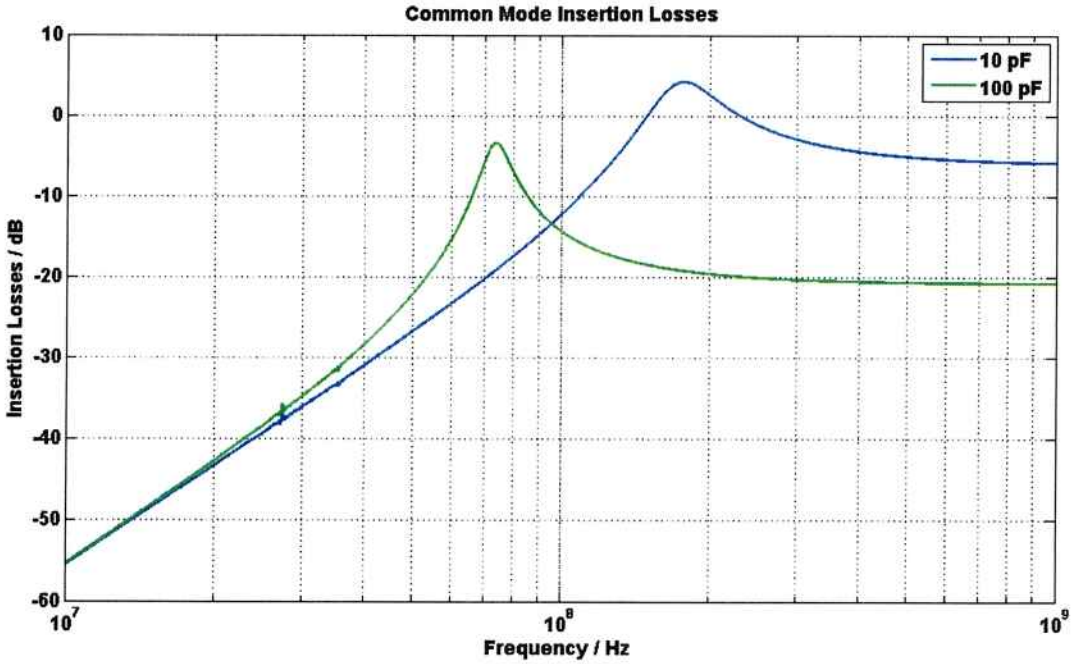

Figure 5.12.: Common Mode Insertion Losses Simulation up to 1 GHz

Measurements to a frequency up to 1 GHz are made for the common mode insertion losses and are plotted in Figure 5.13, and the aforementioned resonance peak exists.

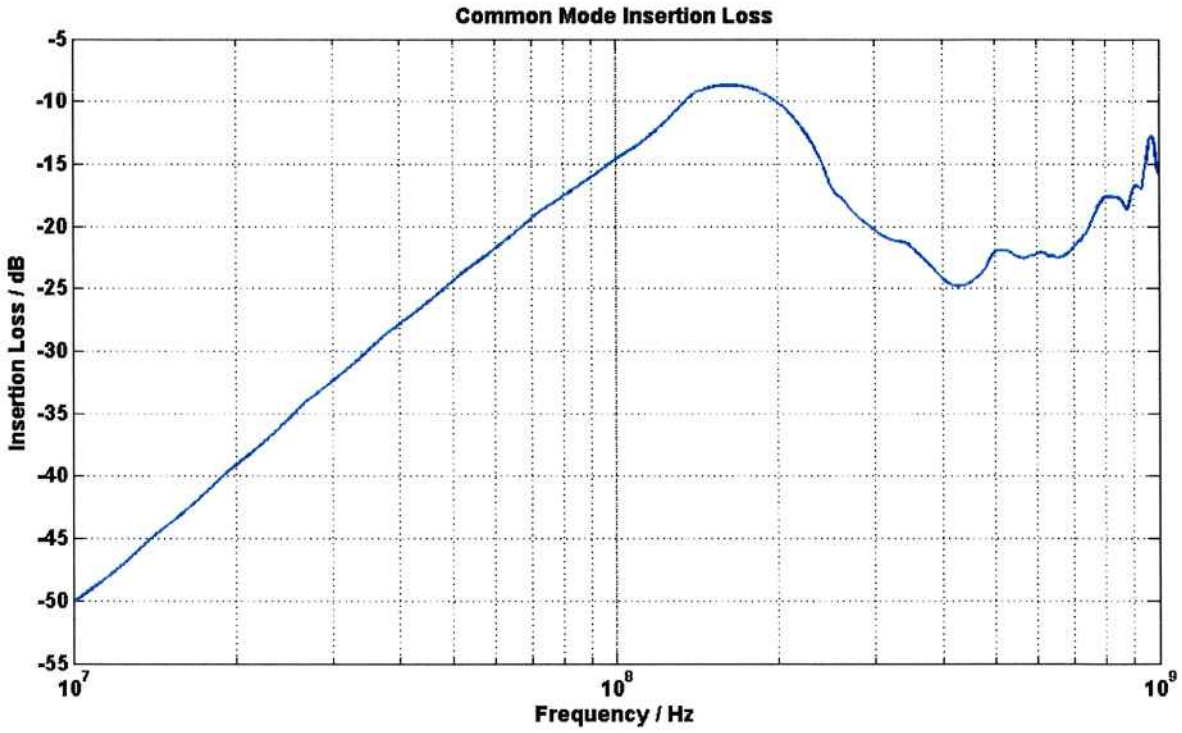

Figure 5.13.: Common Mode Insertion Losses Measurement up to 1 GHz

I - Coupling between X and Y Capacitors and Common Mode Choke

The coupling coefficients between the X Capacitors and Common Mode Choke are of 0.004 for inductive coupling and of 0.01 for capacitive coupling, in RMS mean. For the Y capacitors, the coefficients are of 0.002 for inductive coupling and of 0.01 for capacitive coupling, again in RMS mean. The effects of this coupling are classified as not relevant, except to the fact that they are highly asymmetrical. They are giving a small contribution to the asymmetries between phases in the differential mode losses.

The asymmetries are due to the different distances between the components in the filter. This can be seen in Figure 5.14 and 5.15.

II - Coupling between X and Y Capacitors

Between the X capacitors and the Y capacitors, the coupling factors are of 0.002 for inductive coupling and of 0.0000001 for capacitive coupling, in RMS mean. This coupling is classified as not relevant then, as it has almost no effect in the performance of the filter.

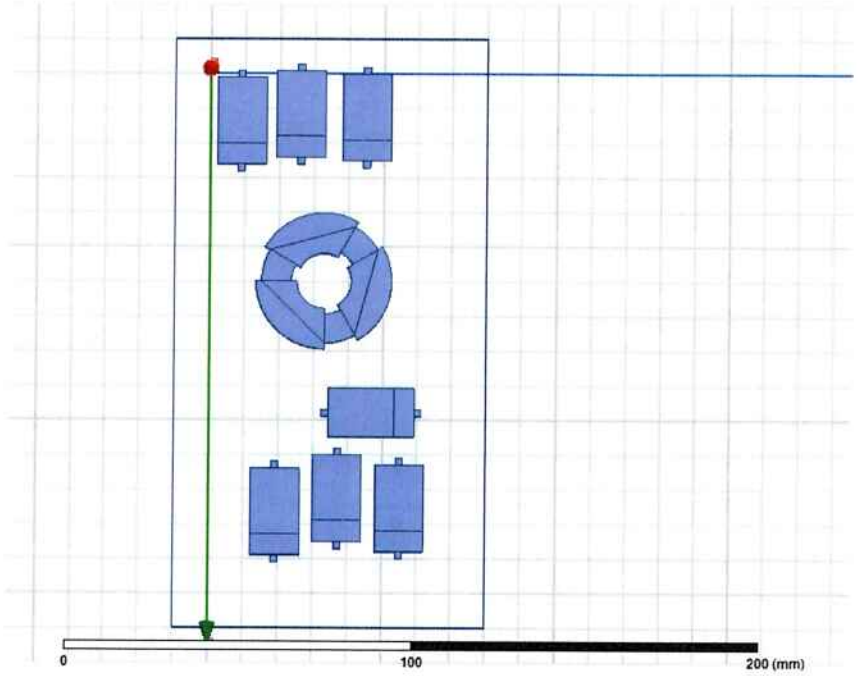

Figure 5.14.: Top View of Filter Model

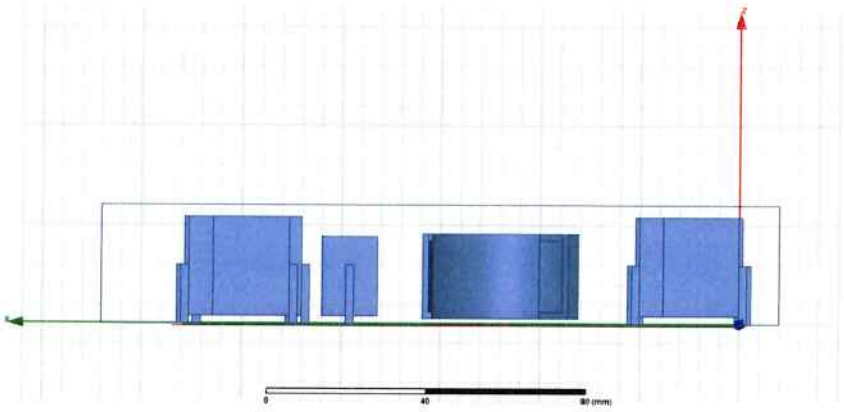

Figure 5.15.: Side View of the Model

III - Coupling between Coil Windings

The inductive coupling of the coil windings is not a stray component but a feature of the common mode choke. The capacitive coupling factor between the coils of the common mode choke is of 0.26 in RMS mean.

Even though the coupling factor is high, the capacitances still lie in the pF range. Since the inductances are not stray ones and the capacitive effects small this coupling classified as not relevant. This coupling works as an additional X capacitive stage.

IV - Coupling in PCB itself and with Other Components

The printed circuit board is classified as a not relevant stray component. The coupling factors for the equivalent PCB arrangement range from 0.0003 to 0.02 for inductive coupling and from 0.03 to 0.09 for capacitive coupling, in RMS mean.

In the frequency of 100 MHz, the wavelength in vacuum equals:

$$\lambda = \frac{c_0}{f} = \frac{3 \cdot 10^8}{100 \cdot 10^6} = 3\ m \tag{5.2}$$

As the filter is smaller than 30 cm, it can be considered as a concentrated elements circuit. However, at higher frequencies, traveling wave effects, such as wave reflections, need to be considered and the circuit must be represented with distributed elements. In this case, the PCB traces (as electrically long lines) are going to have an important role on the filter performance.

Part 5.4: Summary of the Relevance of the Stray Components and Couplings

In this chapter, the relevance of the parasitics is evaluated. Also, the effects of the relevant stray components and couplings are analyzed and exemplified. The criteria for the evaluation are explained in the introduction.

In Table 5.4, the relevance of them is summarized. Many stray components are calculated, but only the stray capacitance of the coils and the stray inductance of the capacitors are most relevant. The coupling between the X capacitors, between the Y capacitors and the coupling between the filter components and the housing is relevant. The other components are not relevant and therefore neglected in the creation of an equivalent circuit model for the filter. Of course for more complex filter topologies, as the ones depicted in Figures 1.8 and 1.9, the number of couplings is going to increase. Therefore, each filter topology must be analyzed separately. Even for more complex topologies the coupling principles and the relevance of them should remain the same.

Table 5.4.: Relevance of the Stray Components and Couplings

Stray Component	Relevance
Stray Inductances of the Capacitors	Most Relevant
Parallel Stray Capacitance of the Coil	Most Relevant
Coupling between X Capacitors	Relevant
Coupling between Y Capacitors	Relevant
Coupling between Filter Components and the Housing	Relevant
Coupling between X and Y Capacitors and Common Mode Choke	Not Relevant
Coupling between X and Y Capacitors	Not Relevant
Coupling between Coil Windings	Not Relevant
Coupling in PCB itself and with Other Components	Not Relevant
Coupling between Y Capacitors	Not Relevant

6 Optimization and Improvement

Part 6.1: State-of-the-art in the Filter Parasitics Compensation

There are many articles and dissertations that aim to improve the performance of EMI filters. Most of the authors are focusing either in the stray couplings effect or in the stray components of the elements themselves. As in Chapter 1, an analysis of three-phase filters, with simultaneous consideration of the stray components and of the stray couplings, together with an analysis of the costs, is due.

In [27], a method to improve the high-frequency performance of filter inductors and common-mode chokes by compensating the stray capacitance is presented, improving the attenuation of an inductor with a stray capacitance of around 10 pF in up to 5 dB. In an inductor with a very high stray capacitance of around 20 pF the improvements are up to 20 dB. The inductors used in this work do not have such a high stray capacitance and therefore smaller improvements are to be expected when this technique is applied.

Capacitors are critical elements in EMI filters, and their behavior influences the filter performance strongly. In [28], coupled windings are used to cancel the stray inductance of the capacitors. When applied to a 100 μF capacitor, this compensation technique provides an improvement of 20 dB in the insertion losses, out to very high frequencies. Integrated filter elements are compared to single capacitors, and the improvements are similar.

Improvements using the stray inductance canceling in the 20 dB range are also claimed in patents. For example, in [29] and [46], the first using a planar coil and the second a wire and a metal strip on the capacitor, similar results are found.

Through changes in the arrangement of the windings of an inductor to minimize mutual couplings, in [39] an improvement of up to 5 dB is achieved at higher frequencies. A first relevant improvement in higher frequencies of up to 20 dB is obtained with canceling of stray inductances in the capacitors. Improvements of up to 30 dB are obtained with a single-phase integrated filter.

Through optimization of the component arrangement and of the PCB traces, in [7] the filter performance is improved in 10 dB at frequencies starting at 1 MHz. In [21], conservative numbers for the filter layout optimization are presented, with improvements of up to 10 dB in the common mode insertion losses. The placement of the components is changed to minimize the inductive couplings in a limited space.

There are many challenges involved in the design of EMI filters, such as design constraints (size, cost and weight), the wide frequency range, the stray components and the saturation of the inductors. A model for the common mode choke is presented in [22], which corresponds to the reality in frequencies up to 1.5 MHz.

In [24], an EMI filter is designed using the compensation of the stray components of the capacitor and of the coils. The filter is to be installed inside of a three-phase PWM converter and therefore an optimization process with volume constraints is presented.

This work focuses not only in the optimization of the characteristics of the filter, but the costs of the improvement techniques are assessed as well. In that way, the implementation of a given technique can be justified economically. In the ideal case, the filter performance should be improved with almost no increase of the costs.

Part 6.2: Optimization and Improvement Process

In the previous chapters, it is possible to see that the performance of the filter is strongly degraded due to the stray components. Measures to mitigate the parasitics are needed to reduce their impact.

In Chapter 5, it is determined that the most relevant stray components are the stray inductance of the capacitors and the parallel stray capacitance of the coil windings. A systematical and structured approach to select the common mode choke material is a key factor to improve the performance of the EMI filter as in [16] and [22]. The stray couplings classified as relevant are also taken into consideration in the optimization.

A list of the aspects considered in the optimization and improvement process follows:

1. Stray Inductance of Capacitors
2. Parallel Stray Capacitance of Coil Windings
3. Stray Couplings
4. Core Material of Common Mode Choke

A - Stray Inductance of Capacitors

The capacitors used in this filter have a stray inductance of 9 nH. Together with the capacitance value, the resonant frequency is calculated in Equation (6.1). In Figure 6.1, it is possible to see the impedance curves of the capacitors used in this work.

$$f_o = \frac{1}{2 \cdot \pi \cdot \sqrt{L \cdot C}} = 0.93MHz \tag{6.1}$$

Theoretically, it is possible to eliminate the stray inductance of the filter completely through cancelling techniques. Using two mutually coupled inductors, as in Figure 6.2, the equivalent circuit diagram in Figure 6.3 results. The negative inductance compensates the stray inductance of the capacitor in the shunt path. To ensure correct function of the coils in the whole frequency range, it is important to use a core material without frequency dependent permeability, like air or glass.

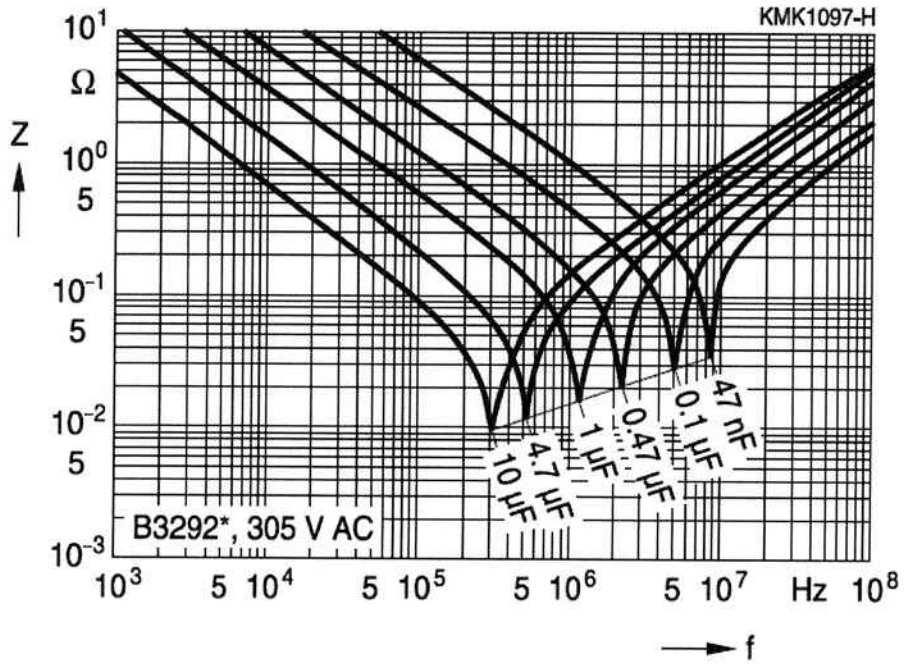

Figure 6.1.: Impedances of the Capacitors [40]

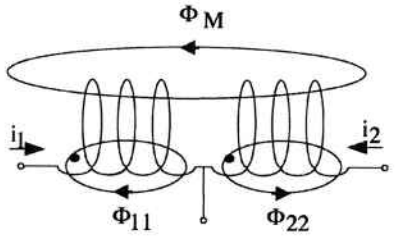

Figure 6.2.: Inductance Cancelling [28]

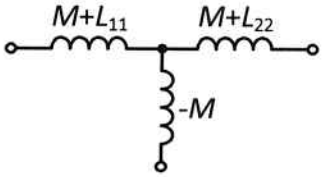

Figure 6.3.: Equivalent Circuit for Inductance Canceling

The mutual inductance must be equal to the inductance to be canceled. The coupling coefficient, the inductances L_{11} and L_{22} are related together in Equation (6.2).

$$M = k \cdot \sqrt{L_{11} \cdot L_{22}} \tag{6.2}$$

In order to evaluate this compensation strategy, a simple test arrangement consisting of one capacitor and two coils arranged as in Figure 6.2 is built. The primary and the secondary winding have the same number of turns.

As in Equation 6.2, the coupling coefficient plays a very important role in this compensation method. In order to maximize coupling, the windings are arranged as in one power transformer, with the secondary coil winded directly over the primary coil.

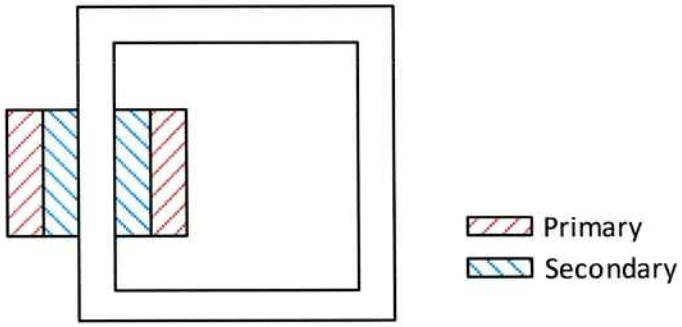

Figure 6.4.: Winding Arrangement

The insertion losses are measured for arrangements of 4x4, 6x6, 8x8 turns and without compensation. In Figure 6.6 the curves for the measurements are plotted. The best results are achieved with 4x4 turns. With 6x6 and 8x8 turns too much compensation is causing degradation of the performance.

Unfortunately, this cancellation technique transforms the two-pin capacitor into a three-pin device, thus limiting the application area to shunt capacitors. The compensation coils could be integrated to the capacitor, but one complicating factor, the stray coupling between the capacitor and the compensation coil, represents a big challenge.

The costs of this cancellation measure depend strongly on the ampacity of the filter, because the higher the nominal current, the thicker the needed copper wire is. There are also additional manufacturing costs due to winding and soldering. In case of cancellation with PCB traces, the material and manufacturing costs become irrelevant.

B - Parallel Stray Capacitance of Coil Windings

In [27], an approach for canceling the parallel stray capacitance is presented. It consists in the parallel connection of the primary of a transformer to the parasitic capacitance to be canceled. The primary side

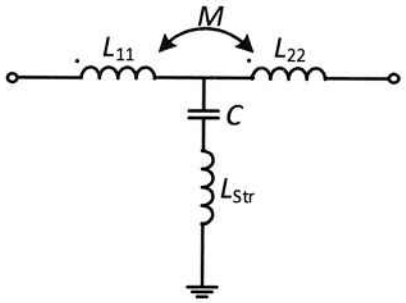

Figure 6.5.: Equivalent Circuit Model

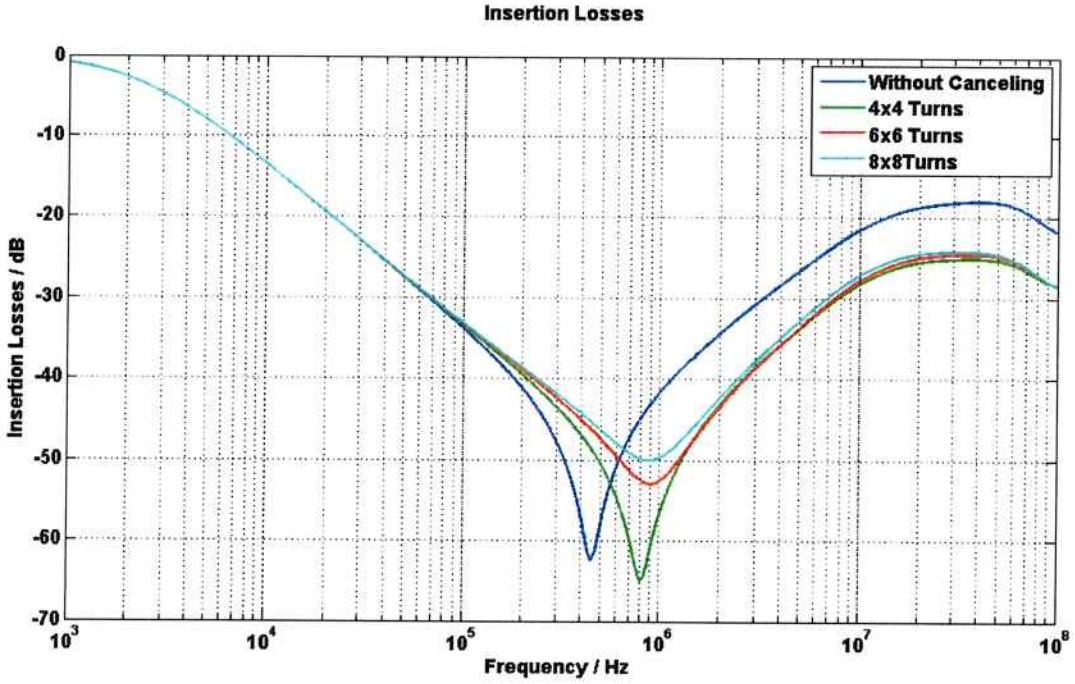

Figure 6.6.: Inductance Canceling Evaluation

is connected to the coil, and the secondary side to a compensation capacitor. This circuit is represented in Figure 6.7.

The values should satisfy Equation 6.3. With this technique a compensation current that cancels the current flowing in the stray capacitance is injected. The high-frequency filtering performance is therefore improved.

To avoid using an additional transformer, the windings of the common mode choke themselves can be used as the primary side, and an additional winding in the choke is used as the secondary side. The compensation winding conducts only small current and therefore can be implemented using wire of smaller gauge.

The values of the parameters are calculated for compensation of the parallel stray capacitance and listed in Table 6.1. As in [27], lower coupling coefficients affect the proper function of the canceling strongly. An in-depth analysis of this effect is done in Section 6.

$$C_{\text{comp}} \cdot m \cdot (1-m) = C_{\text{p}} \tag{6.3}$$

Table 6.1.: Parameters for Cancelling of Parallel Stray Capacitance of Coil Windings

Parameter	Value
C_{p}	5 pF
C_{comp}	29 pF
m	0.78
N_{sec}	10

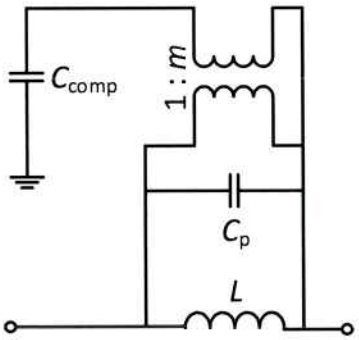

Figure 6.7.: Parallel Stray Capacitance Cancelling

Ceramic capacitors with capacitances of 22 pF and 33 pF are commonly found in the market. As a capacitor of 29 pF is specified (in this case, in other common mode chokes another capacitances are going to be needed), experimental tests are done in order to find the optimal capacitor between the

available ones. The insertion losses of one winding are measured and the results are plotted in Figure 6.8.

With capacitors of 22 pF the best insertion losses characteristic is obtained. An additional resistor of 330 Ω is connected in series with the capacitors in order to dampen the resonance peaks in the frequency of 10 MHz that result in additional insertion losses in the frequency of 25 MHz. In Figure 6.9, it is possible to see a comparison of the winding without and with the coil parallel stray capacitance canceling. An improvement in the range of 5 to 10 dB is verified in frequencies starting from 1 MHz.

The material costs of this compensation technique consist in the less expensive (due to smaller wire gauge) additional windings, capacitors and resistors, which represent approximately 3 % of the total material costs. However, the manufacturing costs increases, as additional soldering and winding is required. If the manufacturer of the common mode choke solders the compensating capacitors directly to the coils, the additional manufacturing costs are eliminated.

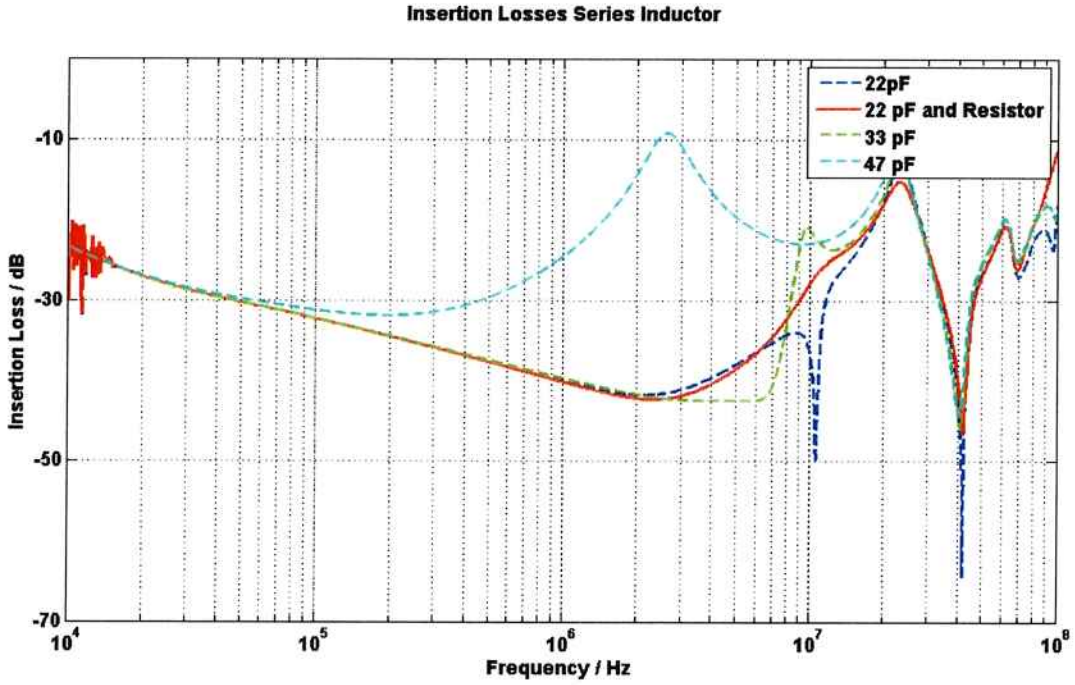

Figure 6.8.: Evaluation of Capacitors

C - Stray Couplings

In order to reduce the coupling between the capacitors, there are two approaches: increase the distance and/or angle between the capacitors or apply shielding. Increasing the distance between the capacitors increases the volume of the filter. Induced currents in the shield increase the losses of the filter, as there are ohmic losses due to induced eddy currents. These losses also increase with the frequency, what contributes to the damping of high frequency emissions. As Equation 6.4 shows, the induced currents are proportional to the frequency, to the mutual inductance and to the inducing current. The shield

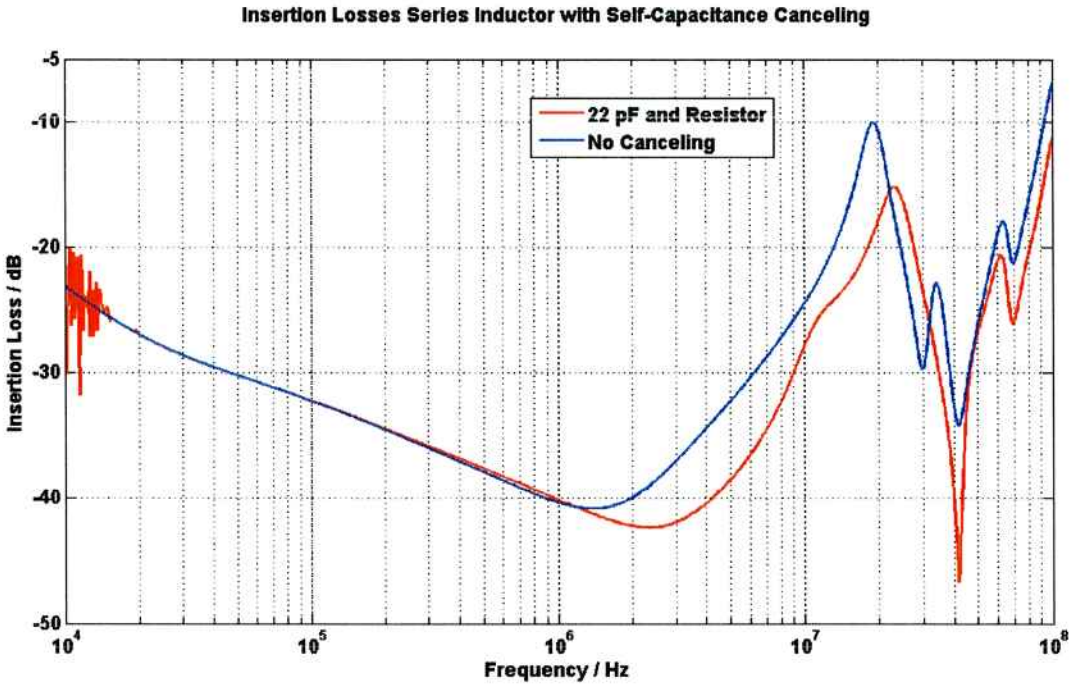

Figure 6.9.: Capacitance Canceling Effect

losses are proportional to the resistivity of the material, to the area, to the thickness of the sheet and to the square of the induced current, as in Equation 6.5.

$$I_{\text{ind}} \sim f \cdot M \cdot I \tag{6.4}$$

$$P \sim \frac{I_{\text{ind}}^2 \cdot \rho \cdot \delta}{A} \tag{6.5}$$

Changing the angle between the capacitor requires changes in the PCB design and perhaps in the manufacturing process of the filter. These changes do not affect the costs of the filter, because the price of the PCB is not affected by the complexity of the layout if the spacing accuracy remains the same.

As seen in Chapter 5, the stray capacitance between the filter components and the housing affects the higher frequency behavior of the filter. This means, through an increase of this parasitic component it is possible to improve the dampening of the filter in frequencies in the range of 100 MHz. Decreasing the distance between the components and the housing is increasing the stray capacitance. By locating all components close to the housing and inserting a thin isolation an approximately ideal Y capacitor bank is created.

To determine the effect of the positioning of the capacitors, a parametric sweep with distance and angle of an two capacitor arrangement (see Figure 6.10) is done. The results of the sweep are plotted in Picture 6.11. The values can be found in Annex B.

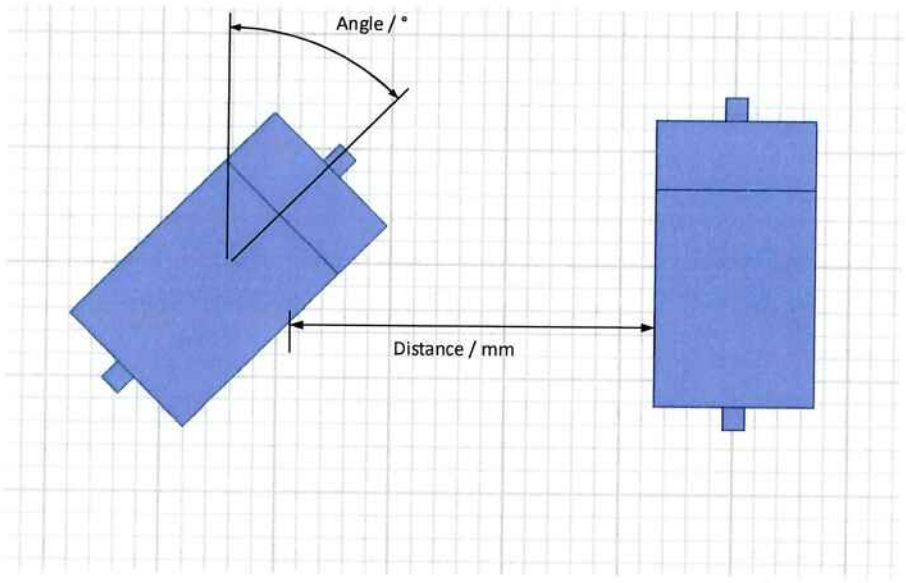

Figure 6.10.: Parameters for Parametric Sweep

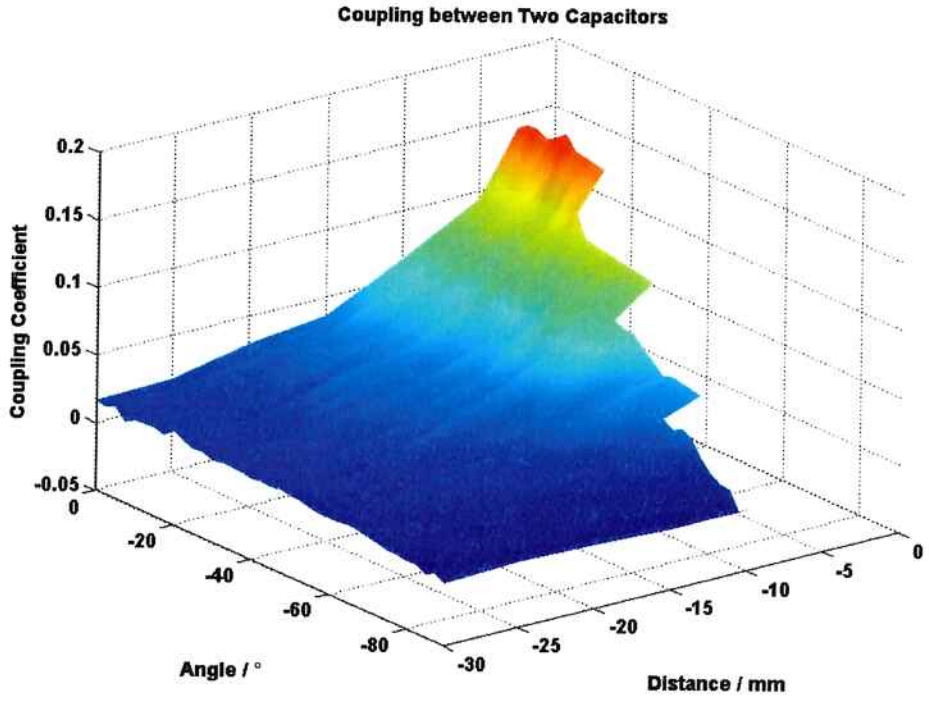

Figure 6.11.: Coupling Coefficient Plot

An increase on the core permeability is directly related to an increase on the equivalent series inductance and resistance for the common mode choke, according to Equations (3.3) and (3.2). This contributes for a higher common mode attenuation, and consequently an improvement in the common mode filter performance.

When a material with higher permeability is used, the stray flux is reduced because less flux lines close in the air. As a result, the stray inductance of the common mode choke is reduced, thus degrading the differential mode performance. This happens because, assuming a constant current, less stray flux results on a smaller inductance.

In Figures 6.12 and 6.13, the complex permeability curves of Vitroperm 500F and T35 Ferrite are plotted. For all frequencies in the range, the nanocrystalline material has a higher absolute permeability than the ferrite material.

Therefore, for a core of the same size, replacing ferrite with nanocrystalline material is going to increase the attenuation of the filter. Also, if an increase in the filter attenuation is not needed, it is possible to reduce the physical dimensions of the coils with the high permeability material. Additionally, with a fixed material volume different toroidal forms can be used. A bigger diameter provides a bigger inductance for the same material volume [22].

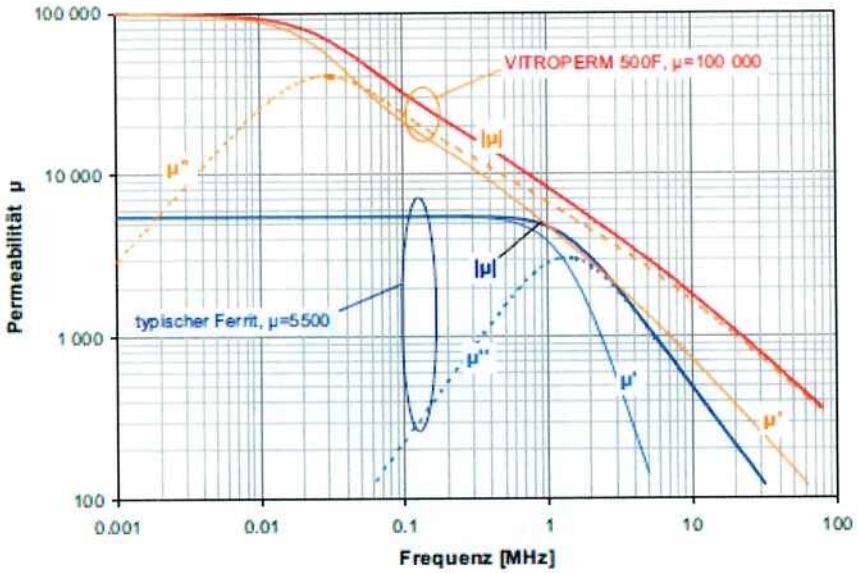

Figure 6.12.: Permeability Characteristic of Vitroperm 500F [43]

Two cores are tested in this work, the TDK/EPCOS T35B64290L0618X035 and the Vacuumschmelze T60006-L2040-W424. Since they have similar geometries, a comparison showing the advantages and disadvantages of each material is possible. Unfortunately, there are additional material costs when a

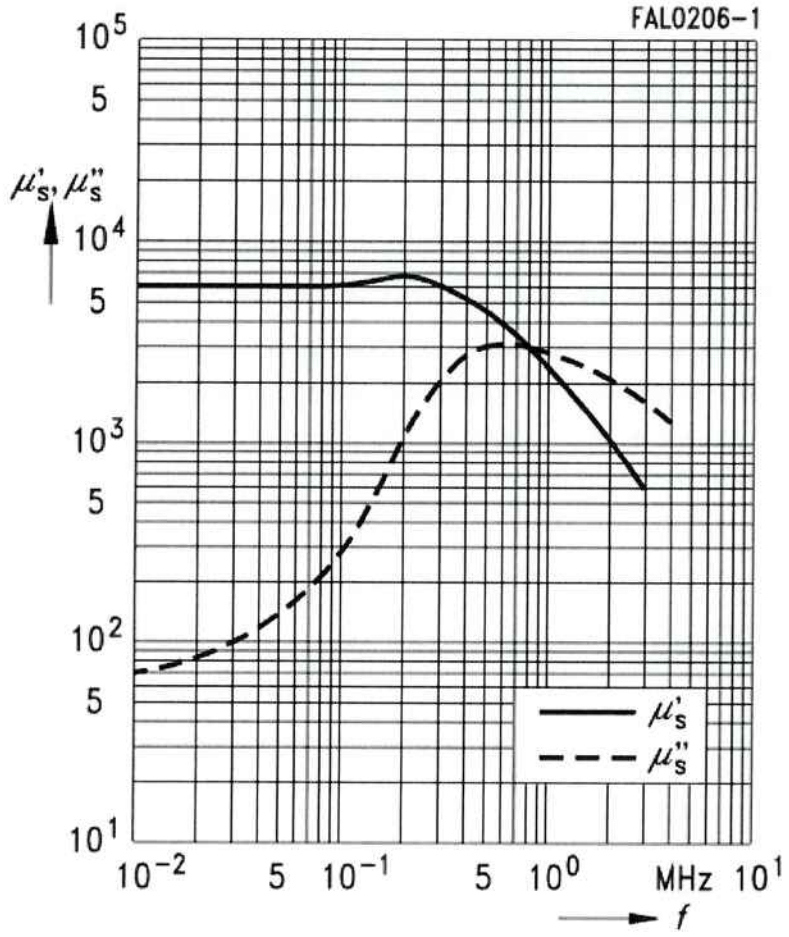

Figure 6.13.: Permeability Characteristic of T35 Ferrite [10]

better performing magnetic core of the same size is used. This is because the price per volume of the nanocrystalline material are higher than of the ferrite material.

Part 6.3: Design of the Reference and Optimized Filter

A - Introduction

A modular approach is used in the prototyping for evaluation of the filter performance with different chokes, capacitors banks and cancellation techniques. The list of the modules and their PCB sheets can be found in Table 6.2. With this approach, it is possible to create a filter prototype with different configurations just by swapping the filter modules.

The parallel stray capacitance canceling of the windings can be turned on and off on the common mode choke module. The compensated X and Y capacitor stages include the canceling coils for the stray inductance of the capacitors, and the uncompensated not.

At first, an approach with shifted PCB trace coils was implemented, however this arrangement has brought no improvement of the insertion loss characteristic. This is due to a design error. In order to correct this problem copper coil windings with a 4x4 turns in center tapped arrangement are soldered to the boards, and the compensation works correctly.

Table 6.2.: Modules List

Module	PCB Sheet in Annex...
Common Mode Choke (T35 and W424)	D.1
Compensated X Stage	D.2
Compensated Y Stage	D.3
Uncompensated X Stage	D.4
Uncompensated Y Stage	D.5

The filter arrangements built with the modules are listed in Table 6.3. The modules are connected in series as in Figure 6.19.

Table 6.3.: Filter Arrangements

Arrangement	Module 1	Module 2	Module 3
I	Compensated X Stage	T35 Common Mode Choke	Compensated Y Stage
II	Compensated X Stage	T35 Common Mode Choke	Compensated Y Stage
III	Uncompensated X Stage	W424 Common Mode Choke	Uncompensated Y Stage
IV	Uncompensated X Stage	W424 Common Mode Choke	Uncompensated Y Stage

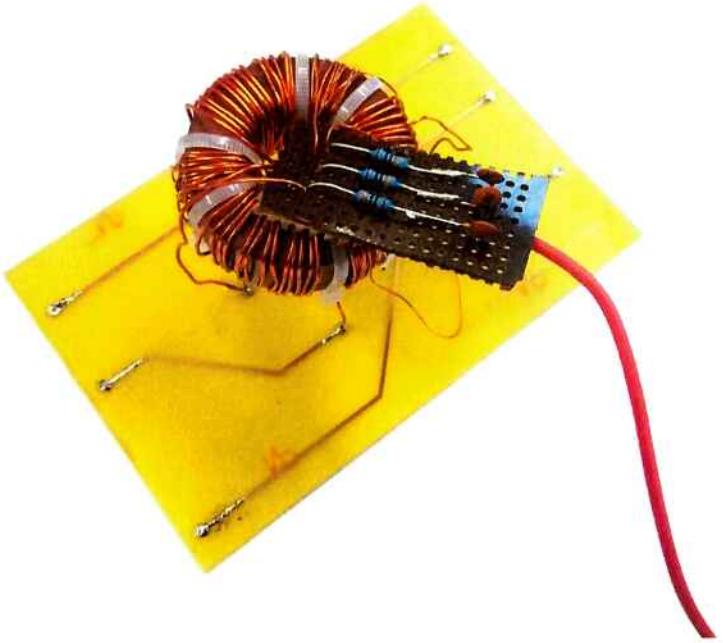

Figure 6.14.: Common Mode Choke

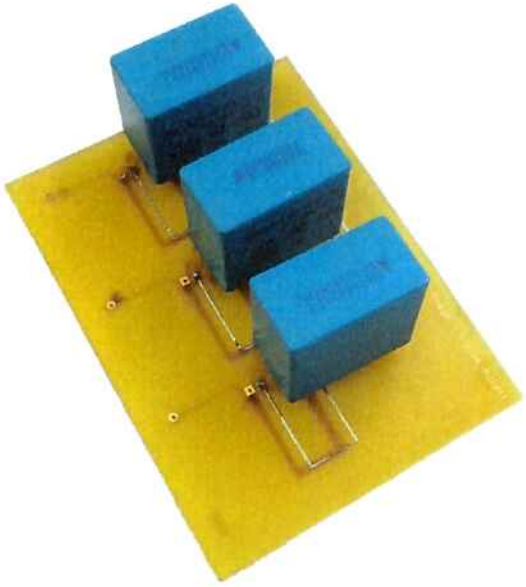

Figure 6.15.: X Capacitor Stage

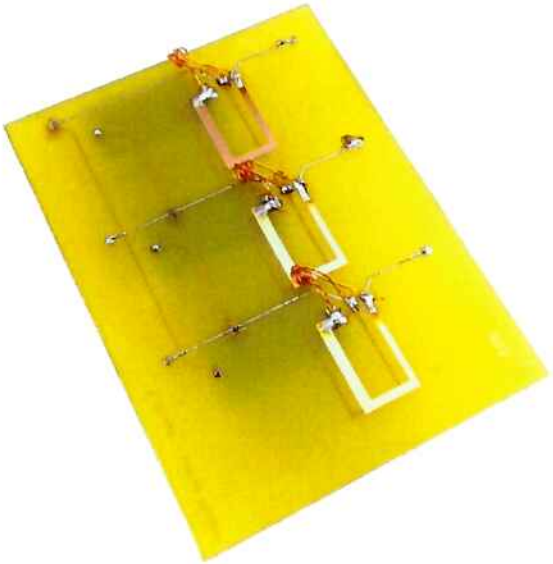

Figure 6.16.: X Capacitor Stage

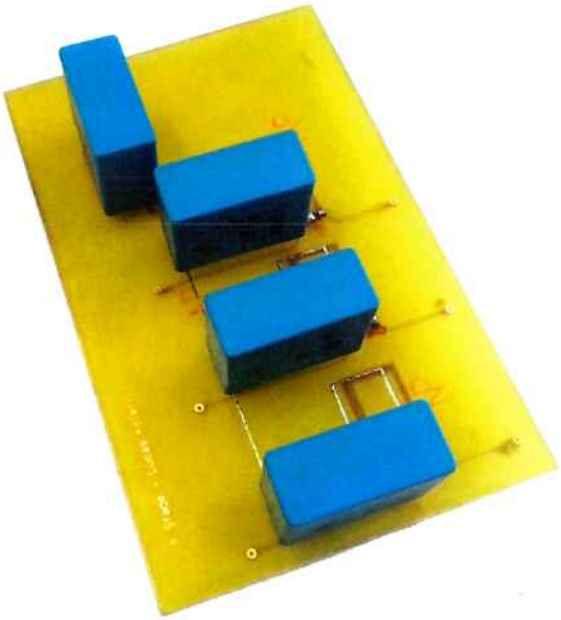

Figure 6.17.: Y Capacitor Stage

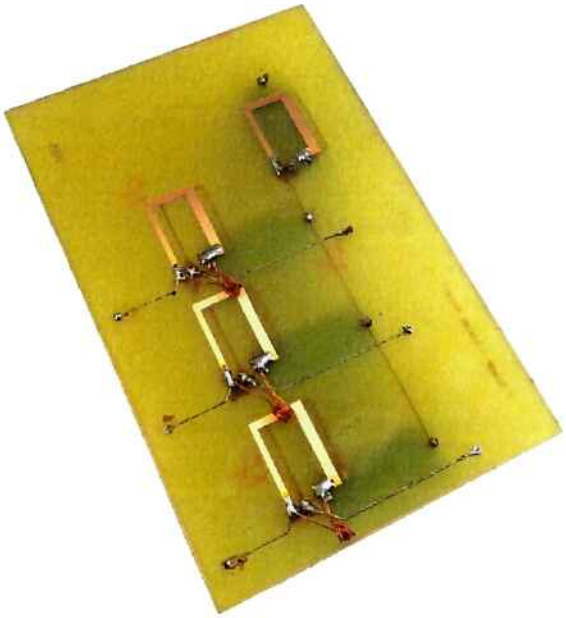

Figure 6.18.: Y Capacitor Stage

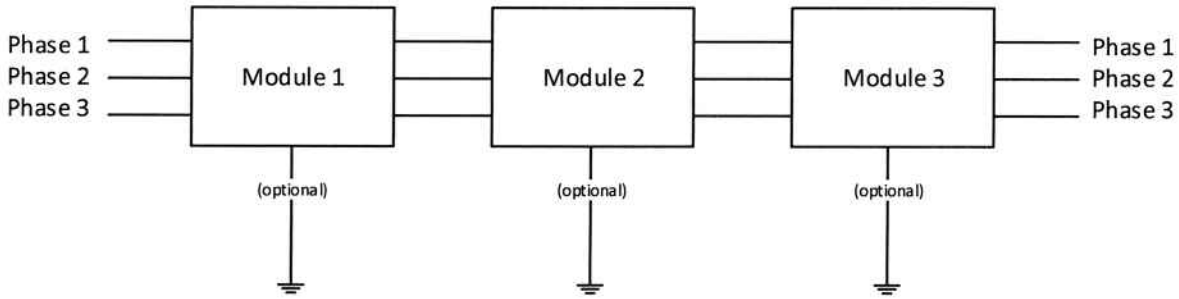

Figure 6.19.: Module Connection

B - Coils for Stray Inductance Cancelling

The use of copper wire coils for compensation is expensive and complex, and thus suitable for high-performance and experimental applications. In order to improve the economic viability, an approach that reduces the manufacturing effort is needed.

An alternative is to use planar coils in the PCB board. As the PCB board is already available in the filter, it does not increase manufacturing costs, as already mentioned. This approach is used in Section 6.

Part 6.4: Performance Evaluation of the Reference and Optimized Filter

In order to evaluate the performance of the arrangements the common mode and differential mode insertion losses are measured. In Table 6.4 the measurements are summarized.

Comparing the measurements 1 with 4 and 5 with 8, it is possible to see that the compensation techniques is improving the differential mode performance of the filter up to 25 dB. Comparing the measurements 9 with 12 and 13 with 16, the filter common mode performance improves in up to 15 dB with compensation.

Through comparison between measurements 1 and 2, 5 and 6, 10 and 11, 13 and 14, it is possible to conclude that the stray inductance canceling is improving the filter performance slightly in the frequency range starting at 200 kHz. From comparison between measurements 1 and 3, 5 and 7, 10 and 12, 13 and 15, it follows that the stray capacitance canceling is improving the filter performance significantly in the frequency range between 1 MHz and 10 MHz.

The measurements 1 and 9 contrast with the measurements 5 and 13 through the use of different cores. It is possible to see that the use of W424 instead of T35 increases the common mode insertion losses in up to 20 dB and the differential mode insertion losses in up to 10 dB.

Part 6.5: Deterioration of the Compensation Techniques through Secondary Stray Components

A - Effect of the Core Permeability in the Compensation of the Parallel Stray Capacitance

As mentioned in [27], the coupling coefficient between the compensation winding and the main winding is affecting the compensation strongly. In order to evaluate this effect, the windings and the core are modeled in Ansys Maxwell and a Parametric Logarithmic Sweep is done, calculating the coupling coefficient for different values of permeability. The results of the simulations are plotted in Figure 6.24. Then, the compensation is evaluated in LTSpice and the insertion losses for different coupling factors are plotted in Figure 6.25.

It is possible to conclude that in order to obtain the proper effect of the compensation technique, a coupling coefficient of at least 0.998 is needed. Thus, a relative permeability of at least 1000 is needed.

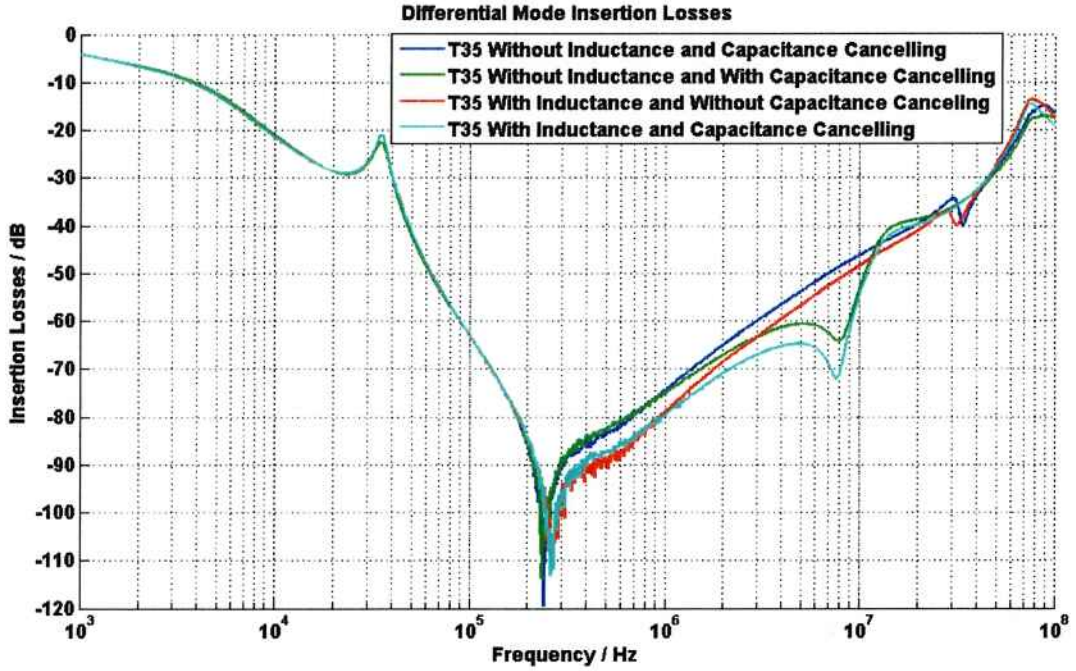

Figure 6.20.: Differential Mode Insertion Losses for T35 Core

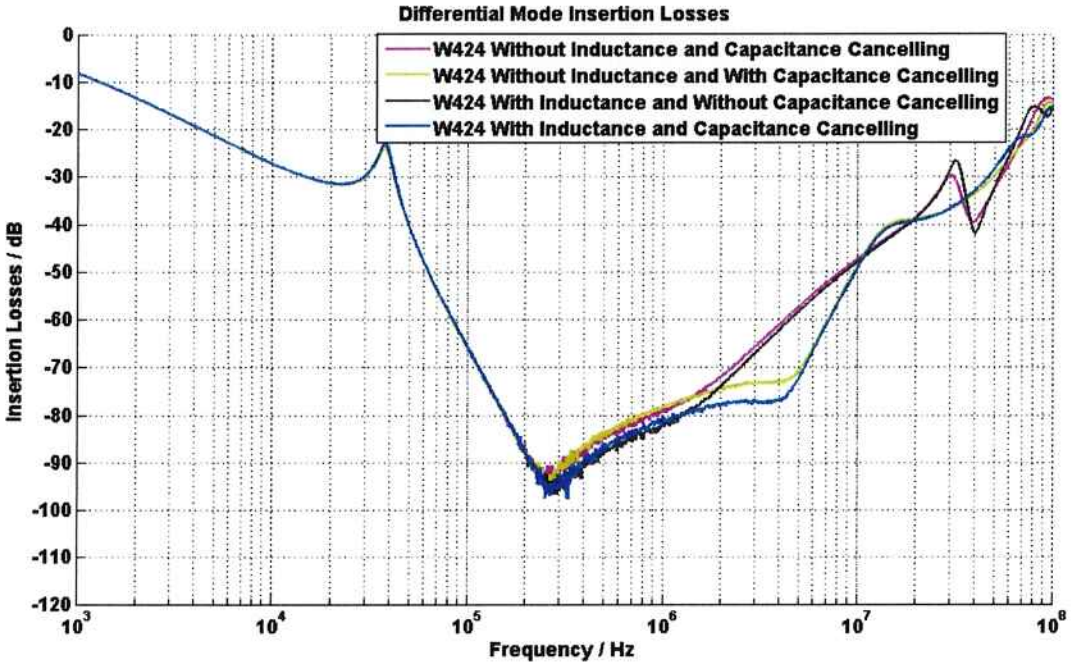

Figure 6.21.: Differential Mode Insertion Losses for W424

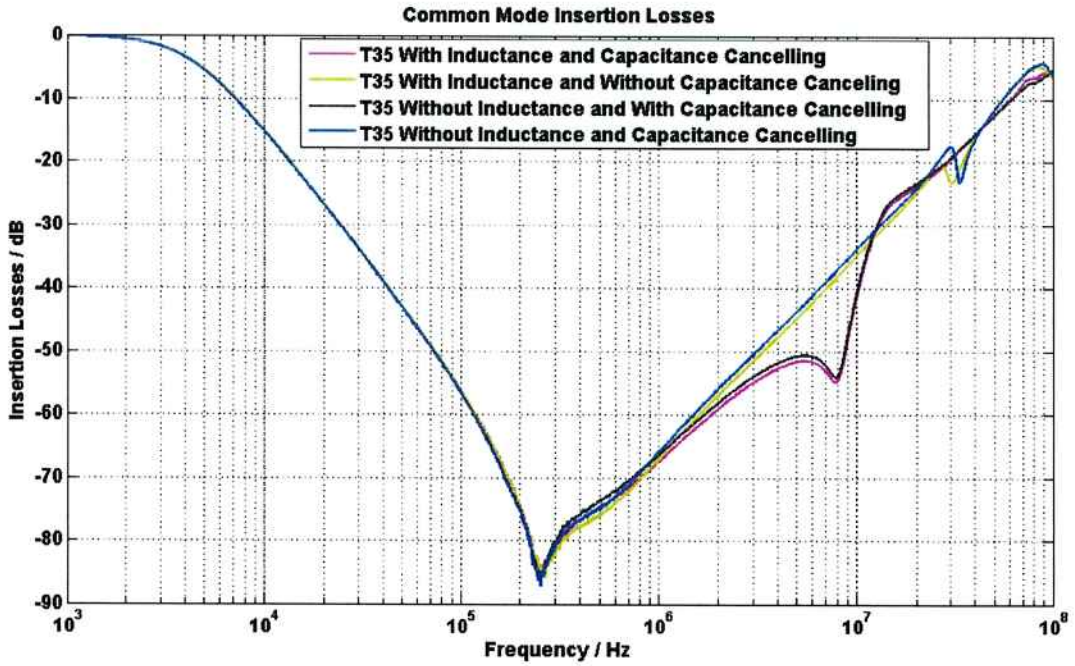

Figure 6.22.: Common Mode Insertion Losses for T35 Core

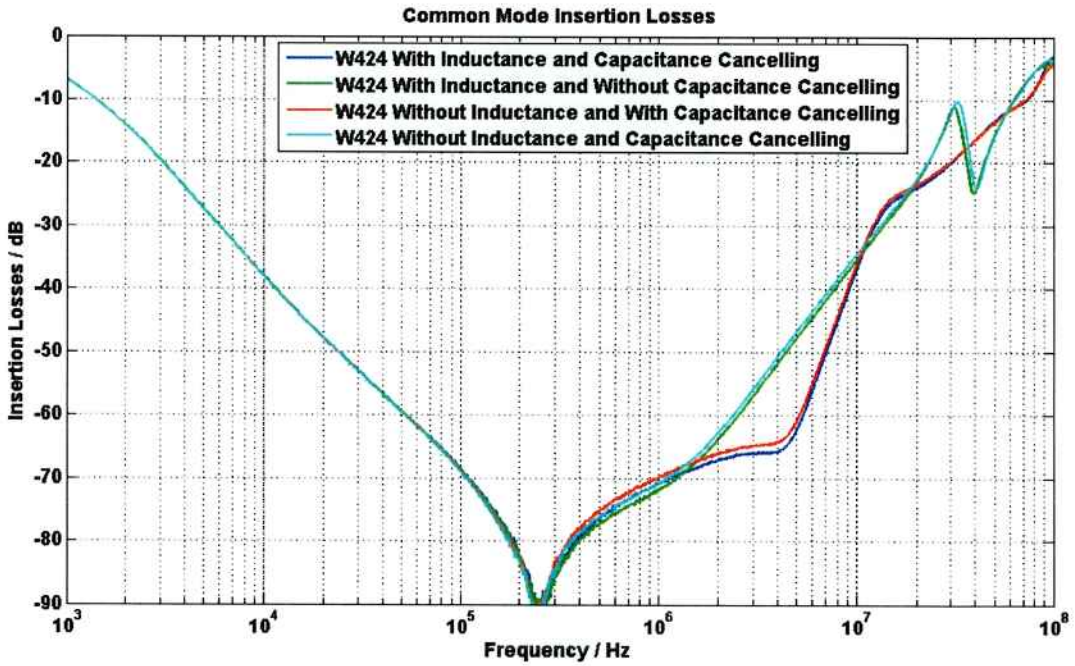

Figure 6.23.: Common Mode Insertion Losses for W424 Core

Table 6.4.: Measurements Summary

	Mode	Core Type	Stray Inductance Comp.	Stray Capacitance Comp.	Figure...
1	Differential Mode	T35	No	No	6.20
2	Differential Mode	T35	Yes	No	6.20
3	Differential Mode	T35	No	Yes	6.20
4	Differential Mode	T35	Yes	Yes	6.20
5	Differential Mode	W424	No	No	6.21
6	Differential Mode	W424	Yes	No	6.21
7	Differential Mode	W424	No	Yes	6.21
8	Differential Mode	W424	Yes	Yes	6.21
9	Common Mode	T35	No	No	6.22
10	Common Mode	T35	Yes	No	6.22
11	Common Mode	T35	No	Yes	6.22
12	Common Mode	T35	Yes	Yes	6.22
13	Common Mode	W424	No	No	6.23
14	Common Mode	W424	Yes	No	6.23
15	Common Mode	W424	No	Yes	6.23
16	Common Mode	W424	Yes	Yes	6.23

In Figures 6.12 and 6.13 it is possible to see that the permeability of the material decreases at higher frequencies. That means that the compensation is not going to work properly in frequencies starting at 10 MHz due to reduced permeability of the magnetic material. Unfortunately, this frequency range is important for the performance of the filter, as the norm limits conducted emissions up to 30 MHz.

Another drawback of this compensation technique is the complexity. It limits the application to high performance experimental applications and is not economically suitable for normal commercial applications, because of the additional windings and the additional passive components that have to be soldered at the board.

B - Effect of the Secondary Stray Effects in the Compensation of the Stray Inductance of the Capacitor

Unfortunately, the performance of the stray inductance canceling is deteriorated by the effect of secondary stray components. There is a stray capacitance between the primary and secondary coils, as well as stray capacitances of the coil to the earth. Additionally, there is a stray inductive coupling between the coil and the capacitor due to their proximity.

The equivalent circuit model of the stray inductance canceling with addition of the secondary stray components is represented in Figure 6.27. In Figure 6.28, the insertion losses of the capacitor without stray inductance canceling are compared with the ideal canceling without any additional stray effect and

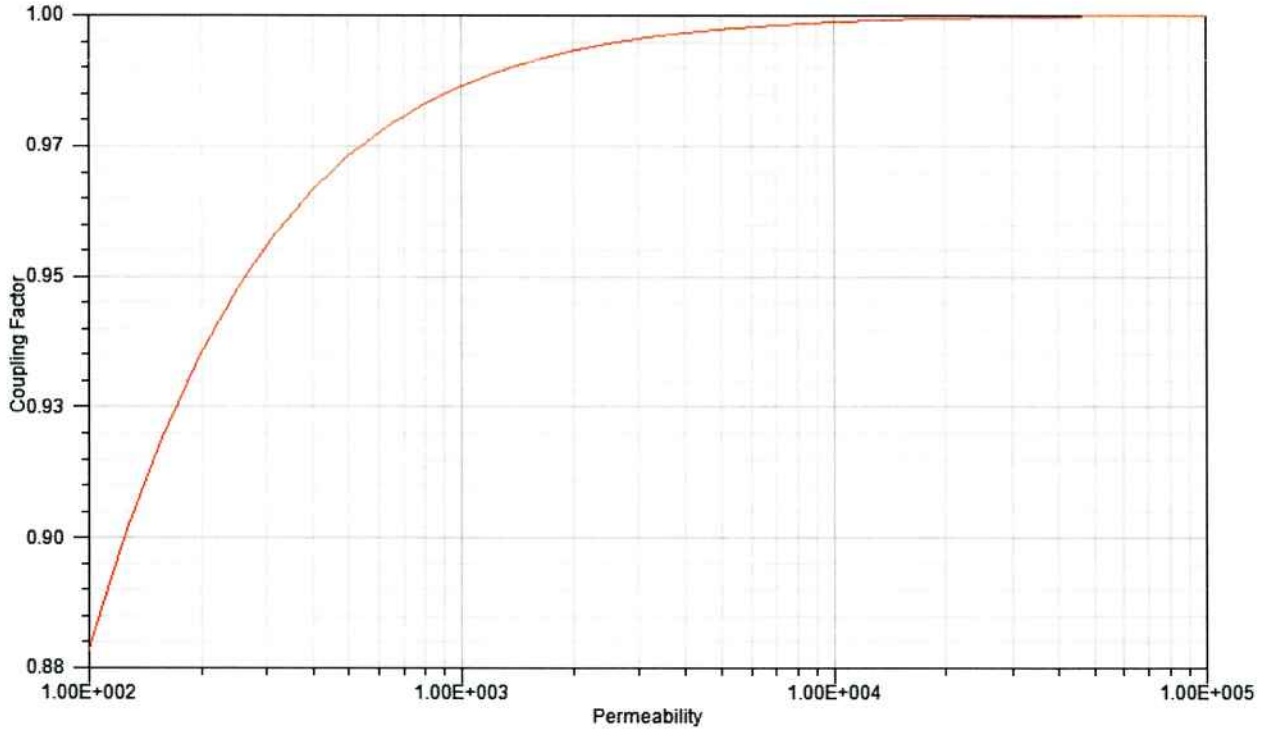

Figure 6.24.: Effect of the Permeability in the Coupling Factor

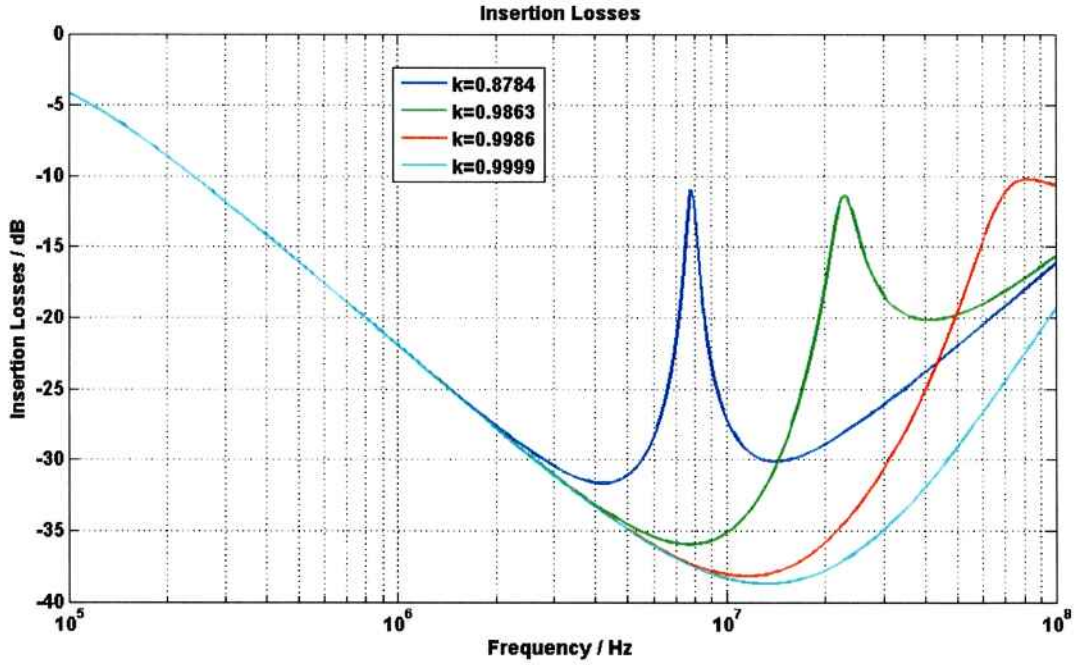

Figure 6.25.: Effect of the Coupling Factor on the Insertion Losses

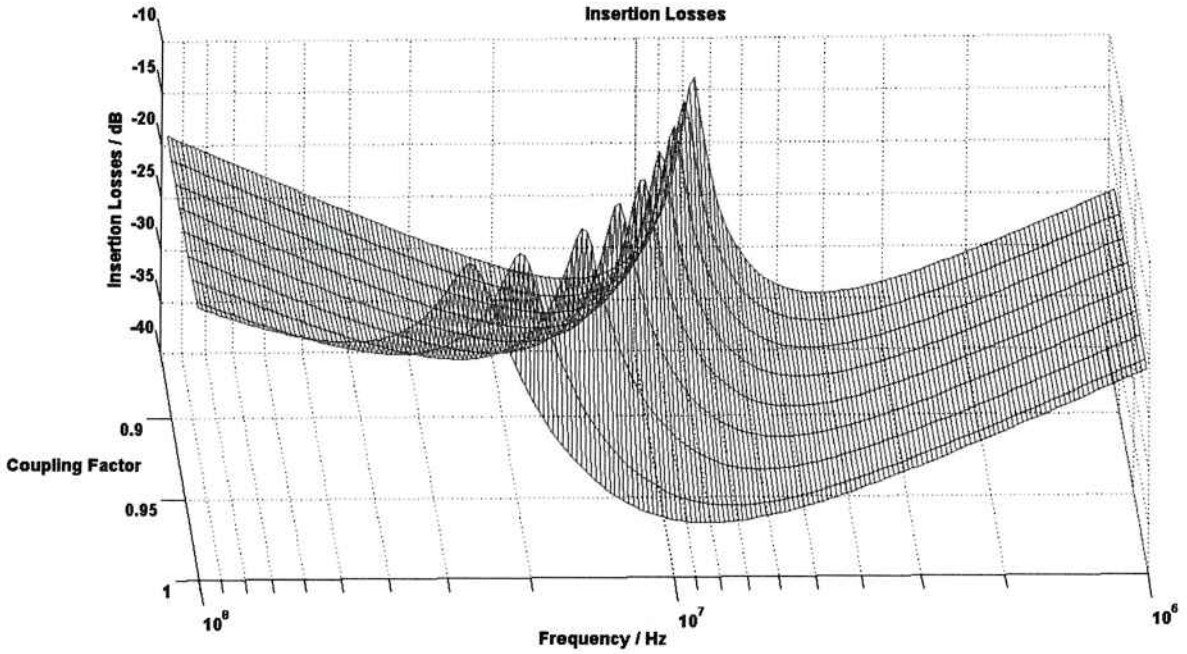

Figure 6.26.: Effect of the Coupling Factor on the Insertion Losses in Three Dimensions

with the complete circuit model with secondary stray components. The values of the parameters used in the simulations are listed in Table 6.5.

Based on the simulations in Figure 6.28 and the measurements in Figure 6.6 it is possible to conclude that the performance of the stray inductance canceling is limited to an increase of up to 20 dB in the insertion losses in the frequency range of interest (1 MHz to 30 MHz).

Table 6.5.: Secondary Stray Parameters

Parameter	Value
L_{11}	25 nH
L_{22}	120 nH
C_{str1}	0.2 pF
C_{str2}	1.1 pF
C_{str3}	1 pF
k_{str1}	0.05
k_{str2}	0.05
ΔL	5 nH

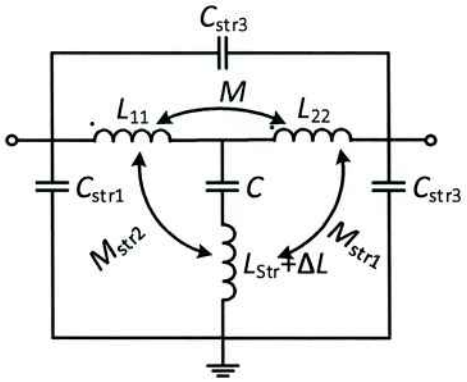

Figure 6.27.: Stray Components in the Compensation of the Stray Inductance

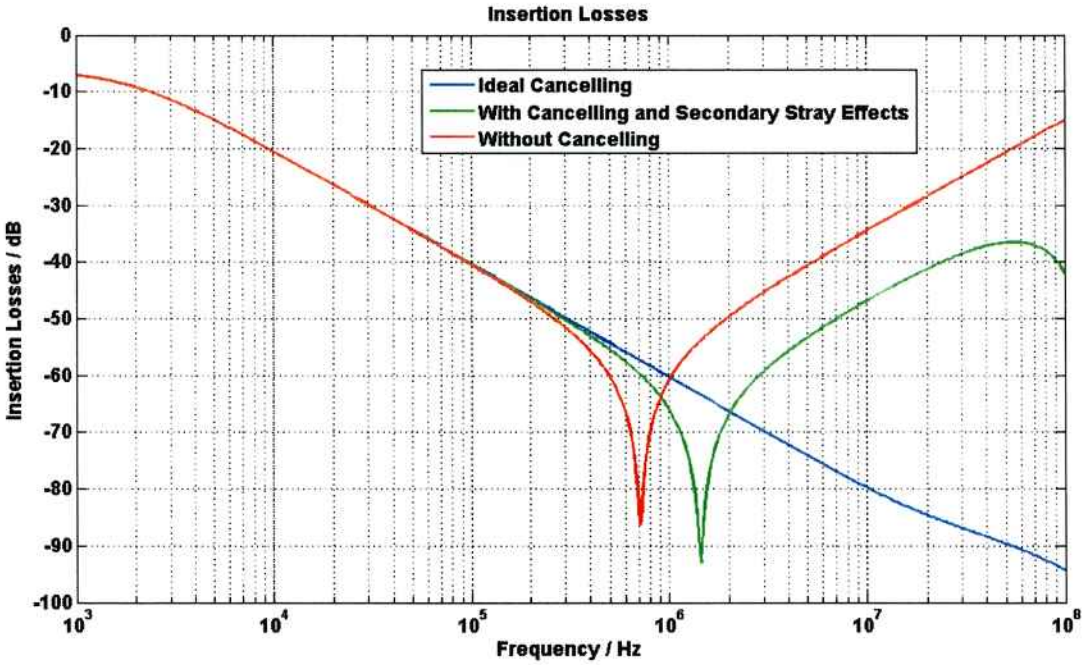

Figure 6.28.: Effect of Deterioration in Stray Inductance Cancelling

Part 6.6: Design of the Enhanced Filter

Using the optimization measures studied in this chapter an enhanced filter prototype is designed and built. It includes the same X and Y capacitor stages and the nanocrystalline core used in the modular filter.

The compensation of the parallel stray capacitance is also used in the enhanced filter prototype. As the common mode choke uses the same Vitroperm T60006-L2040-W424 core and same winding from the modular filter, the values of the compensation resistors and capacitors remain unchanged. The necessary components are now soldered in the PCB board, and not in an additional board as in Figure 6.14.

Additionally, instead of using copper wire coils for stray inductance canceling, the coils are now included in the PCB board. This approach minimizes the manufacturing process and is so effective as the prior one. In order to design the layout of the traces, simulations are done to determine the mutual inductance between the coils. The model is represented in Picture 6.30.

The primary and the secondary coils are designed as rectangular spirals with several turns. In order to maximize the mutual coupling, the secondary is placed inside of the primary coil. Care must be taken that value of the required mutual inductance is not exceeded, as excessive canceling degrades the capacitor performance. Also, the direction of the current flow is crucial. If it is inverted, the coupling factor is not negative anymore and the canceling coils are going to contribute to increase the equivalent series inductance of the capacitor, therefore causing more degradation.

The induced current in the secondary coil due to the current flow in the primary coil is simulated and the results plotted in Figure 6.31.

In Appendix D.6, the layout of the circuit board can be found. Figure 6.29 depicts the prototype. The common mode and differential mode insertion losses are measured and plotted in Figure 6.32 and 6.33, respectively. A comparison of between the prior art and the proposed design is offered in Table 6.6.

Table 6.6.: Comparison Between Reference Filter (Siemens) and Enhanced Prototype

Parameter	Prior Art	Enhanced Design	Relative Change
Filter Volume	5129 cm^3	6020 cm^3	17 %
Differential Mode Insertion Losses	85 dB @ 1.3 MHz	100 dB @ 1.3 MHz	18 %
Common Mode Insertion Losses	20 dB @ 20 KHz	50 dB @ 20 KHz	150 %
Estimated Material Costs	15.75EUR	34.63EUR	120 %

The prices used for the calculation of the material costs for the filter components that cost more than 0.10 EUR are listed below. They are obtained from the website from popular distributors in Europe in the July of 2015 and are subject to variations.

1. T35 ferrite core: 2.03 EUR (RS Components)
2. W424 Vitroperm core: 17.17 EUR (Mouser Electronics)

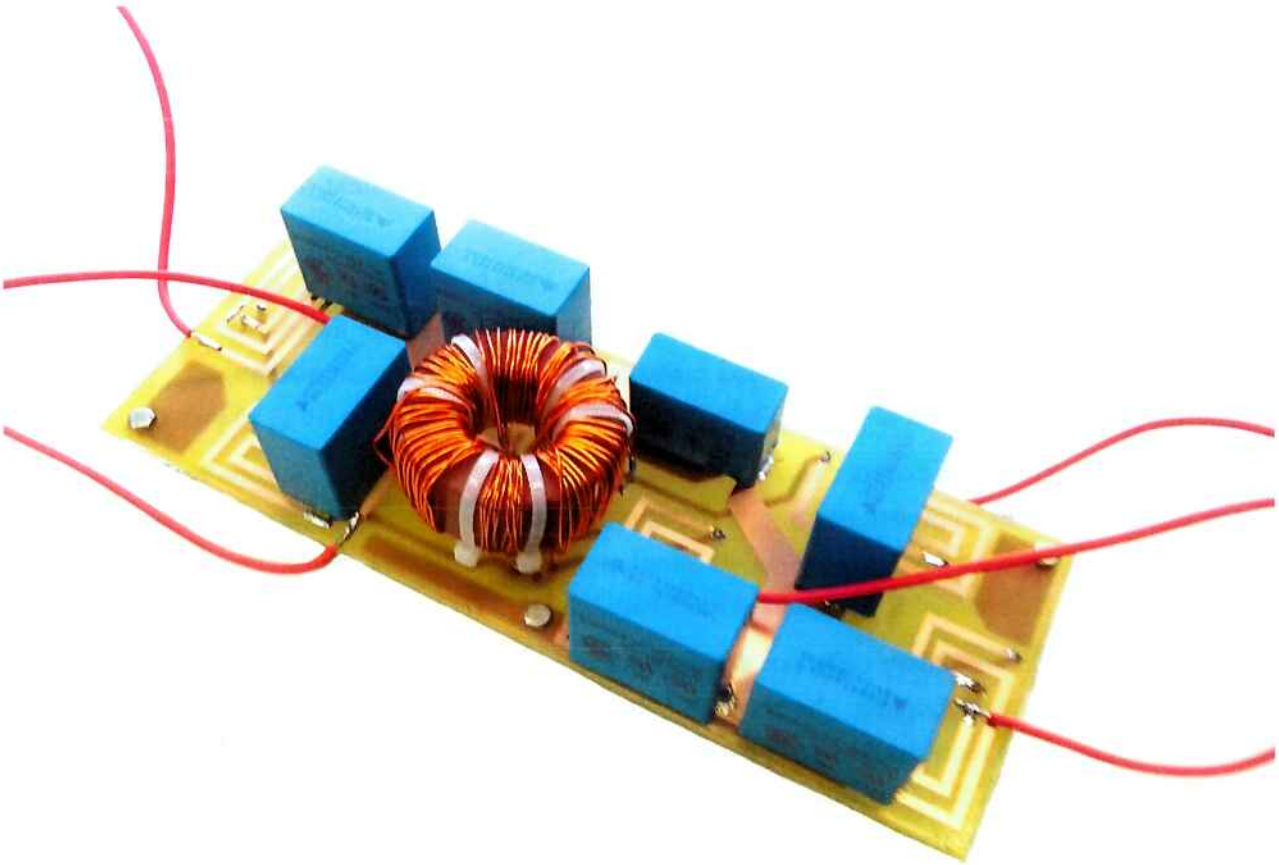

Figure 6.29.: Filter Prototype

3. Copper wire 1.5mm: 0.50 EUR/m (Farnell)
4. 2.2 μF capacitor: 0.89 EUR (RS Components)
5. 3.3 μF capacitor: 1.17 EUR (RS Components)
6. PCB board: 5.77 EUR (RS Components)

The common mode choke has an important role in the total material costs if nanocrystalline material is used. Independently of which core material is used, the capacitors are also decisive, as in total 7 units are needed.

Part 6.7: Determination of the Effect of the Number of Winding Turns on Common Mode Choke

The stray capacitance of one single-layer winding depends only on the number of turns and the turn-to-turn capacitances. It converges to a constant value for a higher number of turns, according to [25]. The turn-to-turn capacitances depend on the parameters of the winding such as wire gauge, coil radius and distance between turns.

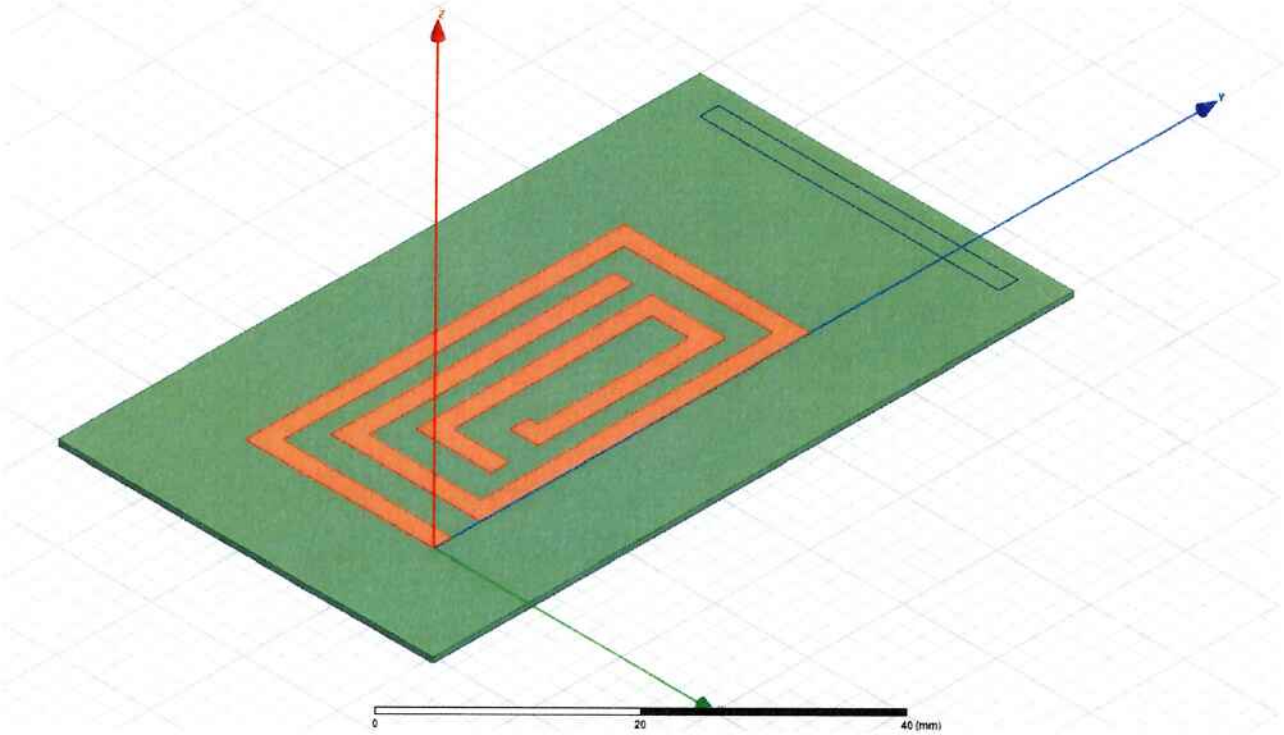

Figure 6.30.: Cancelling PCB Coil Geometry

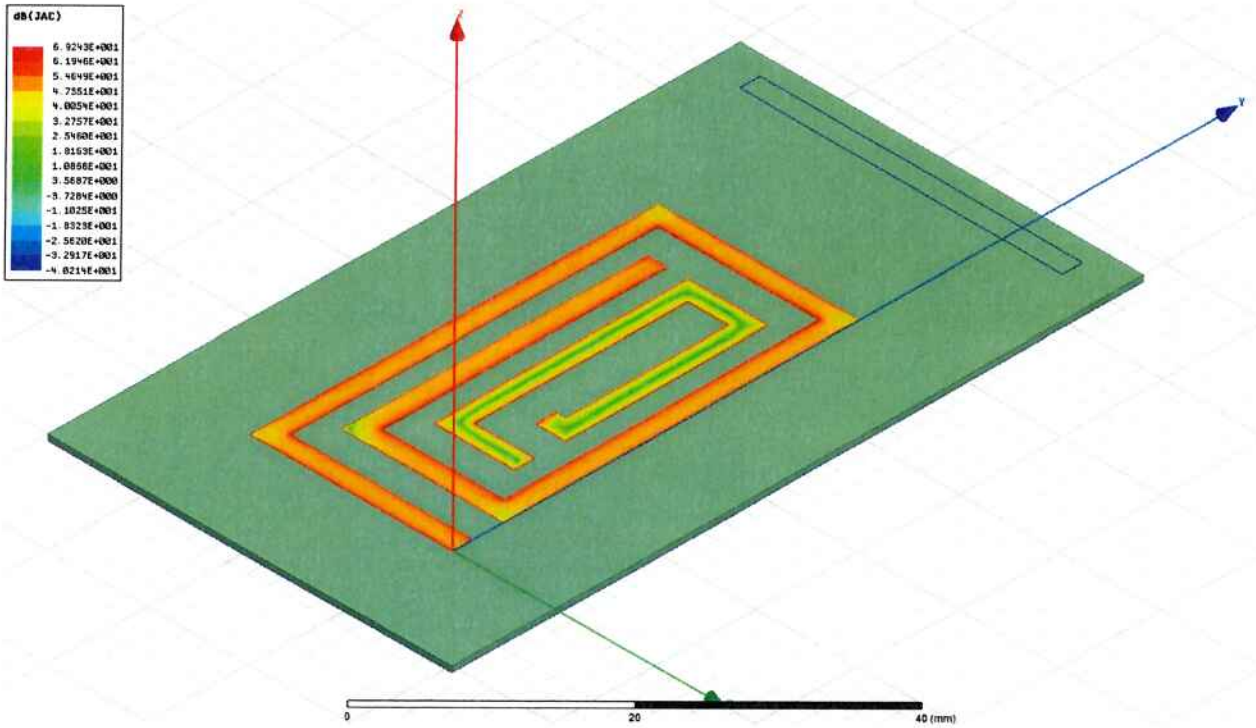

Figure 6.31.: Induction of Current Between Two Coils

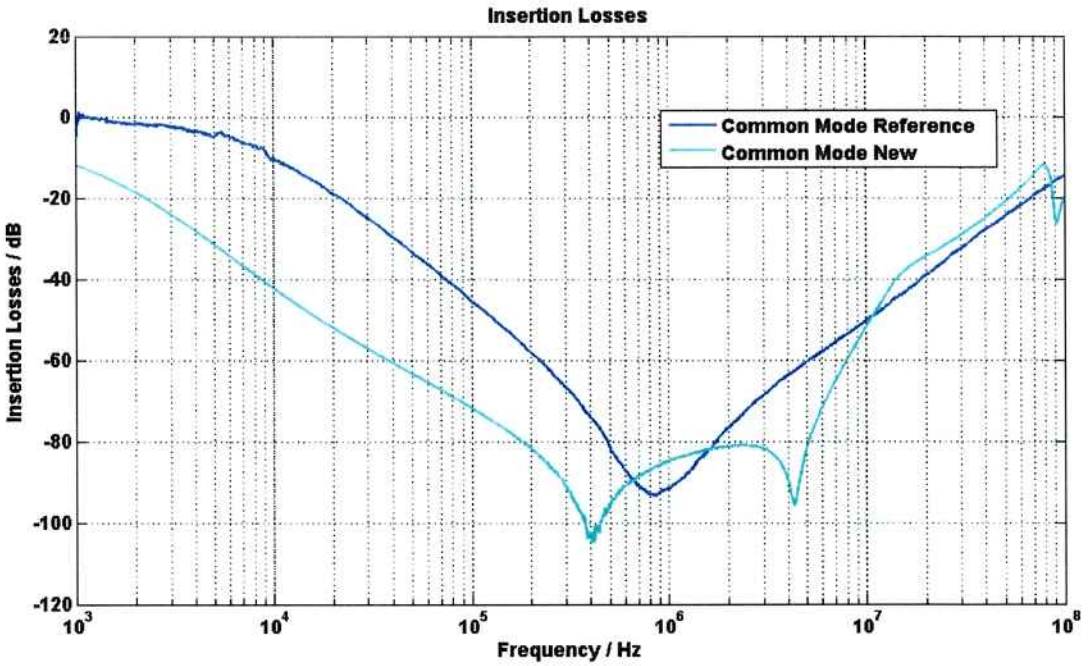

Figure 6.32.: Common Mode Insertion Losses

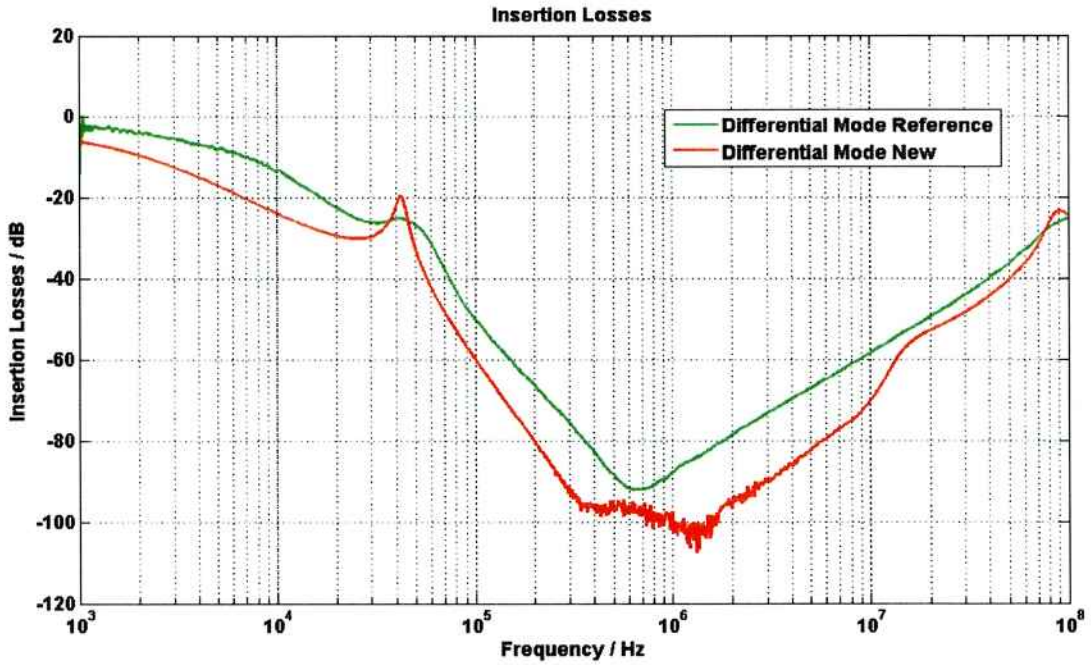

Figure 6.33.: Differential Mode Insertion Losses

The winding is modeled as an inductor and a stray capacitor connected in parallel to it. The resonant frequency of this circuit is calculated in Equation 6.6.

$$f_o = \frac{1}{2 \cdot \pi \cdot \sqrt{L \cdot C}} \tag{6.6}$$

It is possible to see in Equation 6.7 that the inductance of a coil depends on the number of turns of the winding and from the magnetic reluctance, which depends on the permeability, cross section area and length of the core material.

$$L = \frac{N^2}{R_m} \tag{6.7}$$

Substituting 6.7 on 6.6, Equation 6.8 results.

$$f_o = \frac{\sqrt{R_m}}{2 \cdot \pi \cdot N \cdot \sqrt{C}} \tag{6.8}$$

For two windings with different number of turns, it results the relation expressed in Equation 6.9.

$$\frac{f_1}{f_2} = \frac{N_2}{N_1} \cdot \sqrt{\frac{C_2}{C_1}} \tag{6.9}$$

Measurements are made in order to determine if the stray capacitance does not change for a higher number of winding turns. The insertion losses are plotted in Figure 6.34. It is important to note that the same core is used in all experiments. The resonant frequencies are summarized in Table 6.7. With the ratio of the resonant frequencies of coils with two different number of turns, the relationship of the stray capacitance of the windings is calculated.

In Table 6.8, the results of the calculations of the stray capacitance ratios are represented. It is possible to see that the relative change of the stray capacitance is smaller for windings with higher number of turns. That means that the stray capacitance converges, as expected.

Therefore, the method used in Chapter 2 to calculate the parallel stray capacitance of the coils is valid, and can be used for further estimations with different arrangements, given that the number of coil windings is higher than 10.

Table 6.7.: Resonant Frequencies

Number of Turns	Resonant Frequency
9	91 MHz
12	58 MHz
15	42 MHz
18	36 MHz

Table 6.8.: Stray Capacitance Ratios

Winding Turns Change	Stray Capacitance Ratio
9 to 12	1.41
12 to 15	1.21
15 to 18	1.06

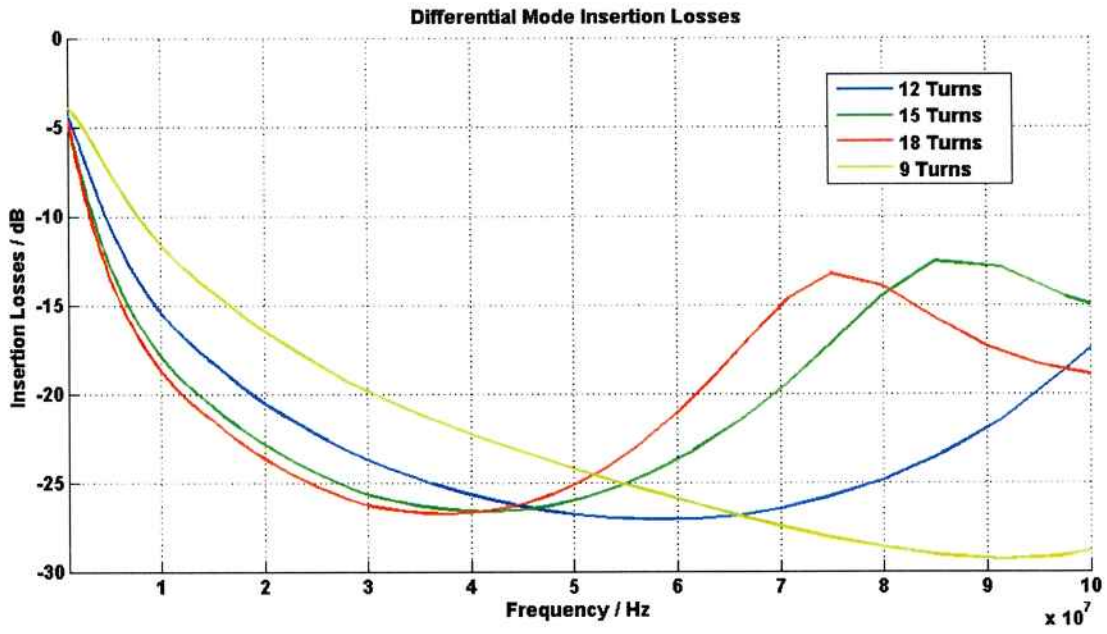

Figure 6.34.: Differential More Insertion Losses for Different Number of Turns

Part 6.8: Summary of Optimization

In the optimization process, the most relevant stray components are assessed and the literature is searched for the compensation techniques available. These techniques involve compensation of the stray inductances and the stray capacitances. Additionally, the stray couplings and the core material of the common mode choke are improved. For evaluation purposes, a set of modules is built, and the performance of different filter arrangements is tested.

The results of the tests show that the compensation techniques used are effective. However, they are subject to deterioration due to secondary stray components, and unfortunately the performance of the ideal filter cannot be reached. The effectiveness of the cancellation techniques are determined, with both measurements and simulations.

Afterwards, an enhanced filter prototype is projected and built using the knowledge acquired from the modeling of the filter. Its performance is evaluated and compared with the reference filter studied in the first chapters of this work.

The common mode insertion losses are increased in 150 % and the differential mode insertion losses are increased in 18 %. On the other side, the filter volume is increased in 17 % and the estimated material costs in 120 %. The main shortcoming of the proposed optimization techniques is the increase of the costs, however, they are in the range of economical viability.

7 Conclusion

Part 7.1: Stray Components and Couplings and their Effect

In order to reduce the electromagnetic interference emitted by power electronic devices, passive EMI filters have to be applied. These filters are intended to attenuate these emissions and comply with the ruling norms.

However, the behavior of the filters differ strongly from the expectations. This is due to the stray components, which degrade the damping characteristics of the filter significantly at higher frequencies. Experimental and simulation results shows that the filter insertion losses of the real filter start to differ strongly compared to the ideal filter at 1 MHz.

The stray components are originated from magnetic and/or electric fields. The degradation of the filter performance is caused by stray inductances or stray capacitances of the filter elements. Stray inductive couplings or stray capacitive couplings between filter elements also cause degradation.

Finite element analysis is used to derive the inductance and capacitance matrices, and thereby obtain the values of the stray components and couplings. To simplify further modeling and development, the stray components are added to the equivalent circuit model of the filter. The common mode and differential mode insertion losses of the filter are simulated.

To validate the simulations, the common mode and differential mode insertion losses of the filter are measured using a network analyzer and compared with simulations. The validation process was successful, with a tolerance of 10 %.

With that, a validated model of the filter is created. This allows prediction of the filter behavior with different simulated noise sources and line impedances. The simulations and the validation are done for one reference filter topology, but can also be extended to foresee the attenuation of filters with more complex topologies and of 4-wire filters as well.

Part 7.2: Comparison of the Stray Components Relevance

With the finite element analysis, the stray inductances and capacitances and stray inductive and capacitive couplings in the filter are obtained. However, they do not have the same impact on the performance of the filter. Hence, they are classified as most relevant, relevant and not relevant.

The calculated parameters are split up in two categories, stray components of filter elements themselves (stray components) and stray couplings between filter elements (stray couplings). These categories are then subdivided in three subcategories, most relevant, relevant and not relevant.

In this analysis, it is concluded that the stray inductance of the capacitor and the stray capacitance of the coils are the most relevant stray components for the filter model.

The coupling between the X capacitors, the coupling between the Y capacitors and the coupling between the filter components and the housing are classified as relevant. Not relevant is the coupling between the X and Y capacitors and the common mode choke, the coupling between X and Y capacitors, the coupling between coil windings and the couplings in the PCB itself and with other components.

The magnetic permeability characteristic of the material used on the core of the common mode choke is not classified as a stray component but affects the filter significantly. Another parasitics, such as the skin effect and the proximity effect, are not considered in this work.

To focus in the optimization and compensation of not relevant stray components and stray couplings is not reasonable, as the degradation of the filter insertion losses caused by them is smaller than 10 dB.

Part 7.3: Optimization and Improvement of the Filter

A literature research is done on the state-of-the-art of filter optimization and improvement. The most relevant stray components, together with the core material, are subject of the improvement process. As they degrade the filter performance significantly, the efforts invested in their compensation lead to the highest improvements.

Coupled magnetic windings are used to compensate the stray inductance of the capacitors. Based on the principle of one transformer, this technique cancels the parasitic effect using a negative mutual inductance. It also adds inductance in the series branch, a desirable side effect.

Injection of a compensation current from an additional winding connected to a capacitor is used to compensate the parallel stray capacitance of the coils. Use of an additional series resistance in the compensation circuit attenuates the resonance between the additional capacitor and the stray inductance of the winding.

Replacement of the ferrite core of the common mode choke core with a nanocrystalline one improves the common mode attenuation of the filter substantially. Unfortunately this increases the material price of the filter.

In order to evaluate the effectiveness of the aforementioned optimization techniques isolated or together, a modular filter prototype is built. The compensation techniques are found to be effective.

Further, a prototype of an enhanced filter is designed. The filter common mode and differential mode attenuation is improved by 150 % and 18 %, respectively, with an increase of material costs of 120 % .

Part 7.4: Future Work

The stray inductance canceling for the capacitors and the parallel stray capacitance compensation for the common mode choke can be applied to the reference filter from Siemens for further evaluation. The number of stages for common mode and differential mode filtration, the structure of those stages,

the arrangement of the common mode and differential mode arrangements between each other and the values and type of the used passive components of the filter can be changed in order to improve the attenuation.

Through combination of multiple cores with different permeabilities in the common mode choke it should be possible to further improve the frequency behavior of the filter. This multi-material core can be applied to one of the filter arrangements. The proposed compensation techniques for the stray components should be investigated, in order to determine if the side effects affect their viability in complex multi-stage filter arrangements.

The filters can also be tested in the working environment. For example, as a part of the installation according to the EN55017 standard, a test receiver together with a line impedance stabilization network can measure the spectrum of emissions of different converters, with and without filtering. Finite element simulations of the filter including the cancellation measures can be done. Additionally, the filter model can be represented as a transfer function or in matrix form to enable insertion in other simulation tools. The model of the filter together with the model of the active front end can be simulated and later on be validated with an experimental arrangement.

A Inductive and Capacitive Coupling Matrices

Inductance

Inductances in mH	Coil 1	Coil 2	Coil 3	X Capacitor 1	X Capacitor 2	X Capacitor 3	Y Capacitor 1	Y Capacitor 2	Y Capacitor 3	Y Capacitor 4
Coil 1	2,31E-03	2,27E-03	2,27E-03	-6,92E-07	-9,86E-07	-6,62E-07	-2,34E-07	-3,34E-07	-2,64E-07	-2,06E-07
Coil 2	2,27E-03	2,31E-03	2,27E-03	3,04E-07	5,63E-07	6,77E-07	2,25E-07	1,72E-07	1,41E-08	6,31E-07
Coil 3	2,27E-03	2,27E-03	2,31E-03	3,46E-07	3,30E-07	2,30E-09	7,96E-09	1,35E-07	2,33E-07	-4,83E-07
X Capacitor 1	-6,92E-07	3,04E-07	3,46E-07	9,08E-06	1,28E-06	2,29E-07	-8,92E-09	-1,11E-08	-9,56E-09	-2,58E-09
X Capacitor 2	-9,86E-07	5,63E-07	3,30E-07	1,28E-06	8,58E-06	1,02E-06	-1,05E-08	-1,54E-08	-1,57E-08	5,73E-09
X Capacitor 3	-6,62E-07	6,77E-07	2,30E-09	2,29E-07	1,02E-06	8,65E-06	-1,33E-08	-2,29E-08	-2,62E-08	1,98E-08
Y Capacitor 1	-2,34E-07	2,25E-07	7,96E-09	-8,92E-09	-1,05E-08	-1,33E-08	8,83E-06	1,16E-06	2,53E-07	2,44E-07
Y Capacitor 2	-3,34E-07	1,72E-07	1,35E-07	-1,11E-08	-1,54E-08	-2,29E-08	1,16E-06	8,74E-06	1,21E-06	4,61E-07
Y Capacitor 3	-2,64E-07	1,41E-08	2,33E-07	-9,56E-09	-1,57E-08	-2,62E-08	2,53E-07	1,21E-06	8,85E-06	-2,88E-07
Y Capacitor 4	-2,06E-07	6,31E-07	-4,83E-07	-2,58E-09	5,73E-09	1,98E-08	2,44E-07	4,61E-07	-2,88E-07	8,81E-06

Inductive Coupling Coefficient

	Coil 1	Coil 2	Coil 3	X Capacitor 1	X Capacitor 2	X Capacitor 3	Y Capacitor 1	Y Capacitor 2	Y Capacitor 3	Y Capacitor 4
Coil 1		0,98622	0,98612	-0,0047818	-0,0070128	-0,0046841	-0,0016426	-0,002352	-0,0018499	-0,0014478
Coil 2	0,98622		0,9863	0,0020989	0,0040018	0,0047901	0,001574	0,0012126	0,000098527	0,004431
Coil 3	0,98612	0,9863		0,0023917	0,0023455	0,00001625	0,000055802	0,00094981	0,001631	-0,0033927
X Capacitor 1	-0,0047818	0,0020989	0,0023917		0,14456	0,025865	-0,00099605	-0,0012419	-0,001067	-0,0002891
X Capacitor 2	-0,0070128	0,0040018	0,0023455	0,14456		0,11881	-0,001208	-0,001782	-0,0018019	0,00065971
X Capacitor 3	-0,0046841	0,0047901	0,00001625	0,025865	0,11881		-0,0015254	-0,0026337	-0,0029918	0,0022717
Y Capacitor 1	-0,0016426	0,001574	0,000055802	-0,00099605	-0,001208	-0,0015254		0,13149	0,028665	0,027625
Y Capacitor 2	-0,002352	0,0012126	0,00094981	-0,0012419	-0,001782	-0,0026337	0,13149		0,13706	0,052576
Y Capacitor 3	-0,0018499	9,8527E-05	0,001631	-0,001067	-0,0018019	-0,0029918	0,028665	0,13706		-0,032584
Y Capacitor 4	-0,0014478	0,004431	-0,0033927	-0,0002891	0,00065971	0,0022717	0,027625	0,052576	-0,032584	

Figure A.1.: Inductance Table and Coupling Coefficient Table

Capacitance

Capacitances in pF	X Capacitor 1	X Capacitor 2	X Capacitor 3	Y Capacitor 1	Y Capacitor 2	Y Capacitor 3	Y Capacitor 4	Coil 1	Coil 2	Coil 3	Ground
X Capacitor 1		-2,21E+00	-2,57E-03	-6,09E-06	-6,09E-06	-6,09E-06	-6,09E-06	-7,21E-02	-5,25E-03	-8,59E-05	-3,49E+04
X Capacitor 2	-2,21E+00		-1,33E+00	-7,75E-07	-7,75E-07	-7,75E-07	-7,75E-07	-1,23E-01	-8,61E-04	-1,36E-03	-2,77E+04
X Capacitor 3	-2,57E-03	-1,33E+00		-7,01E-08	-7,01E-08	-7,01E-08	-7,01E-08	-1,19E-01	-7,99E-05	-2,52E-02	-3,45E+04
Y Capacitor 1	-6,09E-06	-7,75E-07	-7,01E-08		-1,63E+00	-6,64E-03	-4,83E-02	-4,75E-05	-1,09E-02	-3,24E-04	-3,38E+04
Y Capacitor 2	-1,14E-06	-1,47E-07	-5,86E-08	-1,63E+00		-1,63E+00	-7,31E-01	-9,49E-06	-3,94E-03	-2,38E-04	-2,42E+04
Y Capacitor 3	-5,24E-09	-8,29E-08	-3,71E-06	-6,64E-03	-1,63E+00		-4,13E-01	-3,05E-06	-2,79E-05	-5,31E-04	-3,17E+04
Y Capacitor 4	-7,45E-06	-4,16E-06	-1,36E-04	-4,83E-02	-7,31E-01	-4,13E-01		-2,15E-04	-1,45E-01	-1,52E-01	-2,57E+04
Coil 1	-7,21E-02	-1,23E-01	-1,19E-01	-4,75E-05	-9,49E-06	-3,05E-06	-2,15E-04		-2,11E+00	-2,17E+00	-2,11E+04
Coil 2	-5,25E-03	-8,61E-04	-7,99E-05	-1,09E-02	-3,94E-03	-2,79E-05	-1,45E-01	-2,11E+00		-2,15E+00	-2,25E+04
Coil 3	-8,59E-05	-1,36E-03	-2,52E-02	-3,24E-04	-2,38E-04	-5,31E-04	-1,52E-01	-2,17E+00	-2,15E+00		-2,24E+04
Ground	-3,49E+00	-2,77E+00	-3,45E+00	-3,38E+00	-2,42E+00	-3,17E+00	-2,57E+00	-2,11E+00	-2,25E+00	-2,24E+00	

Capacitive Coupling Coefficient

	X Capacitor 1	X Capacitor 2	X Capacitor 3	Y Capacitor 1	Y Capacitor 2	Y Capacitor 3	Y Capacitor 4	Coil 1	Coil 2	Coil 3	Ground
X Capacitor 1		-3,63E-01	-4,82E-04	-1,12E-06	-1,87E-07	-9,53E-10	-1,54E-06	-1,16E-02	-8,45E-04	-1,37E-05	-2,75E-01
X Capacitor 2	-3,63E-01		-2,36E-01	-1,36E-07	-2,29E-08	-1,43E-08	-8,13E-07	-1,87E-02	-1,31E-04	-2,06E-04	-2,07E-01
X Capacitor 3	-4,82E-04	-2,36E-01		-1,40E-08	-1,04E-08	-7,31E-07	-3,05E-05	-2,06E-02	-1,39E-05	-4,38E-03	-2,95E-01
Y Capacitor 1	-1,12E-06	-1,36E-07	-1,40E-08		-2,86E-01	-1,29E-03	-1,06E-02	-8,14E-06	-1,88E-03	-5,53E-05	-2,84E-01
Y Capacitor 2	-1,87E-07	-2,29E-08	-1,04E-08	-2,86E-01		-2,81E-01	-1,43E-01	-1,45E-06	-6,02E-04	-3,61E-05	-1,81E-01
Y Capacitor 3	-9,53E-10	-1,43E-08	-7,31E-07	-1,29E-03	-2,81E-01		-8,97E-02	-5,15E-07	-4,72E-06	-8,95E-05	-2,63E-01
Y Capacitor 4	-1,54E-06	-8,13E-07	-3,05E-05	-1,06E-02	-1,43E-01	-8,97E-02		-4,13E-05	-2,79E-02	-2,90E-02	-2,42E-01
Coil 1	-1,16E-02	-1,87E-02	-2,06E-02	-8,14E-06	-1,45E-06	-5,15E-07	-4,13E-05		-3,15E-01	-3,23E-01	-1,54E-01
Coil 2	-8,45E-04	-1,31E-04	-1,39E-05	-1,88E-03	-6,02E-04	-4,72E-06	-2,79E-02	-3,15E-01		-3,20E-01	-1,65E-01
Coil 3	-1,37E-05	-2,06E-04	-4,38E-03	-5,53E-05	-3,61E-05	-8,95E-05	-2,90E-02	-3,23E-01	-3,20E-01		-1,63E-01
Ground	-2,75E-01	-2,07E-01	-2,95E-01	-2,84E-01	-1,81E-01	-2,63E-01	-2,42E-01	-1,54E-01	-1,65E-01	-1,63E-01	

Figure A.2.: Capacitance Table and Capacitive Coupling Table

B Coupling between Two Capacitors

Angle/° and Distance/mm	-30	-27,5	-25	-22,5	-20	-17,5	-15	-12,5	-10	-7,5	-5	-2,5	0	
-90	-2,79E-03	-1,80E-03	-8,18E-04	-1,62E-03	-2,42E-03	-3,61E-03	-4,80E-03	-4,46E-03	-4,13E-03	NaN	NaN	NaN	NaN	
-87,5	9,61E-04	-2,10E-04	-1,38E-03	-7,65E-04	-1,49E-04	-2,00E-03	-3,85E-03	-6,94E-03	-1,00E-02	NaN	NaN	NaN	NaN	
-85	-2,31E-03	-2,58E-04	1,79E-03	1,01E-03	2,36E-04	2,14E-03	4,05E-03	3,69E-03	3,32E-03	NaN	NaN	NaN	NaN	
-82,5	1,53E-03	1,09E-03	6,57E-04	1,54E-03	2,42E-03	6,31E-03	1,02E-02	7,16E-03	4,13E-03	NaN	NaN	NaN	NaN	
-80	8,99E-04	2,42E-03	3,94E-03	3,78E-03	3,63E-03	5,24E-03	6,84E-03	7,82E-03	8,80E-03	NaN	NaN	NaN	NaN	
-77,5	2,21E-03	2,13E-03	2,04E-03	2,94E-03	3,84E-03	7,44E-03	1,11E-02	1,41E-02	1,72E-02	NaN	NaN	NaN	NaN	
-75	2,41E-03	4,36E-03	6,31E-03	6,97E-03	7,64E-03	1,02E-02	1,27E-02	2,03E-02	2,79E-02	NaN	NaN	NaN	NaN	
-72,5	4,27E-03	5,21E-03	6,16E-03	8,08E-03	1,00E-02	1,09E-02	1,18E-02	2,17E-02	3,16E-02	NaN	NaN	NaN	NaN	
-70	5,69E-03	6,65E-03	7,60E-03	1,06E-02	1,36E-02	1,50E-02	1,64E-02	2,23E-02	2,82E-02	NaN	NaN	NaN	NaN	
-67,5	7,39E-03	7,15E-03	6,90E-03	9,53E-03	1,22E-02	1,58E-02	1,93E-02	2,62E-02	3,31E-02	4,30E-02	NaN	NaN	NaN	
-65	8,18E-03	8,37E-03	8,56E-03	1,23E-02	1,61E-02	2,02E-02	2,43E-02	3,07E-02	3,72E-02	4,44E-02	NaN	NaN	NaN	
-62,5	7,12E-03	9,29E-03	1,15E-02	1,41E-02	1,67E-02	2,24E-02	2,81E-02	3,32E-02	3,84E-02	4,58E-02	NaN	NaN	NaN	
-60	6,75E-03	9,53E-03	1,23E-02	1,50E-02	1,77E-02	2,25E-02	2,74E-02	3,73E-02	4,71E-02	4,71E-02	NaN	NaN	NaN	
-57,5	6,84E-03	8,68E-03	1,05E-02	1,39E-02	1,72E-02	2,31E-02	2,89E-02	3,48E-02	4,07E-02	4,49E-02	NaN	NaN	NaN	
-55	8,06E-03	1,03E-02	1,25E-02	1,48E-02	1,72E-02	2,39E-02	3,06E-02	3,50E-02	3,95E-02	5,20E-02	NaN	NaN	NaN	
-52,5	9,94E-03	1,21E-02	1,42E-02	1,72E-02	2,02E-02	2,38E-02	2,73E-02	3,86E-02	4,99E-02	5,85E-02	NaN	NaN	NaN	
-50	1,07E-02	1,23E-02	1,40E-02	1,86E-02	2,32E-02	2,63E-02	2,93E-02	4,55E-02	6,16E-02	6,57E-02	NaN	NaN	NaN	
-47,5	1,17E-02	1,14E-02	1,12E-02	1,88E-02	2,64E-02	3,20E-02	3,75E-02	4,99E-02	6,24E-02	6,64E-02	NaN	NaN	NaN	
-45	1,05E-02	1,23E-02	1,42E-02	1,75E-02	2,08E-02	2,99E-02	3,90E-02	5,23E-02	6,56E-02	6,91E-02	9,01E-02	NaN	NaN	
-42,5	1,13E-02	1,44E-02	1,74E-02	2,08E-02	2,42E-02	2,94E-02	3,47E-02	4,73E-02	5,99E-02	7,03E-02	9,15E-02	NaN	NaN	
-40	1,01E-02	1,20E-02	1,39E-02	2,00E-02	2,60E-02	3,36E-02	4,12E-02	5,55E-02	6,99E-02	7,48E-02	9,29E-02	NaN	NaN	
-37,5	1,16E-02	1,37E-02	1,57E-02	1,98E-02	2,39E-02	3,11E-02	3,84E-02	5,14E-02	6,44E-02	8,11E-02	9,42E-02	NaN	NaN	
-35	1,17E-02	1,38E-02	1,58E-02	2,23E-02	2,89E-02	3,23E-02	3,57E-02	4,96E-02	6,34E-02	7,98E-02	9,56E-02	NaN	NaN	
-32,5	1,21E-02	1,59E-02	1,96E-02	2,34E-02	2,73E-02	3,47E-02	4,22E-02	4,79E-02	5,35E-02	8,21E-02	9,70E-02	NaN	NaN	
-30	1,08E-02	1,36E-02	1,65E-02	2,14E-02	2,64E-02	3,18E-02	3,72E-02	4,70E-02	5,68E-02	7,66E-02	9,84E-02	NaN	NaN	
-27,5	1,37E-02	1,53E-02	1,70E-02	2,38E-02	3,06E-02	3,42E-02	3,79E-02	4,92E-02	6,05E-02	8,01E-02	9,98E-02	NaN	NaN	
-25	1,30E-02	1,40E-02	1,51E-02	2,11E-02	2,72E-02	3,31E-02	3,91E-02	4,95E-02	5,98E-02	8,90E-02	1,18E-01	NaN	NaN	
-22,5	1,59E-02	1,75E-02	1,91E-02	2,59E-02	3,28E-02	3,77E-02	4,27E-02	5,48E-02	6,69E-02	8,36E-02	1,00E-01	1,37E-01	NaN	
-20	1,97E-02	1,68E-02	1,40E-02	2,03E-02	2,66E-02	3,35E-02	4,03E-02	5,17E-02	6,30E-02	8,43E-02	1,06E-01	1,39E-01	NaN	
-17,5	1,31E-02	1,61E-02	1,91E-02	2,11E-02	2,30E-02	3,24E-02	4,17E-02	5,21E-02	6,25E-02	7,94E-02	9,63E-02	1,40E-01	NaN	
-15	1,52E-02	1,63E-02	1,74E-02	2,29E-02	2,84E-02	3,58E-02	4,32E-02	5,27E-02	6,23E-02	8,01E-02	9,79E-02	1,41E-01	NaN	
-12,5	1,47E-02	1,50E-02	1,52E-02	2,10E-02	2,67E-02	3,33E-02	3,98E-02	5,37E-02	6,76E-02	8,95E-02	1,11E-01	1,51E-01	NaN	
-10	1,41E-02	1,52E-02	1,63E-02	2,23E-02	2,82E-02	3,52E-02	4,22E-02	5,38E-02	6,53E-02	8,56E-02	1,06E-01	1,45E-01	NaN	
-7,5	9,69E-03	1,43E-02	1,89E-02	2,13E-02	2,36E-02	3,47E-02	4,57E-02	5,50E-02	6,42E-02	8,37E-02	1,03E-01	1,41E-01	NaN	
-5	1,75E-02	1,89E-02	2,04E-02	2,44E-02	2,84E-02	3,44E-02	4,03E-02	5,09E-02	6,16E-02	8,34E-02	1,05E-01	1,45E-01	NaN	
-2,5	1,42E-02	1,62E-02	1,82E-02	2,20E-02	2,59E-02	3,34E-02	4,09E-02	5,25E-02	6,42E-02	8,29E-02	1,02E-01	1,45E-01	NaN	
0	1,61E-02	1,67E-02	1,74E-02	2,33E-02	2,93E-02	3,24E-02	3,56E-02	4,97E-02	6,39E-02	7,89E-02	9,39E-02	1,39E-01	1,84E-01	

Figure B.1.: Coupling between Two Capacitors

C Coupling Summary

Inductive Coupling			Capacitive Coupling		
Components	Coupling Factor	Relevance	Components	Coupling Factor	Relevance
X Capacitors and Common Mode Choke	0,00406301	Not Relevant	X Capacitors and Common Mode Choke	0,010157807	Not Relevant
Y Capacitors and Common Mode Choke	0,002089965	Not Relevant	Y Capacitors and Common Mode Choke	0,011623863	Not Relevant
X Capacitors and Y Capacitors	0,001718722	Not Relevant	X Capacitors and Y Capacitors	8,83341E-06	Not Relevant
X Capacitors	0,089047313	Relevant	X Capacitors	0,203920642	Not Relevant
Y Capacitors	0,072012012	Relevant	Y Capacitors	0,153982166	Not Relevant
Common Mode Choke	0,805239817	Relevant	X Capacitors and Housing	0,261657496	Relevant
PCB and X Capacitors	0,022825572	Not Relevant	Y Capacitors and Housing	0,245435323	Relevant
PCB and Y Capacitors	0,020674981	Not Relevant	Common Mode Choke and Housing	0,161078629	Relevant
PCB and Common Mode Choke	0,000350273	Not Relevant	Common Mode Choke	0,260928659	Not Relevant
PCB	0,011088	Not Relevant	PCB and X Capacitors	0,066697251	Not Relevant
			PCB and Y Capacitors	0,055419784	Not Relevant
			PCB and Common Mode Choke	0,032687119	Not Relevant
			PCB and Housing	0,1669874	Relevant
Note: All RMS Coupling Factors					
Range: 0 (No Coupling) to 1 (Perfect Coupling)			PCB	0,092938589	Not Relevant

Figure C.1.: First Table

Inductive Coupling	Common Mode Choke	Y Capacitors	X Capacitors	PCB
Common Mode Choke	0,805239817	0,002089965	0,00406301	0,000350273
	Not Stray	Not Relevant	Not Relevant	Not Relevant
Y Capacitors		0,072012012	0,001718722	0,020674981
		Relevant	Not Relevant	Not Relevant
X Capacitors			0,089047313	0,022825572
			Relevant	Not Relevant
PCB				0,011088
				Not Relevant

Capacitive Coupling	Common Mode Choke	Y Capacitors	X Capacitors	Housing	PCB
Common Mode Choke	0,260928659	0,011623863	0,010157807	0,161078629	0,032687119
	Not Relevant	Not Relevant	Not Relevant	Relevant	Not Relevant
Y Capacitors		0,153982166	0,000008833	0,245435323	0,055419784
		Not Relevant	Not Relevant	Relevant	Not Relevant
X Capacitors			0,203920642	0,261657496	0,066697251
			Not Relevant	Relevant	Not Relevant
Housing				Not Avaiable	0,1669874
				Not Avaiable	Relevant
PCB					0,092938589
					Not Relevant

Figure C.2.: Second Table

Components	Coupling Factor, Inductive	Coupling Factor, Capacitive	Relevance, Summary	Effect	Mitigation	See Chapter
Parallel Capacitance of Common Mode Choke	N/A	N/A	Most Relevant	Shifting of Curve Amplitude	Compensation	5.1 and 6.1
Stray Inductance of Capacitors	N/A	N/A	Most Relevant	Shifting of Valley Frequency	Compensation	5.1 and 6.1
PCB and Housing	N/A	0,1669874	Relevant	Higher Frequency Peak (Amplitude and Frequency)	Not needed	5.2
X Capacitors	0,0899047313	0,203920642	Relevant	Assymetry between Phases	Arrangement	5.2
Y Capacitors	0,072012012	0,153982166	Relevant	Shifting of Valley Frequency	Atrrangement	5.3
X Capacitors and Housing	N/A	0,261657496	Relevant	Higher Frequency Peak (Amplitude and Frequency)	Not needed	5.2
Y Capacitors and Housing	N/A	0,245435323	Relevant	Higher Frequency Peak (Amplitude and Frequency)	Not needed	5.2
Common Mode Choke and Housing	N/A	0,161078629	Relevant	Higher Frequency Peak (Amplitude and Frequency)	Not needed	5.2
Common Mode Choke	N/A	0,260928659	Not Relevant	N/A	N/A	5.2
PCB and X Capacitors	0,022825572	0,066697251	Not Relevant	N/A	N/A	5.3
PCB and Y Capacitors	0,020674981	0,055419784	Not Relevant	N/A	N/A	5.3
PCB and Common Mode Choke	0,000350273	0,032687119	Not Relevant	N/A	N/A	5.3
PCB	0,011088	0,092938589	Not Relevant	N/A	N/A	5.3
X Capacitors and Common Mode Choke	0,00406301	0,010157807	Not Relevant	N/A	N/A	5.3
Y Capacitors and Common Mode Choke	0,002089965	0,011623863	Not Relevant	N/A	N/A	5.3
X Capacitors and Y Capacitors	0,001718722	8,83341E-06	Not Relevant	N/A	N/A	5.3

Figure C.3.: Third Table

D PCB Sheets

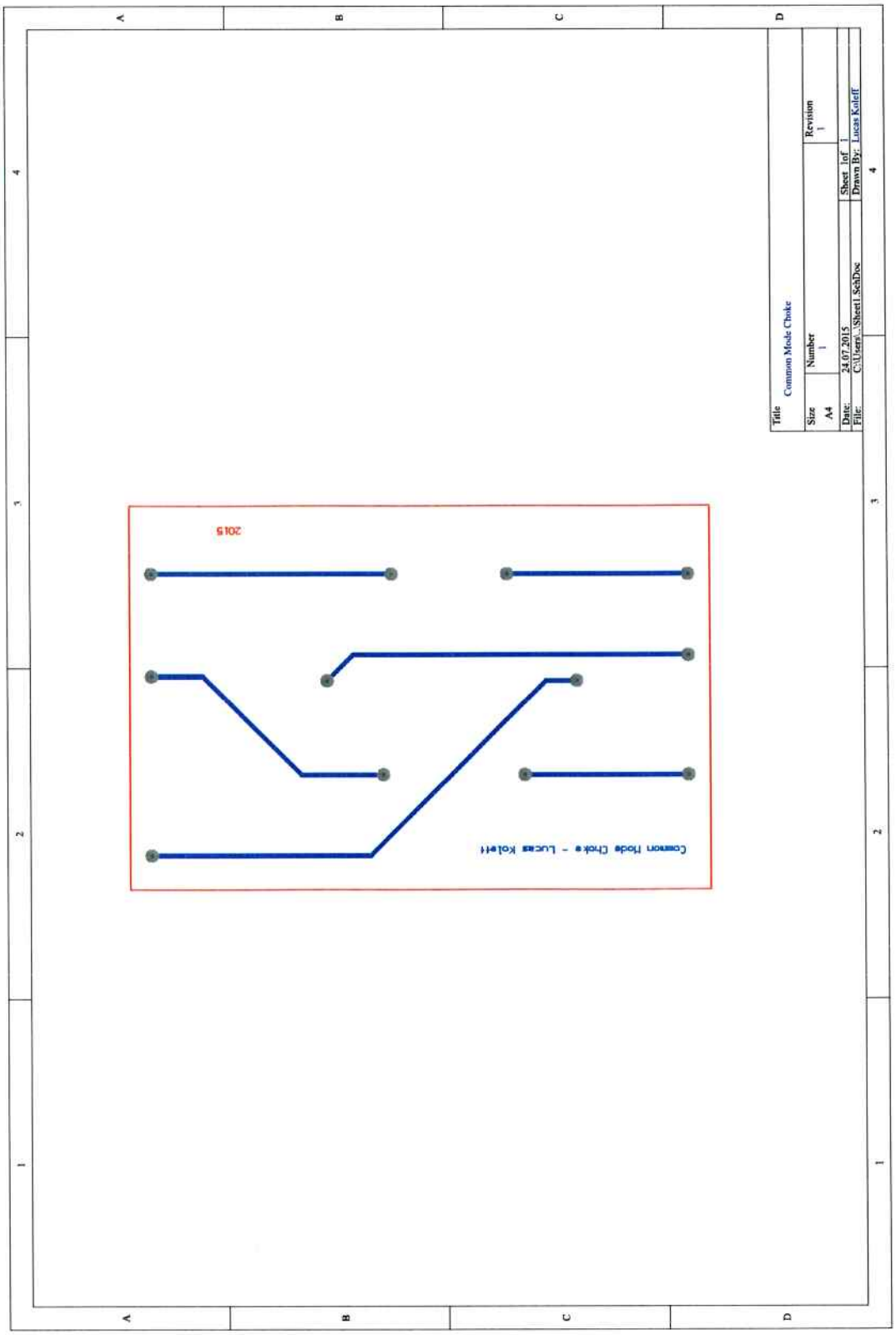

Figure D.1.: Common Mode Choke

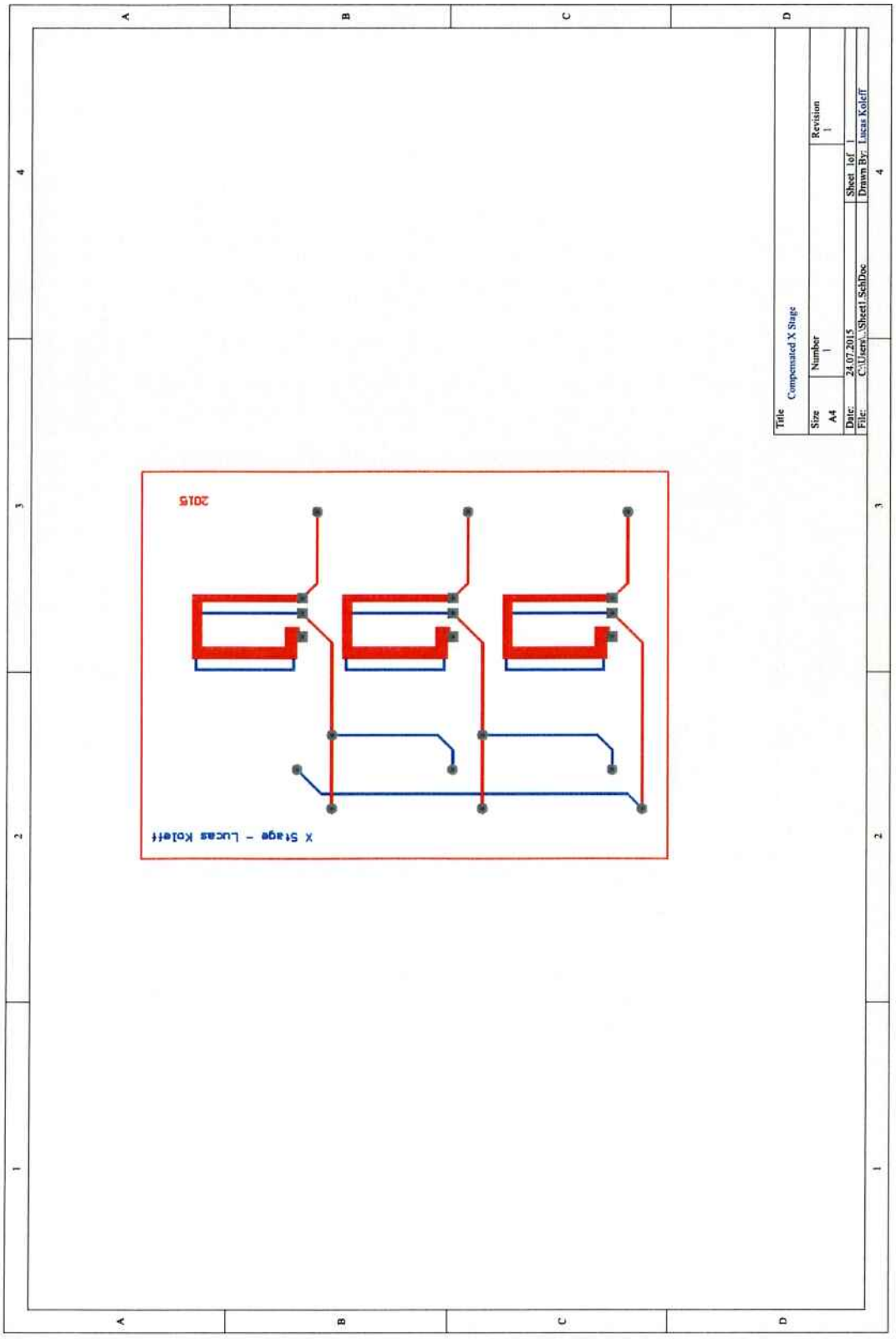

Figure D.2.: Compensated X Stage

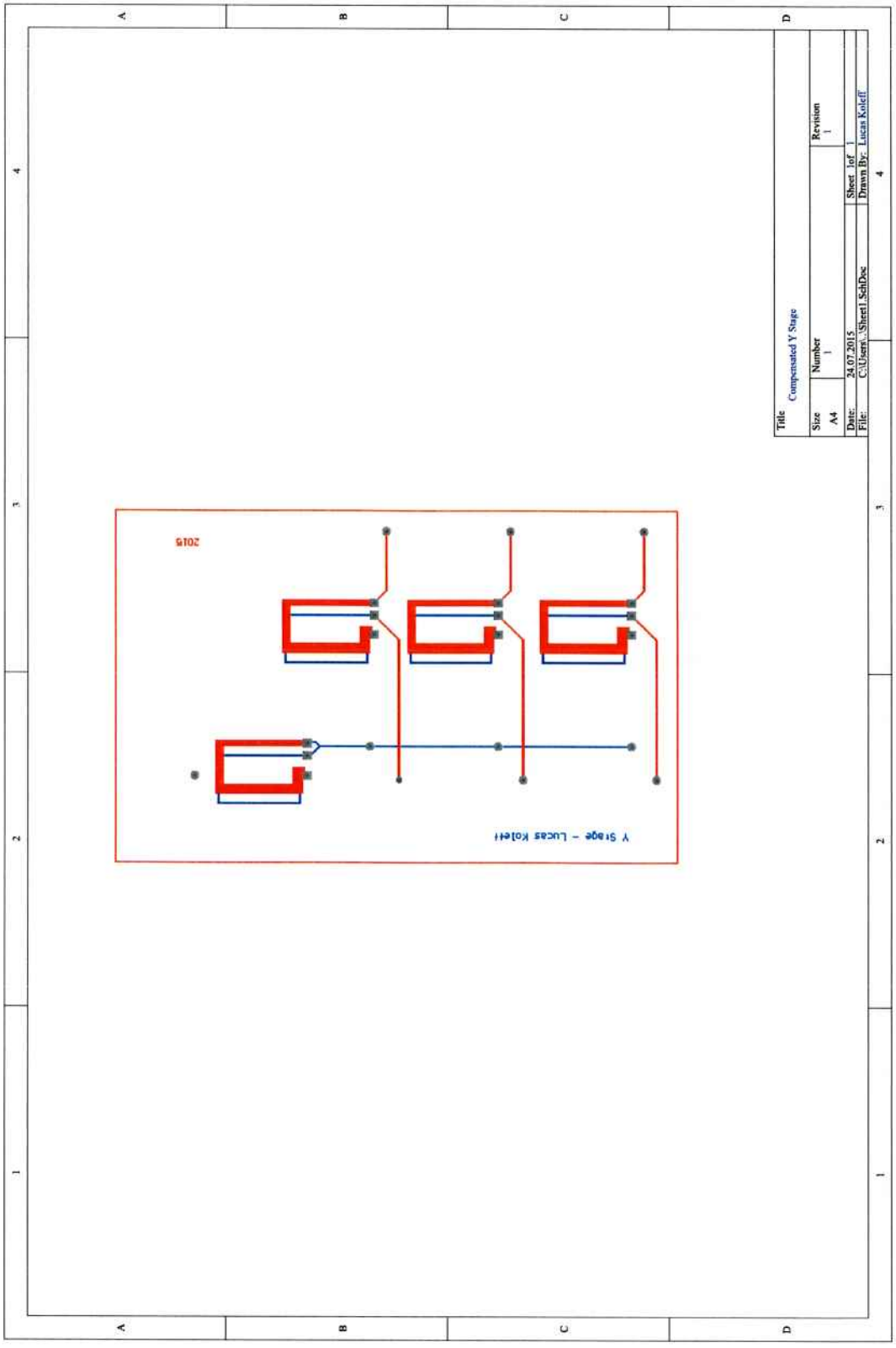

Figure D.3.: Compensated Y Stage

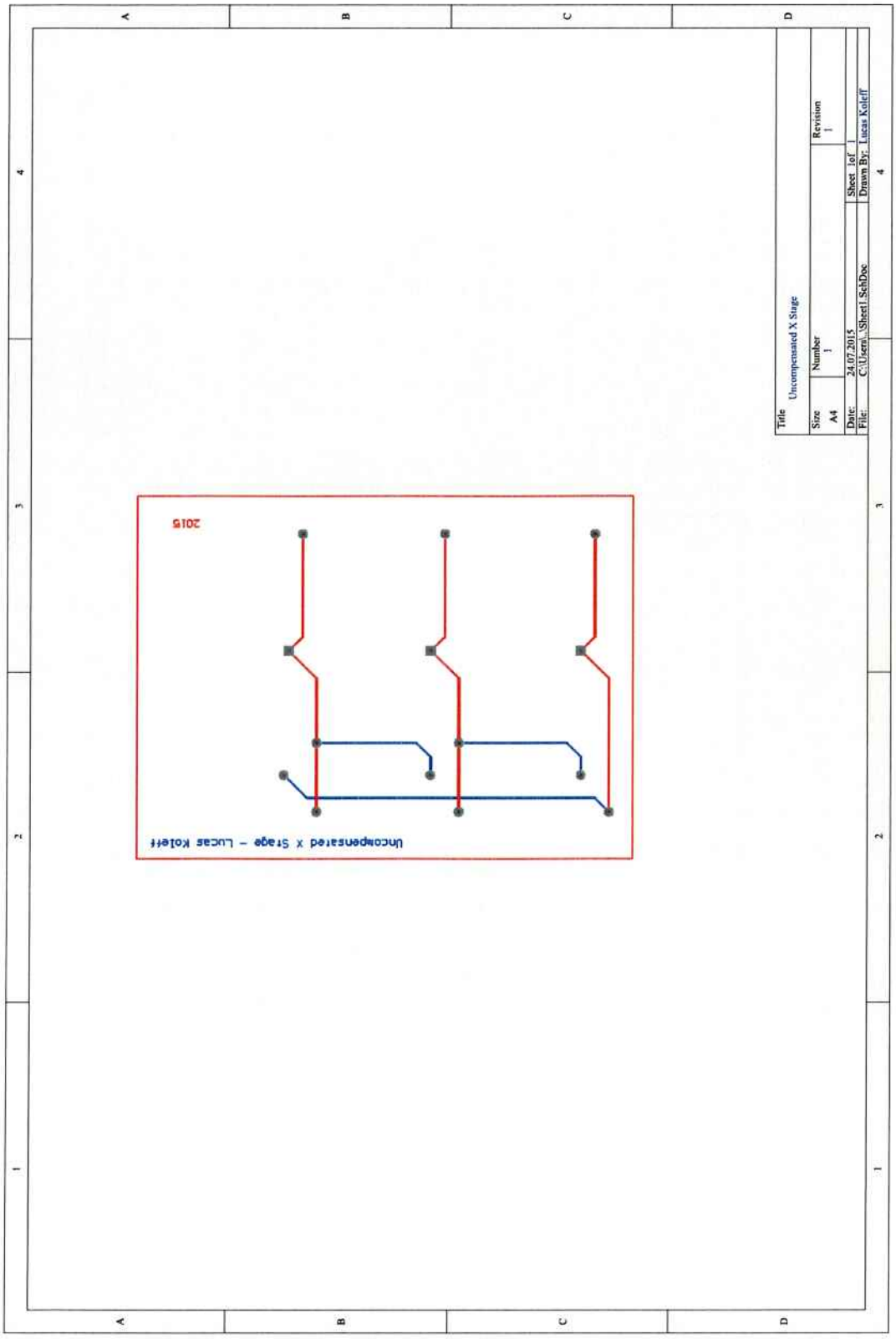

Figure D.4.: Uncompensated X Stage

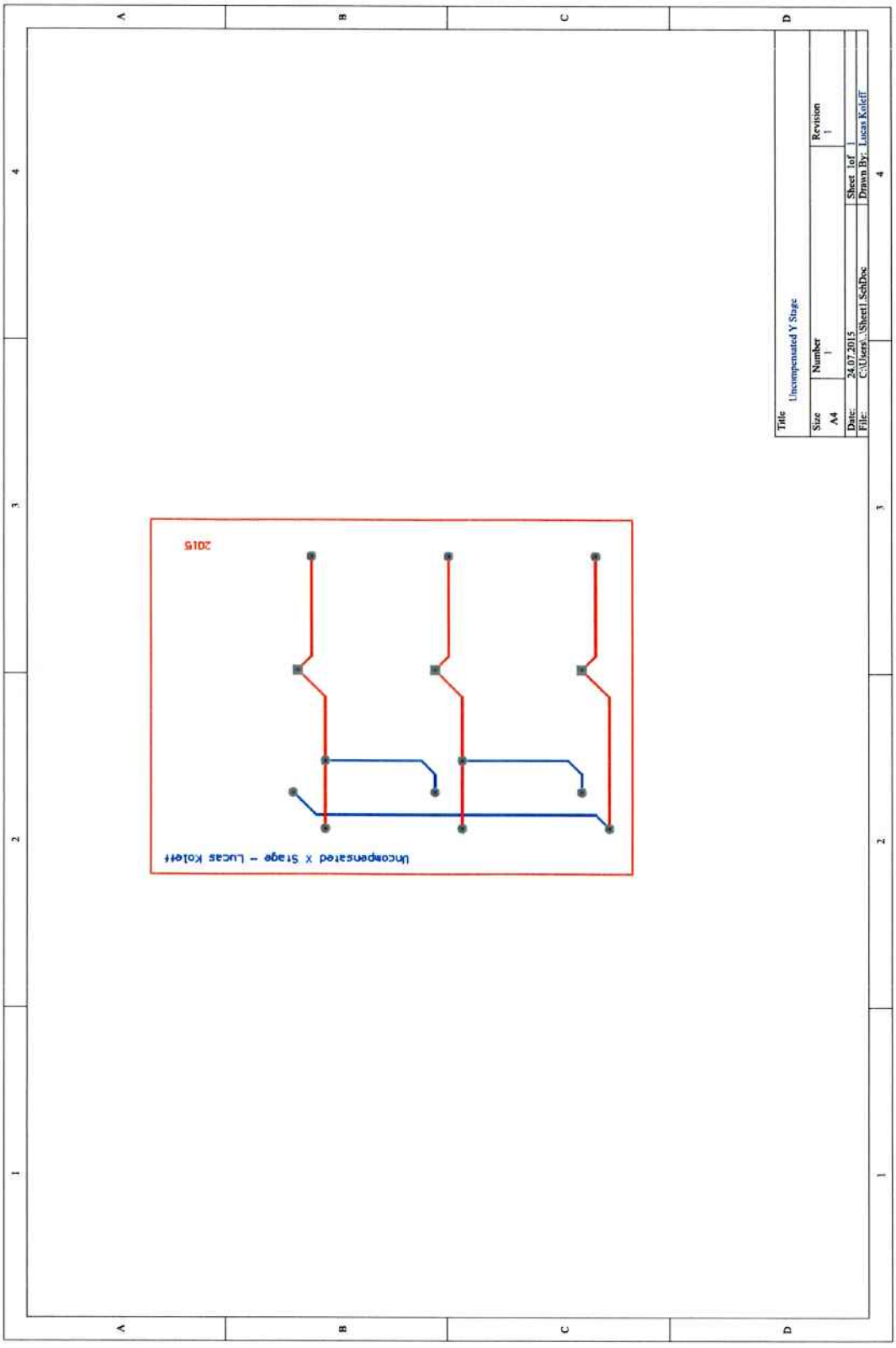

Figure D.5.: Uncompensated Y Stage

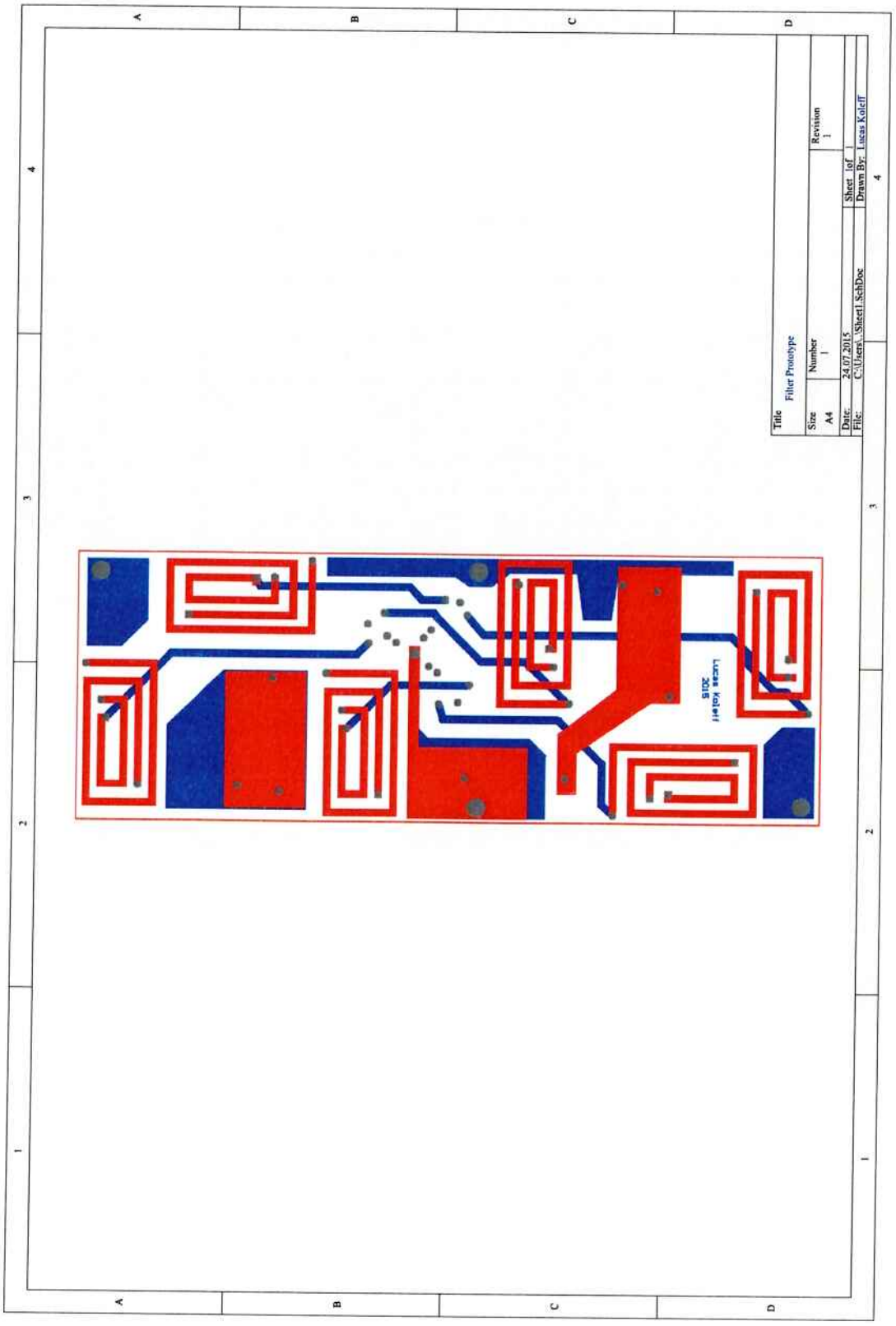

Figure D.6.: Filter Prototype

E Measurement Equipment

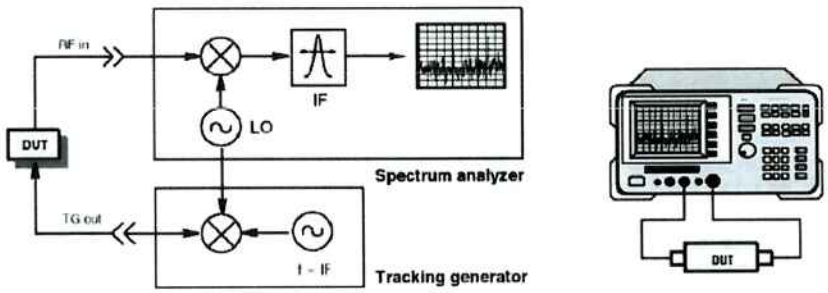

Figure E.1.: Intermediate Frequency of Network Analyser [3]

In order to measure the insertion losses of the filter a vector network analyser is used. This measurement equipment sends a test signal (incident signal) through one of its two ports, and measures the signal that is reflected by the device under test and comes back in the sending port and the signal that is transmitted through the device under test and comes in the receiving port. This process is repeated in the other director. Equations E.1 and E.2 show how the scaterring parameters can be obtained from the signals, in decibels. Figure E.2 illustrates the scattering parameters.

Figure shows the connection of the device under test to the network analyser, as well as the internal oscillator. In order to be able to operate at higher frequencies, the input and output signals are multiplied by the local oscillator in order to shift the spectrum and fit into the bandwidth of the measurement circuit. This is similar to the super-heterodyne receiver principle used in telecommunications. The intermediate frequency bandwidth determines the size of one division of the frequency spectrum of the whole measurement range. If the bandwidth is too big, a significant part of the noise is not filtered. So the bandwidth should be kept small, even though the network analyser takes longer to finish one measurement.

$$S_{11} = 20 \cdot log(\frac{V_{\text{reflected1}}}{V_{\text{incident1}}}), \quad S_{22} = 20 \cdot log(\frac{V_{\text{reflected2}}}{V_{\text{incident2}}}) \tag{E.1}$$

$$S_{12} = 20 \cdot log(\frac{V_{\text{transmitted2}}}{V_{\text{incident1}}}), \quad S_{21} = 20 \cdot log(\frac{V_{\text{transmitted1}}}{V_{\text{incident2}}}) \tag{E.2}$$

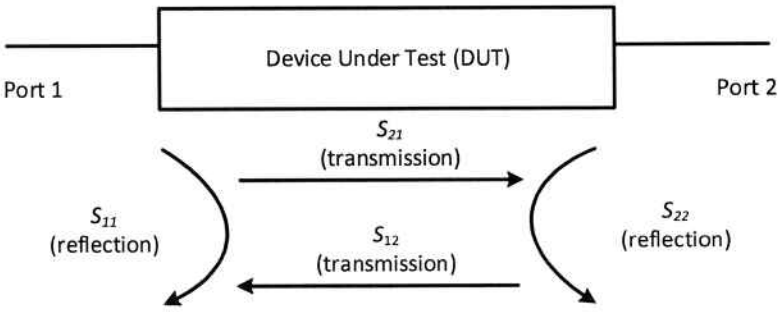

Figure E.2.: Scaterring Parameters

Bibliography

[1] A. Lissner, E. Hoene, B. Stube, S. Guttowski, "Predicting the influence of placement of passive components on emi behaviour," *EPE 07 Paper 0033*.

[2] A. Nagel, R. W. De Doncker, "Systematic design of emi-filters for power converters - industry applications conference, 2000. conference record of the 2000 ieee."

[3] Agilent, "Network analyzer basics."

[4] An Zhou, C. Joubert, M. Bensetti, F. de Daran, "Study and modeling of inter-component coupling to optimize emc filter."

[5] Ansys, "Maxwell online help."

[6] Clayton R. Paul, *Electromagnetic Compatibility*, second edition ed. Wiley.

[7] T. De-Oliveira, J.-L. Schanen, J.-M. Guichon, and L. Gerbaud, "Optimal stray magnetic couplings for emc filters," *IEEE Transactions on Industry Applications*, vol. 49, no. 4, pp. 1619–1627, 2013.

[8] ——, "Optimal stray magnetic couplings for emc filters," *IEEE Transactions on Industry Applications*, vol. 49, no. 4, pp. 1619–1627, 2013.

[9] E. Hoene, A. Lissner, S. Guttowski, "Symposium: Prediction of emi behaviour in terms of passive component placement."

[10] EPCOS, "Ferrites and accessories, siferrit, material t35."

[11] M. Ferch, "Magnetec presentation vde nordbayern may 15, 2014."

[12] Fred C. Lee, Shuo Wang, *Characterization and Cancellation of High-Frequency Parasitics for EMI Filters and Noise Separators in Power Electronics Applications*, 2005.

[13] Gundars Asmanis, Aivis Asmanis, and Denis Stepins, "Mutual couplings in three phase t-type emi filters."

[14] Heinz M. Schlicke, "Assuredly effective filters," *IEEE Transactions on Electromagnetic Compatibility*, 1976.

[15] http://electronicdesign.com/, "Emc table."

[16] Illia Manushyn, "Assessment and classification of the soft magnetic material cores for emi filter application," in *Energy Science Technology Karlsruhe 2015*.

[17] Ivana Kovaevi, Andreas Maesing, Thomas Friedli, Johann. W. Kolar, "Electromagnetic modeling of emi input filters."

[18] I. F. Kovaceevic, T. Friedli, A. M. Musing, and J. W. Kolar, "Full peec modeling of emi filter inductors in the frequency domain," *IEEE Transactions on Magnetics*, vol. 49, no. 10, pp. 5248–5256, 2013.

[19] I. F. Kovacevic, T. Friedli, A. M. Muesing, and J. W. Kolar, "3-d electromagnetic modeling of emi input filters," *IEEE Transactions on Industrial Electronics*, vol. 61, no. 1, pp. 231–242, 2014.

[20] M. Kovacic, Z. Hanic, S. Stipetic, S. Krishnamurthy, and D. Zarko, "Analytical wideband model of a common-mode choke," *IEEE Transactions on Power Electronics*, vol. 27, no. 7, pp. 3173–3185, 2012.

[21] Laurent Taylor, Wenhua Tan, Xavier Margueron, Nadir Idir, "Reducing of parasitic inductive couplings effects in emi filters."

[22] Leonidas Kotzamanidis, *Investigation of the Core Material Effect on the Damping Characteristics of the Common-Mode Choke*, 2015.

[23] Lingyin Zhao, J. D. van Wyk, "Electromagnetic modeling of an integrated rf emi filter," *Industry Applications Conference 38th IAS Annual Meeting. Conference Record*, 2003.

[24] Marcelo Lobo Heldwein, "Emc filtering of three-phase pwm converters."

[25] A. Massarini and M. Kazimierczuk, "Self-capacitance of inductors," *Power Electronics, IEEE Transactions on*.

[26] Munro et al., "Emi filter topology for power inverters," Patent US 5,552,976.

[27] T. C. Neugebauer and D. J. Perreault, "Parasitic capacitance cancellation in filter inductors," *IEEE Transactions on Power Electronics*, vol. 21, no. 1, pp. 282–288, 2006.

[28] T. C. Neugebauer, J. W. Phinney, and D. J. Perreault, "Filters and components with inductance cancellation," *IEEE Transactions on Industry Applications*, vol. 40, no. 2, pp. 483–491, 2004.

[29] Perreault et al., "Method and apparatus to provide compensation for parasitic inductance of multiple capacitors," Patent US 7,589,605 B2.

[30] S. Guttowski, S. Weber, E. Hoene, A. Lissner, W. John, H. Reichl, "Simulating electromagnetic interactions in high power density converters," 2005.

[31] S. Weber, M. Schinkel, S. Guttowski, W. John, H. Reichl, "Calculating parasitic capacitance of three-phase common-mode chokes."

[32] S. Zangui, K. Berger, C. Vollaire, E. Clavel, R. Perrussel, B. Vincent, "Modeling the near-field coupling of the emc filter components."

[33] Schaffner, "Fn 258 datasheet."

[34] ——, "Fn 3100 datasheet."

[35] ——, "Fn351h datasheet."

[36] Schurter, "Fmbc ll - power entry modules with line filter."

[37] Shuo Wang, "Characterization and cancellation of high-frequency parasitics for emi filters and noise separators in power electronics applications," Ph.D. dissertation, Virginia Polytechnic Institute, May 11, 2005.

[38] Shuo Wang, F. C. Lee, and van Wyk, Jacobus Daniel, "A study of integration of parasitic cancellation techniques for emi filter design with discrete components," *IEEE Transactions on Power Electronics*,

vol. 23, no. 6, pp. 3094–3102, 2008.

[39] Shuo Wang, Rengang Chen, Fred C. Lee and J. D. van Wyk, "Improved passive filter configurations for high-frequency conducted emi in power electronics," *EPE 2005 - Dresden*, 2005.

[40] TDK, "Film capacitors emi suppression capacitors (mkp): Datasheet."

[41] B. Touré, J.-L. Schanen, L. Gerbaud, T. Meynard, J. Roudet, and R. Ruelland, "Emc modeling of drives for aircraft applications: Modeling process, emi filter optimization, and technological choice," *IEEE Transactions on Power Electronics*, vol. 28, no. 3, pp. 1145–1156, 2013.

[42] Vacom, "Emc and variable speed drives."

[43] Vacuumschmelze, "Nanokristallines vitroperm emv produkte."

[44] S. Wang, F. C. Lee, D. Y. Chen, and W. G. Odendaal, "Effects of parasitic parameters on emi filter performance," *IEEE Transactions on Power Electronics*, vol. 19, no. 3, pp. 869–877, 2004.

[45] S. Wang, van Wyk, Jacobus Daniel, and F. C. Lee, "Effects of interactions between filter parasitics and power interconnects on emi filter performance," *IEEE Transactions on Industrial Electronics*, vol. 54, no. 6, pp. 3344–3352, 2007.

[46] Wang et al., "Emi filter and frequency filters having capacitor with inductance cancellation loop," Patent US 2006/0 132 257 A1.

[47] White et al., "Common-mode emi filter," Patent US 5,838,216.